#### **TOPICAL REVIEW**

## Applications of nanomagnets as dynamical systems: II

To cite this article: Bivas Rana et al 2022 Nanotechnology 33 082002

View the article online for updates and enhancements.

#### You may also like

- <u>Applications of nanomagnets as dynamical</u> <u>systems: I</u>

Bivas Rana, Amrit Kumar Mondal, Supriyo Bandyopadhyay et al.

 A novel and reliable interlayer exchange coupled nanomagnetic universal logic gate design

Venkat Mattela, Sanghamitra Debroy, Santhosh Sivasubramani et al.

- Computational logic with square rings of

Hanu Arava, Peter M Derlet, Jaianth Vijayakumar et al.



## IOP ebooks™

Bringing together innovative digital publishing with leading authors from the global scientific community.

Start exploring the collection-download the first chapter of every title for free.

IOP Publishing Nanotechnology

Nanotechnology 33 (2022) 082002 (34pp)

https://doi.org/10.1088/1361-6528/ac2f59

#### **Topical Review**

# Applications of nanomagnets as dynamical systems: II

Bivas Rana<sup>1,2,\*</sup>, Amrit Kumar Mondal<sup>3</sup>, Supriyo Bandyopadhyay<sup>4,\*</sup> and Anjan Barman<sup>3,\*</sup>

E-mail: abarman@bose.res.in, sbandy@vcu.edu and bivran@amu.edu.pl

Received 26 April 2021, revised 16 September 2021 Accepted for publication 13 October 2021 Published 30 November 2021



#### **Abstract**

In Part I of this topical review, we discussed dynamical phenomena in nanomagnets, focusing primarily on magnetization reversal with an eye to digital applications. In this part, we address mostly wave-like phenomena in nanomagnets, with emphasis on spin waves in myriad nanomagnetic systems and methods of controlling magnetization dynamics in nanomagnet arrays which may have analog applications. We conclude with a discussion of some interesting spintronic phenomena that undergird the rich physics exhibited by nanomagnet assemblies.

Keywords: nanomagnetism, applications of nanomagnets, magnetization dynamics, external control of magnetization processes, spin waves, spintronics

(Some figures may appear in colour only in the online journal)

#### 1. Introduction

The much-feared impending demise of Moore's law that has guided the electronics industry for the last seven decades has stimulated research into encoding information in alternate state variables, such as an electron's or hole's spin degree of freedom, instead of the charge degree of freedom. This has spawned the field of spintronics where information is stored, processed, sensed, and communicated with the aid of an electron's or a hole's spin. Among various alternative ideas of non-Boolean algebra in spintronics, wave-based or quasi-particle-based information and computation technology has emerged as one of the most promising ideas. In this regard, spin waves (SWs) [1], i.e. collective dynamics of electron spins coupled by exchange and dipolar interaction in ordered

magnetic materials, have emerged. The SWs can encode information by using their wave properties, e.g. frequency, phase, amplitude, and polarization, without the requirement of any translational motion of charge particles causing current flow, and thus can significantly reduce energy consumption. The quasiparticles associated with SWs are known as magnons. Magnonics, which deals with SWs or magnons, is a young and rapidly evolving research field [2–5]. Interestingly, SWs can have a wide range of frequencies from few Gigahertz to few Terahertz with corresponding wavelengths extending from few tens of micrometer down to few tens of nanometer [6-10]. The SW properties are not only determined by the structural and material parameters of the constituent magnetic materials, but also by their static magnetic configuration which is sensitive to an external bias magnetic field. Moreover, various types of interactions such as magnetostatic, symmetric and asymmetric exchange, anisotropies,

<sup>&</sup>lt;sup>1</sup> Institute of Spintronics and Quantum Information, Faculty of Physics, Adam Mickiewicz University in Poznań, Uniwersytetu Poznanskiego 2, Poznań 61-614, Poland

<sup>&</sup>lt;sup>2</sup> Center for Emergent Matter Science, RIKEN, 2-1 Hirosawa, Wako 351-0198, Japan

<sup>&</sup>lt;sup>3</sup> Department of Condensed Matter Physics and Material Sciences, S. N. Bose National Centre for Basic Sciences, Block JD, Sector III, Salt Lake, Kolkata 700 106, India

<sup>&</sup>lt;sup>4</sup> Department of Electrical and Computer Engineering, Virginia Commonwealth University, Richmond, VA, 23284, United States of America

<sup>\*</sup> Authors to whom any correspondence should be addressed.

etc also actively control the SW properties. The crucial advantage is that SWs in magnonic devices are easily reconfigurable unlike information carriers in photonic or phononic devices.

Aided by the understanding of SW properties in various magnetic nanostructures [11-26], research on magnonics in the last decade also focused on various technical issues related to device applications [27-33]. Initially, the study of SW properties was performed mainly on magnetic films with thicknesses around hundreds of nanometers [34]. With significant advancement of thin film deposition and nanofabrication technology, the investigation of SW properties in various types of confined magnetic structures such as magnetic thin films and their heterostructures [6, 35–37], magnetic nanodots [11, 14, 38], connected nanomagnets [18, 21], stripes [15-17], antidots [24, 25], nanowires [16, 26], nanoparticles [22, 23] etc have become possible. Nanomagnets can be the potential testbeds to investigate the properties of SWs not only to probe their fundamental behavior, but also to explore their huge potential for applications in future spintronic devices [39–42]. In fact, nanomagnets come with extra 'knobs' to control static magnetic configuration via tuning of their shapes, sizes, aspect ratios, and geometrical arrangement into arrays. Hence, the SW properties, which strongly depend upon the ground state magnetic configurations (microstates), can be easily tailored just by altering the geometry and physical arrangement of the nanomagnets.

Some of the major technical challenges for the development of magnonic devices are to find efficient ways for excitation, manipulation, control and detection of SWs. The method should preferably consume low power and must be compatible with high-speed nanoscale microwave devices. The relativistic spin-orbit coupling (SOC), which couples electronic spins with its orbital motion, can serve this purpose. An external perturbation, e.g. electric field, can control the spins through SOC. With significant advancements in thin film deposition and nanofabrication technology, a number of SOC mediated physical phenomena have been explored at the surfaces and interfaces [43] of thin films, such as perpendicular magnetic anisotropy (PMA) [44, 45], interfacial Dzyaloshinskii-Moriya interaction (DMI) [46-48], Rashba spin-orbit coupling (RSOC) [49, 50] and interfacial damping [51]. All these phenomena have proved to be very efficient for developing all-electric field controlled magnonic devices based on ultrathin ferromagnetic heterostructures.

Apart from magnonics, nanomagnets also have applications in other fields of spintronics. It is well known that magnetism arises from the quantum mechanical spin degree of freedom of charge carriers and nuclei in a solid. A *single domain* nanomagnet, consisting of  $\sim 10^4$  electron spins, behaves like one single giant *classical* spin in which all the spins together rotate coherently in unison when the magnetization rotates [52]. Consequently, nanomagnets can exhibit some interesting spintronic effects directly related to device applications. In fact, spintronics, or spin electronics, is a multidisciplinary research field that deals with the investigation of spin properties; control and manipulation of spins in solid state devices in order to perform myriad tasks such as

computing, information storage, communication, sensing and so on. The gamut of spintronics spans such disparate topics as nitrogen-vacancy (NV) centres in diamonds to act as spin qubits [53], topological spin textures [54], spin based classical computing [55], SW-based information processing [56], spin transistors [57, 58], spin batteries [59-61], spintronic photodetectors [62], spin current generation [63], spin transport [64] and spin dynamics in macroscale systems [65]. Among them the generation of spin polarized current, spin relaxation and spin detection are three major tasks in modern spintronics, and they often involve nanomagnets. When spin currents are injected into the nanomagnets, they can effectively generate and/or modulate the dynamic behavior of the magnetization leading to many spintronic devices such as microwave generator, SW amplifier, attenuator, nano-oscillator, etc.

In this second part of the topical review, we discuss various aspects of magnetization dynamics in both interacting and non-interacting ensembles of nanomagnets. This part is arranged in the following way. After a brief introduction of the topic, we discuss various potential methods for the excitation of SWs and their detection, in addition to their advantages and disadvantages. Then, we review some groundbreaking works on the investigation of SWs in various confined magnetic media such as single nanomagnet, onedimensional (1D) and two-dimensional (2D) arrays of nanomagnets, and connected nanomagnets. We present the dispersion relations of SWs in nanomagnet arrays calculated by the plane wave method (PWM) and also discuss the effects of geometrical parameters on the SW properties in nanomagnet arrays. This is followed by a discussion on the control of nanomagnet dynamics by an external magnetic field and/or an electric field. Subsequently, we discuss spintronic effects on nanomagnet dynamics. In particular we discuss the established methods for spin current generation, magnetoresistance, spin current induced torques and mechanical torque on spins. This part of the topical review is concluded with future perspectives and various challenges in this field of research.

## 2. Experimental methods for exciting and detecting magnetization dynamics in nanomagnets

## 2.1. Experimental techniques for exciting magnetization dynamics

There are several ways to excite precessional magnetization dynamics in nanomagnets and their arrays. Radio-frequency (RF) Oersted field is one very popular method. For this purpose, coplanar waveguides (CPWs) are fabricated on top of the nanostructures and the RF current induced Oersted field is employed to excite ferromagnetic resonance (FMR) (figure 1(a)) [66]. In some cases, nanostructures are fabricated between the signal and ground lines of a CPW. Conventional microstrip antennae are also used for exciting FMR and SWs (figure 1(b)) [67]. The Oersted field induced by a microwave current passing through a microstrip antenna can couple with

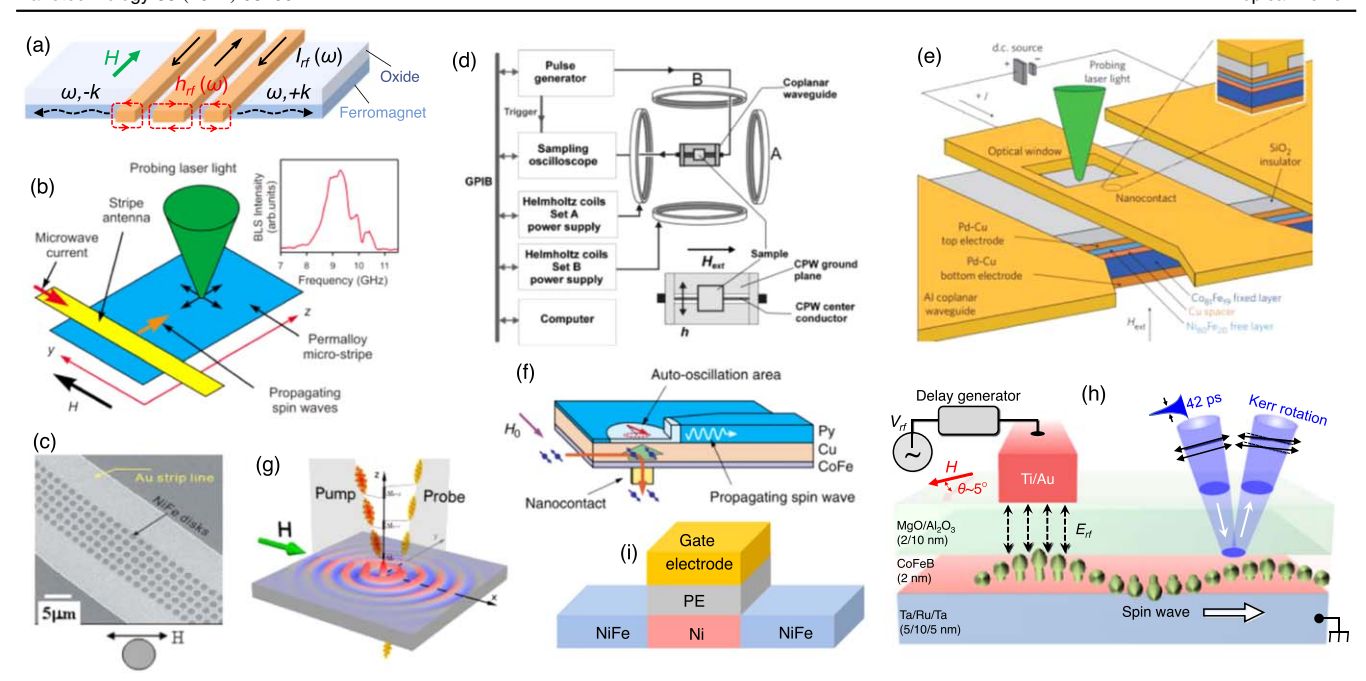


Figure 1. (a) Schematic diagram shows SW excitation by radio frequency (RF) Oersted field. A RF current is passed through a microwave antenna to generate spatially nonuniform RF Oersted field, which then inductively couples to the SWs having frequency ( $\omega$ ) same as the RF current. (b) Schematic diagram of a device for the excitation of SWs by microstrip antennae. The excited SWs can be probed by optical means, e.g. Brillouin light spectroscopy (BLS). Reprinted (figure) with permission from [67], Copyright (2008) by the American Physical Society. (c) SEM micrographs of the arrays of permalloy (Py) microdots deposited on a Au microstrip line. Reproduced from [68] with permission of the American Institute of Physics. (d) Schematic illustration of a pulsed inductive microwave magnetometer (PIMM). The magnetic sample is placed on top of the coplanar waveguide (CPW). Reprinted from [69], with the permission of AIP Publishing. (e) Schematic diagram represents the cross-section of a sample used for spin-transfer torque induced SW excitation. Reprinted by permission from Springer Nature Customer Service Centre GmbH: Springer Nature, Nature Nanotechnology, [71], Copyright © 2011, Nature Publishing Group. (f) Schematic illustration of a device used for the excitation of SWs by pure spin current. Reproduced from [72]. CCBY4.0. (g) Schematic diagram shows the excitation of SWs by femtosecond laser pulses. Reproduced from [73]. CCBY4.0. (h) Schematic diagram of a device and experimental set up for the excitation of SWs by voltage-controlled magnetic anisotropy (VCMA) and detection by optical means. Reprinted from [74], with the permission of AIP Publishing. (i) The schematic diagram shows the excitation of SWs by magneto-electric cell (ME cell).

the SW modes and excite propagating SWs. In some cases, arrays of nanomagnets and thin films are directly deposited on a wide metal strip line for exciting magnetization dynamics (figure 1(c)) [68]. The FMR technique is a robust method to characterize the dynamic properties of nanostructured magnetic materials [69]. Here, magnetic materials are placed inside a microwave cavity having a single resonant frequency with high quality (Q)-factor. When the applied bias magnetic field satisfies the resonant condition, the FMR of the magnetic materials under study is excited, and the absorption of microwave power in the cavity reaches a peak. The absorption is measured as a function of the bias magnetic field and typically exhibits a Lorentzian line shape, from whose linewidth, one can obtain information about the damping or loss in the magnetic material [70].

Dynamical properties of magnetic materials are often measured with a pulsed inductive microwave magnetometer (PIMM), which utilizes CPW as a source of fast magnetic field pulses provided by a pulse generator, and also an inductive flux sensor which can measure the fast pulse data using a digital sampling oscilloscope (figure 1(d)) [69, 75]. Oersted fields are not suitable for nanostructured devices owing to their spatially non-localized nature which precludes addressing individual devices. However, there are some

special techniques, which enable spatially uniform global microwave Oersted fields to excite shorter wavelength SWs which are more compatible with nanomagnets. For instance, naturally or artificially created magnetic nonuniformities on a thin film can be employed to excite short wavelength SWs. The FMR of a magnetic nanorod placed on top of a magnetic thin film can create localized dynamic dipolar field which can also be employed to excite short wavelength SWs. [76]. Furthermore, short wavelength SWs can be excited from the smooth interfaces between two magnetic films [77]. Spin current induced torques (spin transfer torque (STT)/spinorbit torque (SOT)) are another potential method for exciting magnetization dynamics in nanostructured magnetic elements [71]. For exciting FMR using STT, one patterns the magnetic material into sub-micrometre sized elements, or injects the spin current from a sub-micrometre sized nanocontact. By changing the sample geometry, it is also possible to create pure spin current and excite FMR in magnetic thin films by SOT (figure 1(f)) [72]. The key advantages of exciting FMR with STT and SOT are that local excitations are possible and the excited FMR can also be amplified [78]. However, all the above-mentioned charge current induced methods dissipate considerable amount of power owing to inherent Joule heating. Irradiation with a femtosecond pulsed laser beam is yet another efficient way for exciting FMR and coherent SWs in nanomagnets (figure 1(g)) [73, 79].

Femtosecond laser pulses can generate coherent SWs in magnetic thin films in an efficient manner after partially or fully demagnetizing the magnetic materials within sub-picosecond time scales [73]. The key advantages of this method are the local nature of the excitation technique and the ability to choose the propagation direction of excited SWs by shaping the laser pulse. Owing to ever-present thermal agitation, the spins in magnetic materials always oscillate in an incoherent manner, which excites very low intensity SWs even in the absence of other external perturbations [80]. The periodic heating and cooling by a laser can thermally excite SWs which are studied for characterizing various dynamical parameters [48]. This method obviates the need for complex device fabrication.

The voltage-controlled magnetic anisotropy (VCMA), originated from electric field induced modification of electron population at the Fermi level of 3d bands in FMs, is an emerging technique for exciting picosecond magnetization dynamics of magnetic thin films and nanostructures. Nozaki et al [81] and Zhu et al [82] demonstrated that FMR can be excited by VCMA in magnetic nanostructures with submicrometer dimensions accompanied by ultralow power consumption which can be more than two orders of magnitude lower than that in current induced STT excitation. VCMA is also suitable for the excitation of coherent propagating SWs in FM thin films (figure 1(h)) [74]. A practical SW device can be fabricated by placing a metal gate electrode on top of an oxide layer deposited on top of the FM layer, i.e. a waveguide (WG). An alternating voltage of microwave frequency is applied at the gate electrode to launch a microwave electric field into the oxide layer. The microwave periodically modulates the perpendicular magnetic anisotropy (PMA) of the FM layer underneath the gate electrode via the VCMA effect. At the resonance frequency, coherent SWs are excited and propagate along the WG.

Use of a magneto-electric cell (ME cell) [83] is another approach for exciting magnetization dynamics with an electric field. As shown in figure 1(i), a FM SW bus (NiFe) has a magnetostrictive layer made of embedded (Ni), which, in turn, has a piezoelectric layer (PE) on top. The periodic deformation created in the piezoelectric layer by applying an RF voltage across the top gate electrode is then transferred to the Ni layer. This results in a perturbation of the magnetization of the Ni layer, and consequent creation of SWs at the resonance condition [84].

It is also possible to excite magnetization dynamics in nanomagnets indirectly. When nanomagnets are placed sufficiently close to each other, they are coupled via magnetostatic interactions which can transfer magnetization dynamics induced in one nanomagnet to the next, and so on. When a spin-torque nano-oscillator (STNO) is delineated over a small portion of an extended thin film, the oscillatory motion of the nano-oscillators can emit SWs in the FM film [85]. Likewise, oscillatory motion of magnetic vortices can also emit SWs into an adjacent magnetic channel [86].

## 2.2. Experimental techniques for detecting magnetization dynamics

There are numerous methods for detecting magnetization dynamics occurring in nanomagnets. Whenever the dynamics is excited with microwave excitation involving CPW and microstrip lines, the resonance signals are typically measured by inductive coupling using CPWs in the manner of antennas [87]. In magnetic heterostructures, the magnetization dynamics of magnetic layers are detected via spin pumping and the inverse spin Hall effect (ISHE) or the inverse Edelstein effect in the form of a dc voltage. Homodyne detection is another sensitive technique for detecting resonance signals from sub-hundred nanometer magnetic elements with subnanometer thickness. In this case, the probed magnetic layer is fashioned into the free layer of a magnetic tunnel junction (MTJ). The time varying MTJ resistance due to the oscillation of the soft layer's magnetization is mixed with the time varying current through the junction, resulting in a rectified dc voltage. In STT or SOT induced FMR, the resonance signals are also detected via a dc voltage. In this case anisotropic magnetoresistance due to the oscillation of magnetization is mixed with the RF current passing through the magnetic layer giving rise to a finite dc voltage. Recently, inverse VCMA has been reported as another interesting technique for detecting resonance signals [88]. The anomalous Hall effect is another technique to detect FMR signals.

Optical techniques are ideal for the detection of FMR signals locally in a non-invasive way. Time-resolved magneto-optical Kerr effect (TR-MOKE) is one of the most sensitive and widely used optical techniques for locally detecting dynamic magnetic signals from various types of magnetic nanostructures [12]. In Brillouin light scattering (BLS) spectroscopy, the inelastic scattering of photons from the magnons (quanta of SWs) is utilized for detecting SW signals [89]. The single NV centers in diamond is a phasesensitive technique which can locally probe SWs in a very efficient manner [90]. However, practical application of this sensitive probing technique would be quite challenging as the FM films are required to be deposited on a diamond film containing NV centers, which may significantly increase the complexity of the device fabrication process. In ME cells, the inverse of the above discussed process is used for detecting SW signals. Some of the non-conventional methods for detecting FMR signals are magnetic resonance force microscopy (MRFM) [91], magnon-induced heat [92], nuclear resonant scattering [93], and time resolved x-ray magnetic circular dichroism [94].

#### 3. SWs in confined magnetic media

Investigation of magnetization dynamics in patterned microstructures providing spatial confinement to the SWs started in the late 1990s. In a seminal work, Heibert *et al* reported the investigation and imaging of magnetization precession and relaxation dynamics in an 8  $\mu$ m wide Py disk [11]. The Py disk was delineated at the centre of a lithographically

patterned gold coil which was connected with a biased photoconductive switch made of GaAs. The photoconductive switch was triggered by a pulsed laser of 2 ps pulse-width to produce a pulsed magnetic field along the out-of-plane direction to the Py disk under the application of in-plane bias magnetic field. The time-varying precessional oscillation was measured with a time-resolved scanning Kerr effect microscope (TRSKEM) having 0.7  $\mu$ m spatial resolution. The biasfield dependence of precession frequency was fitted using the Kittel formula to extract various magnetic parameters, including a damping constant of 0.008 for Pv. The space-time evolution of magnetization was imaged by fixing the time delay and then scanning the disk under a focused probe laser spot. This yields a non-uniform spatial distribution, indicating the presence of modal frequencies in this confined structure. In another interesting work, Jorzick et al used BLS spectroscopy to measure the SW spectra in rectangular elements having lateral dimensions of  $1 \times (1-2) \mu m^2$  and stripes with 1  $\mu$ m × 90  $\mu$ m area [95]. Thermal magnons were measured in the backscattered geometry. The spectra revealed a number of eigenmodes in the system consisting of Damon-Eshbach (DE), backward volume (BV) and perpendicular standing SW (PSSW) geometry. In particular, they observed the existence of a new, spatially localized SW mode of exchange nature in these elements with the localization caused by the inhomogeneity of the internal field. In 2003, Barman et al used TRSKEM to study the precessional magnetization dynamics of a  $10 \times 10 \ \mu \text{m}^2$  square permalloy (Ni<sub>81</sub>Fe<sub>19</sub>) element [96]. Time-resolved Kerr rotation signal measured from the center of the element revealed the presence of a fourfold anisotropy in the precession frequency due to the internal field generated by the nonuniform static magnetization. The damping was much larger when the static magnetic field was applied along the diagonals of the square element. The dynamic images revealed this to be associated with spatial nonuniformity at the centre of the element. Initially, the dynamic magnetization was found to be nonuniform at the edges of the element, slowly extending towards the centre [97]. These authors thoroughly investigated the dephasing of SW modes by extensive imaging of the dynamic magnetization through the measurement of Kerr rotation signals from various positions from the element, combined with micromagnetic simulations, which revealed various dynamic modes. The number of antinodes in modal oscillation extracted from dynamic images was found to be larger along the diagonal than along the edge of the square causing the observed increase in damping due to dephasing of modes (figure 2) [98]. These authors later systematically studied the anisotropy in the apparent damping in samples with varying shape [99] and aspect (width/thickness) ratio and found it to become stronger with decreasing aspect ratio [100]. Extensive micromagnetic simulation study revealed the spatial profile of each resonant mode, which showed a uniform centre mode, localized edge modes (EMs), and other localized modes with nodal planes oriented perpendicular to the bias magnetic field [101]. Belov et al studied modal oscillations in a 4  $\mu$ m Ni<sub>80</sub>Fe<sub>20</sub> element with a central pinhole to show that the spatial pattern of the magnetization oscillation response depends sensitively on weaker variations of the static magnetization. They also observed a spatially nonuniform damping in this sample as a result of conversion of energy into shorter wavelength modes in the vicinity of the domain boundaries [102].

Barman *et al* also studied coherent suppression of precessional dynamics in circular shaped Ni<sub>81</sub>Fe<sub>19</sub> microdots with varying aspect ratio with a shaped magnetic field pulse. To achieve coherent suppression, the static magnetic field was adjusted in such a way that the effective torque acting upon the magnetization vanishes after one cycle of precession. Interestingly, the coherent suppression was found to be more spatially nonuniform in samples with smaller aspect ratio owing to the dephasing of multiple SW modes as confirmed from the measured time-resolved Kerr images and micromagnetic simulations [103]. With continuing advancement of nanofabrication capabilities, the focus in this field gradually shifted to studying the dynamics of single and arrays of nanomagnets as described in the following section.

#### 3.1. SWs in single nanomagnets

Investigation of the intrinsic dynamics of single nanomagnet in the deep nanoscale regime and at extremely fast timescale is of pure fundamental interest. The spatial confinement should suppress domain formation in the nanoscale in accordance with Brown's fundamental theorem. An individual nanomagnet is expected to behave like a macrospin comprising of a large number of isotropic spins aligned together. However, apart from strain and magnetocrystalline anisotropies, nanomagnets with non-ellipsoidal shapes often exhibit shape anisotropy arising from geometric configuration. Furthermore, the magnetic configuration may vary depending upon the orientation of an applied magnetic field with respect to the anisotropy field. Size reduction from micrometer to nanometer scale results in transitions between various magnetic microstates, namely multidomain, magnetic vortex, quasi-single domain and single domain state. Consequently, the magnetization dynamics show a variety of behaviour, such as domain wall oscillation, vortex core gyration, radial and azimuthal modes of SWs, confined, localized and standing SW modes etc.

Despite the experimental studies of SW spectra in arrays of submicron magnetic structures in early 2000 using FMR [104] and BLS [105] techniques, the investigation of intrinsic magnetization dynamics of isolated nanomagnets was missing. In 2003, Kiselev et al addressed an outstanding question of the type of magnetic motions that can be generated by STT. By performing electrical measurement on a magneticmultilayer nanopillar structure of  $130 \, \text{nm} \times 70 \, \text{nm}$  lateral dimensions (80 nm Cu/40 nm Co/10 nm Cu/3 nm Co/2 nm Cu/ 30 nm Pt fabricated on an oxidized silicon wafer), they showed that the nanopillar can act like a nanoscale motor which converts energy from a dc electrical current source into a high-frequency magnetic oscillator. The oscillator may serve as a microwave source whose operational frequency can even be tuned over a wide frequency range by the current and the magnetic field [106]. In 2004, Demidov et al performed



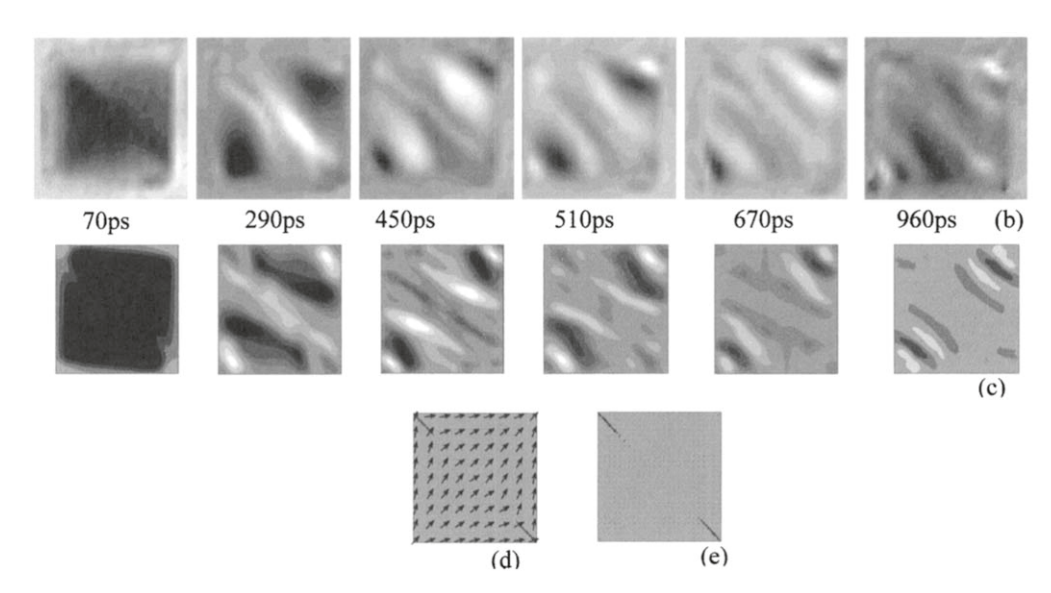


**Figure 2.** (a) The geometry of the experiment is illustrated for the measurement of dynamic images of magnetization (b). The simulated dynamic images are shown in (c). The simulated static magnetization configuration (d) and corresponding total internal magnetic field (e) are shown. The grey color scale in all the images represents the out-of-plane components of the magnetization (static and dynamic) and the internal field. Reprinted (figure) with permission from [98], Copyright (2004) by the American Physical Society.

micro-focused BLS measurement to demonstrate the radiation of SWs from a sub-micrometer sized Py element into the surrounding CoFe microstructure [35]. They showed that the radiation occurs at two discrete frequencies (around 10-12 GHz) which are basically the frequencies of the quantized SW modes of the magnetic element. This means when a sub-micrometer sized magnetic element is deposited on top of another micrometer sized magnetic element with a copper layer sandwiched in between, it can be used as a source of microwave radiation. Koch et al investigated timeresolved STT induced magnetization reversal in nanosecond timescale in a spin-valve nanomagnetic junctions subjected to a pulsed bias current with current-perpendicular-to-plane geometry [107]. In another important work, Krivorotov et al in 2005, investigated STT driven time-resolved magnetization dynamics of a Cu/IrMn/Py/Cu/Py/Cu nanopillar system of  $130 \,\mathrm{nm} \times 60 \,\mathrm{nm}$  lateral dimensions [108]. Their experimental results were in excellent agreement with the predictions of the Slonczewski spin-torque model [109], i.e. STT reduces the effective magnetic damping for applied charge currents less than a critical current. At higher currents, STT was able to drive phase-coherent precessional dynamics. It could drive precessional switching with switching times less than 1 ns having narrow statistical distributions, which is a very exciting result for magnetic-memory applications. Later, in 2006, x-ray microscopy technique was used to image the switching process of magnetization in a spin transfer structure [110]. Switching was found to occur by lateral motion of a magnetic vortex across a nanoscale element instead of coherent magnetization reversal.

Optical detection of time-domain magnetization dynamics in single nanomagnets with dimensions well below the diffraction limit inspired the application of the cavityenhanced MOKE (CEMOKE) technique. The ps magnetization dynamics of individual Ni nanomagnets with different sizes was reported by Barman et al in 2006 by exploiting time-resolved CEMOKE [12]. They observed a sharp and non-monotonic variation in the precession frequency from sub-GHz to few GHz range as the magnetic microstates of cylindrical magnets underwent a transition from multidomainto single-domain state (figure 3). Interestingly, the damping associated with the coherent precessional mode of these cylindrical nanomagnets decreased rapidly with decreasing diameter to finally settle down to its intrinsic value in the single domain regime. The bias field dependence of the precessional frequency confirmed the presence of an extrinsic contribution to damping in these micrometer sized magnets [101]. Around the same time, Laraoui et al reported ultrafast laser-induced spin dynamics, including demagnetization, precession [13] and relaxation [111] of CoPt<sub>3</sub> single dots with sub-micrometer dimensions using an all-optical TR-MOKE set up having high spatio-temporal resolution achieved by using a reflective confocal Kerr microscope. An initial fast relaxation time of few ps was observed owing to the energy exchange of electrons and spins with the lattice, followed by a slow relaxation time of hundreds of ps originating from the energy exchange of electrons and lattice with the environment. Liu et al investigated the time-resolved magnetization dynamics of single 160 nm wide Py disks in 2008 using timeresolved Kerr microscopy. A distinct hysteresis of the

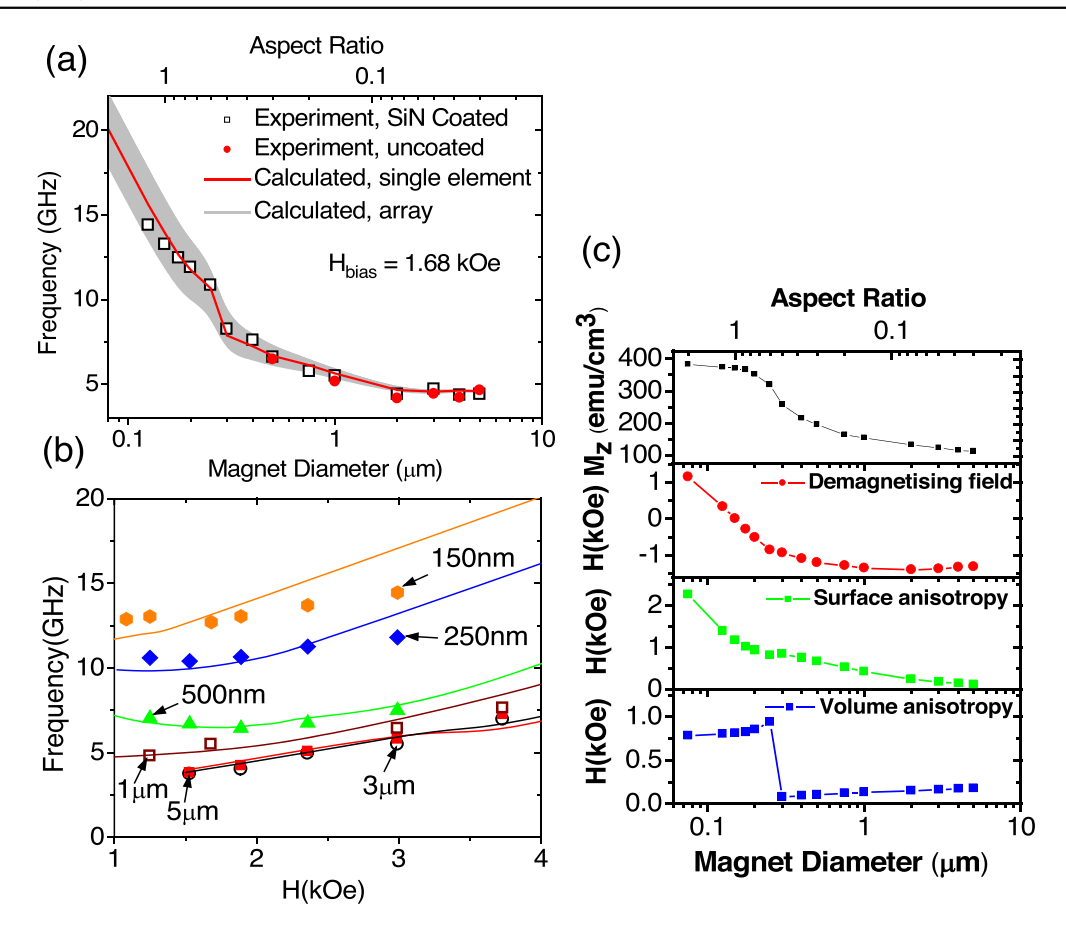


Figure 3. Theoretical modelling of the bias magnetic field and diameter dependence of experimentally measured precession frequencies. (a) The uniform precession mode frequencies measured from uncoated and 70 nm thick SiN-coated magnets are plotted as a function of magnet diameter and aspect ratio at  $H_{\text{bias}} = 1.68$  kOe. The calculated precession frequencies of single magnets are represented by solid line and the possible range of precession frequencies in arrays of magnets separated by 56 nm are shown by the grey shaded region. (b) Experimental (solid points) and calculated (curves) precession frequencies are plotted as a function of bias magnetic field ( $H_{\text{bias}}$ ). (c) The out-of-plane magnetization component ( $M_z$ ) and the contributions from various magnetic field terms are plotted as a function of magnet diameter and aspect ratio. Reprinted with permission from [12]. Copyright © 2006, American Chemical Society.

fundamental mode frequency was observed as a function of the in-plane bias field owing to the evolution of the internal spin configuration from vortex to quasi-single domain states. The critical fields to trigger the vortex nucleation and annihilation processes were determined in this study [112]. In 2011, remarkable advances in studying single nanomagnet dynamics were reported, when Rana et al investigated the time-resolved precessional magnetization dynamics of an isolated 50 nm wide square Py dot showing a dominant spin wave edge mode (EM) without the appearance of a center mode (CM) [14]. The characteristic dynamic frequency of a smaller dot is generally very different from that of a larger dot. This allows one to resolve the high-frequency dynamics of 150 nm sized single magnetic dots against the lower frequency background of larger nanomagnets by overcoming the optical diffraction limit as shown by Liu et al [113]. Naletov et al studied azimuthal and radial eigenmodes of Py/Cu/Py nanopillars with spin-valve like structures using MRFM. They established a rule for exciting selected resonant modes by adjusting the excitation geometry [114]. Interestingly, the EM in an individual nanomagnet can be suppressed by exciting larger amplitude coherent precession of the CM, as shown by Keatley *et al.* This study paved the way for the development of nanoscale STT oscillators and bi-stable switching devices where more uniform spin dynamics is desirable [115].

In a further study, pure spin current induced antidamping torque was found to set the magnetization precession into auto-oscillation mode by compensating for its intrinsic damping [85]. Investigations showed that spin current induced spin-orbit torque (SOT), generated by passing a charge current through a heavy metal layer adjacent to a nanomagnet, can switch the magnetization of the nanomagnet in a deterministic way. This can be utilized to develop nanomagnetic logic and field-free clocking analogous to current CMOS technology [116]. Hybrid magnonics arising from strong coupling of magnon with phonon, photon or other magnons has emerged as an interesting topic for quantum transduction. One of the important developments in this direction was the direct observation of strong magnonphonon coupling (MPC) in a single nanomagnet by varying the direction of the applied magnetic field [117]. Surface acoustic wave (phonon)-induced switching of magnetization in dipole-coupled nanomagnets also established a successful

Boolean operation recently [118]. More recently, hybrid magneto-dynamical modes was observed in single magnetostrictive Co quasi-elliptical dots deposited on a piezoelectric substrate using TR-MOKE microscope as described in detail in section 8.7.4 [119] of part I.

#### 3.2. SWs in 1D arrays of nanomagnets

The study of picosecond magnetization dynamics in periodic arrays of nanomagnets is motivated by many potential applications. Such arrays may be thought of as artificial 'crystals', known as magnonic crystals (MCs), in analogy with a material crystal that provides a periodic potential landscape for an electron wave or a photonic crystal that provides a periodic refractive index landscape for an electromagnetic wave. Just as there are electronic band structures in a material crystal and photonic band structures in a photonic crystal, there are magnonic band structures in an MC, which can be tailored by choosing the pitch (or periodicity) of the array, as well as the shapes and materials of the nanomagnets. The study and control of magnonic band configurations in nanomagnet arrays is very important for developing various types of magnonic devices such as microwave filters, attenuators, sensors, transistors, logic gates and so on. The dynamic behaviour of a single nanomagnet depends upon the ground state of magnetization, which, in turn, is determined by the shape, size, material parameters, strength and orientation of any external magnetic field, strain, etc. Interestingly, the dynamic behaviour of nanomagnet arrays is discernibly different from that of the individual nanomagnets making up the array owing to the magnetostatic interaction among the nanomagnets. The latter, again, depends upon the shape, size, material parameters and interelement separation, as well as the orientation and strength of any external magnetic field. Magnonic bands can be engineered by manipulating these parameters. In this topical review, we will restrict our discussion only to arrays of magnetic stripes and dots. Discussion of other shapes can be found in [120].

Gubbiotti et al experimentally investigated collective magnetization dynamics in 1D periodic arrays of Py nanowires of width 175 nm and pitch 35 and 175 nm. For closely spaced nanowires, the strong dipolar coupling among the magnetic stripes led to the formation of collective modes in which the lowest frequency modes were found to be dispersive (i.e. the SW frequency depended on the wavevector). This indicated that the SWs had a non-zero group velocity because the dipolar coupling allowed the SWs to travel through the array. For nanowires spaced farther apart, the SW modes were found to be dispersionless owing to absence of dipolar coupling among the stripes [15]. In this case, the group velocity was zero indicating that the weak dipolar coupling does not allow a SW to travel though the array (from one nanomagnet to the next). In ensuing studies, they investigated the collective magnetization switching behaviour and collective SW modes in 1D arrays of nanowires of alternating width [16, 121]. The switching mechanism was observed to be very sensitive to the thickness to width ratio of the nanowires. A number of collective and dispersive SW modes were observed whose frequency periodically oscillated with respect to the wavevector encompassing several Brillouin zones, induced by the artificial periodicity of the array. The amplitude of oscillation was larger for the low-frequency mode and smaller for the high frequency modes. Interestingly, each mode existed in a range of frequency separated from the neighboring mode by a prohibited frequency zone, reminiscent of 'bands' and 'bandgaps' [16]. Notably, neighboring nanomagnets could be coerced into either parallel or antiparallel magnetizations by varying a bias magnetic field. The magnonic bands for 'parallel' ground state were markedly different from those of the 'antiparallel' state [122].

Topp et al utilized microwave assisted switching and minor-loop measurement to prepare various ground states of magnetization such as ferromagnetic state, multidomain state and antiferromagnetic states in periodically arranged magnetic nanowires [123]. They investigated collective SW modes in various ground states of magnetization and observed that the SW dispersion character can be substantially tuned by this method of arranging nanomagnets into 1D arrays. Kostylev et al showed that in these types of 1D arrays, the frequency gaps or band gaps are partial, i.e. the stop bands for SW propagation along the major axis of nanowires overlap with the passbands for SW propagation perpendicular to it [124]. However, this feature can be suppressed by using 2D arrays of nanomagnets. Wang et al investigated magnonic band structures in 1D MCs formed by magnetic nanostripes made of alternating materials: namely cobalt and Py. A number of dispersive SW modes separated by magnetic-field-tunable band gaps was observed [125]. Interestingly, an increase in bandgap was observed with the increase of cobalt stripe width, whereas it decreases with the increase of Py stripe width (figure 4) [126]. The center frequency bandgap is more sensitive to the stripe width of Py than that of cobalt. The reason behind this is the variation of effective saturation magnetization and exchange length which increases with the increase of cobalt width but decreases with the increase of Py width. Gubbiotti et al investigated collective SWs in another type of 1D MCs where each stripe is made of two magnetic layers either with the same (rectangular cross section) or with different width (L-shaped cross section) [127]. For the rectangular cross section, the lowest frequency fundamental mode originates from the in-phase precession of the magnetization in the two layers, whereas the higher frequency mode is spawned by the out-of-phase precession of the magnetization in the two layers. In the case of L-shaped cross-section, two dispersive SW modes with a sizable magnonic band width were observed. One of the modes was the fundamental mode in the thick segment and another was the fundamental mode in the thin segment of each nanowire. Moreover, by carefully tuning the overlayer thickness, the mode frequencies and their spatial profiles could be significantly tuned [128].

In a very recent study, it has been demonstrated that if the coupling between the magnetic layers in a multilayered ferromagnetic structure can be changed from exchange to dipolar by inserting a thin metallic layer between consecutive layers and systematically varying its thickness, then the

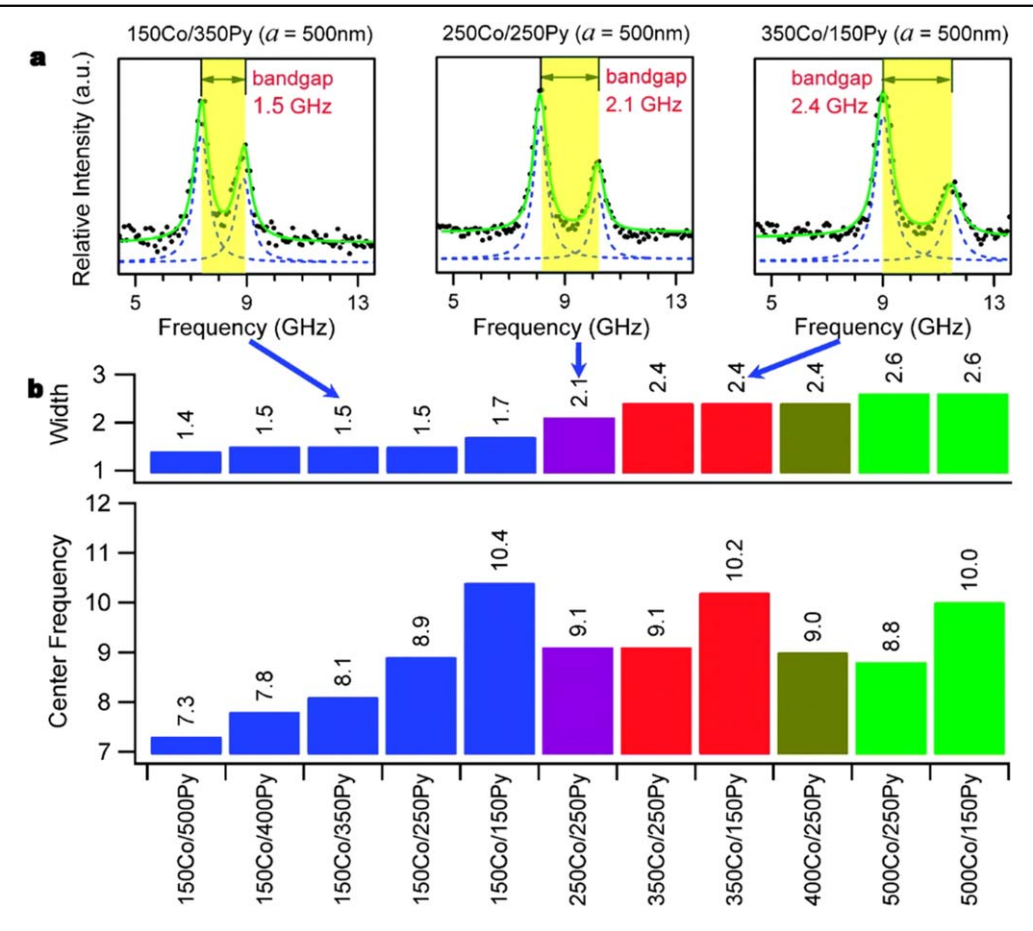


Figure 4. (a) BLS spectra recorded from 150 nmCo/350 nmPy, 250 nmCo/250 nmPy and 350 nmCo/150 nmPy samples at the first Brillouin zone boundary  $q = \pi/a$  (where lattice constant a = 500 nm). (b) The first bandgap widths and center frequencies (in GHz), measured from 11 MCs studied, are plotted. Reprinted with permission from [126]. Copyright © 2010, American Chemical Society.

collective magnetization dynamics can be significantly modified [129]. In fact, it is possible to stabilize the magnetizations of two neighbouring layers either in the parallel or in the antiparallel configuration. Several modes can be excited depending upon the static magnetization configuration as well as the relative phase (in-phase or out-of-phase) of dynamic magnetizations between the two layers within the same nanowire. Saha et al investigated collective SW dynamics of 1D arrays of magnetic nanostripes with varying width down to 50 nm [17]. For the narrowest stripe with 50 nm width, the inter-stripe magnetostatic interaction became negligible, which enabled the detection of magnetization dynamics of a single stripe. When a magnetic field was applied along the long axes of the nanostripes, the 50 nm wide stripes showed a uniform mode and a pure BV-like standing SW mode, whereas the wider stripes showed a uniform mode, a combination of BV- and DE-like standing SW mode, and a pure BV-like standing SW mode. However, the collective mode frequencies and their spatial profiles changed significantly when the bias magnetic field was rotated along the width of the nanostripes.

Another interesting type of 1D MC is periodically arranged corrugated magnetic stripes [18]. The advantage of these types of MC is that the SW frequencies and corresponding band gaps can be significantly tuned just by rotating

the in-plane bias magnetic field which essentially modifies the internal magnetization configuration. It was found that the EMs are more sensitive to the degree of corrugation than the CMs.

#### 3.3. SWs in 2D arrays of nanomagnets

The study of SW dynamics in 2D periodic arrays of nanomagnets begun with theoretical investigations of the effect of inter-dot dipolar coupling on the dynamical behaviour in different array geometries and under different magnetic field orientations [130, 131]. Soon thereafter, it was experimentally demonstrated that a single SW mode, observed in an unpatterned magnetic thin film, is split into a number of modes when the film is patterned into a 2D array of square magnetic dots, because of the presence of a demagnetization area inside each dot [132]. Notably, it was observed that the mode frequencies strongly depend on the interdot separation and orientation of the external magnetic field [104].

A flurry of experimental investigations followed the early work, which demonstrated the presence of multiple SW modes in magnetic nanodots with uniform and nonuniform ground states of magnetization [105, 133, 134]. It was observed that the magnetization dynamics became more nonuniform with reduction in the dot diameter (in the submicrometer size scale) owing to nonuniform ground state of

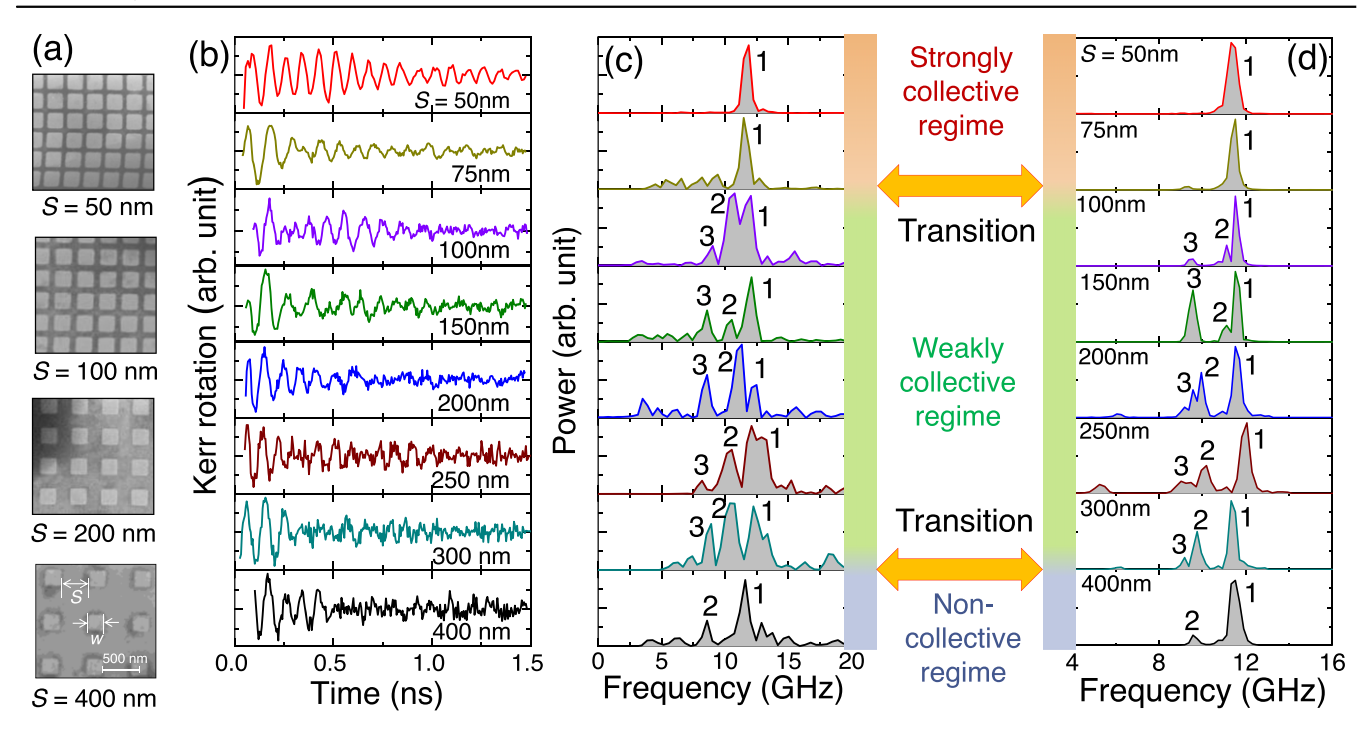


Figure 5. (a) Scanning electron micrographs of the arrays of 200 nm wide (W), 20 nm thick permalloy dots with varying interdot separation (S). (b) Experimental time-resolved Kerr rotations and (c) corresponding fast Fourier transform (FFT) spectra are plotted for the permalloy square dot arrays. (c) FFT spectra of simulated time-varying magnetization data obtained from  $7 \times 7$  array of permalloy dots with same specifications as in the experiment. Reproduced from [144]. © IOP Publishing Ltd. All rights reserved.

magnetization [135, 136]. Interestingly, low frequency SW modes were found to originate from the demagnetized edges of the magnetic dots and became more prominent with reduction of dot size. The resonance linewidth associated with the EM is generally higher than that of the CM since the EM is highly sensitive to imperfections and variations in the shape and size of the dots [19]. The dynamic modes in arrays of magnetic dots also show anisotropic behavior in their characteristic frequency as one varies the applied magnetic field orientation. This behaviour stems from the combined effect of static and dynamic effective magnetic fields inside the magnetic dots [20, 137–139]. The number of symmetries in the anisotropy is determined by the shape of individual dots and the symmetry of their lattice arrangement [20, 139–141]. The collective magnetization dynamics were extensively studied for various shapes of the magnetic dots [38, 142, 143] such as square [14, 138, 144], circular [139, 140, 145, 146], triangular [147], rectangular, elliptical, diamond, stadium [148], cross [20, 149–151] etc and were found to be significantly affected by the shape of the individual dots. In 2010 Kryuglyak et al first imaged collective modes of magnetization dynamics in 2D arrays of magnetic dots with timeresolved scanning Kerr microscopy [148]. It was observed that the SWs were confined within the whole array as if the latter behaved like a single element made of a continuous material. Micromagnetic simulations have been widely used to analyze the nature of the collective magnetization dynamics of magnetic dot arrays. These simulations revealed that various types of modes appear because of the collective oscillations of different groups of dots in an array with

well-defined phase relationships which are determined by the structure and the geometry of the array and its constituent nanoelements [20, 21, 38, 79, 138–140, 142, 143, 146, 150]. Rana et al studied magnetization dynamics of 2D arrays of magnetic dots by systematically varying the interdot separation (figure 5(a)). A smooth transition from strongly collective magnetization dynamics to non-collective dynamics was observed with the increase in the interdot separation (figures 5(b)–(d)) [14, 144]. Surprisingly, strongly collective to non-collective transition was also observed just by varying the in-plane bias magnetic field orientation from  $0^{\circ}$  to  $45^{\circ}$ with respect to the symmetry axis of the dot array [138]. This is because the static and dynamic magnetostatic stray fields, which control the collective precessional dynamics, are also affected by the in-plane orientation of bias magnetic field. Arrays of magnetic dots, made of the same element but with different sizes, show very interesting collective dynamics. A significant variation in the number of dynamical modes, their profiles, and slopes of the magnonic bands are observed when the in-plane orientation of the bias magnetic field is varied [152–154]. In nanometer scale magnetic dots, defects in the form of edge roughness, local thickness variation, etc can generate new resonant modes and quench the existing modes in isolated as well as arrays of magnetic dots [155].

#### 3.4. SWs in connected nanomagnets

Connected nanomagnets have attracted interest over the last two decades because of their intrinsic large shape anisotropy which aids an efficient transfer of energy in space [18, 21, 156]. A MC is said to be a *connected dot* (CD) if all

the magnetic nanodots are physically connected. A CD system can display properties characteristic of dots and/or antidots (AD). Antidot arrays typically exhibit higher SW propagation velocity and hence longer propagation wavelength at a given frequency. However, the primary difference between a CD array and an AD array is that the latter generally does not have regular shaped connector channels. The CDs have rarely been studied in the context of magnonics. The 1D bicomponent magnonic CD system with uniform width has been studied both experimentally and theoretically [125, 157]. SW dynamics in 1D magnonic quasicrystals arranged in a Fibonacci sequence with Pv NWs of two different widths have been used to precisely tune SW spectra. This system shows a two-step hysteresis loop and its field dispersion shows two discontinuities at the transition points between ferromagnetic order and antiferromagnetic order. The observed properties of the Fibonacci structures are promising for applications in magnonic devices for data processing and wave-based computing [158].

More recently, an analytical model of a graded-index (GRID) 1D slab, with a finite spatial gradient of saturation magnetization or anisotropy, predicted phase coherent refraction of SW at desirable angles. The fundamental SW mode can be guided coherently in the GRID slab along a bend in a magnonic WG [159]. Subsequently, an alternative way was discovered where the 1D stripe or nanowire was replaced by a connected pseudo-1D MC with tilted rectangular and/or rounded rectangular shape [18, 21]. This system is capable of magnonic band structure reconfiguration via subtle tuning of the external magnetic field orientation. It has the potential for implementing logic gate functionality by virtue of the anisotropy in SW dispersion and bandgap. At the first Brillouin zone boundary, the magnonic bandgap can show an asymmetric dependence on the azimuthal angle of the bias magnetic field [160]. In another connected tilted rectangular nanodot system, the magnonic band structure and bandgap were observed to depend strongly on the magnetic history driven spin texture [21]. Depending upon the magnetic history, leaf-, S-, and shifted-core vortex states could be stabilized, which presented drastically different potential landscapes to the propagating SWs passing through the nanochannels (NCs) connecting the dots. More importantly, at the same bias field value, two different spin textures were obtained as a consequence of magnetic field-induced bifurcation giving rise to a reconfigurable magnonic band structure. In square nanodots connected by rectangular NCs, the SW modes are affected by magnetic coupling as well as by selective channeling of SW modes [161]. The selective channeling of SW modes through NCs may be utilized to develop an electronic demultiplexer [162]. On the other hand, artificial spin-ice structures formed of connected nanobars or nanoelements arranged in a square or honeycomb (Kagome) lattice are also interesting due to their metastable ground-state spin configuration. Because SWs are very sensitive to internal fields, SW dynamics can also be affected by the creation of monopole-anti-monopole pairs and Dirac strings in these systems [156, 163].

#### 3.5. Spin-wave dispersion in nanomagnet arrays

During the last two decades, the field of reconfigurable magnonics has increasingly focused on 1D and 2D MCs. including pseudo-1D MC [18, 125, 157, 164]. The SW dynamics in these systems can be efficiently reconfigured by tuning active parameters such as magnetic field strength and orientation, magnetic history, electric field, strain, spin texture, etc, as well as passive parameters such as size, shape, lattice constant, lattice symmetry, and constituent materials. SW dispersion is usually measured with BLS [165] and analytically investigated with the help of PWM [166], dynamical matrix method [167], micromagnetic simulation software such as OOMMF [168] and Mumax3 [169]. The magnetostatic SW dispersion relation is primarily governed by the long wavelength magneto-dipole interaction and the short wavelength exchange interaction. In the following subsection, we illustrate the PWM for calculation of SW dispersion in some model nanostructures.

3.5.1. Plane wave method (PWM). In this method, the Landau–Lifshitz (LL) equation is solved for a magnetic structure (MC in this case) using Bloch's theorem [166, 170] assuming 0 K temperature when no thermal noise is present. The temporal evolution of the magnetization vector (M(r,t)) in the structure is described by:

$$\frac{\partial \boldsymbol{M}(\boldsymbol{r},t)}{\partial t} = -\gamma \mu_0 \boldsymbol{M}(\boldsymbol{r},t) \times \boldsymbol{H}_{eff}(\boldsymbol{r},t). \tag{1}$$

Here,  $H_{eff}(\mathbf{r},t)$  is the effective magnetic field given by:

$$H_{eff}(r,t) = H + H_d + H_{ex}, \tag{2}$$

where  $\mathbfit{H}_{\mathrm{d}}$  is the total demagnetizing field that can be expressed as:

$$H_d = H_d(r) + h_d(r)e^{i2\pi\nu t}$$
(3)

The quantities  $H_d(r)$  and  $h_d$  are the static and the dynamic dipolar field components, and they satisfy the magnetostatic Maxwell's equations. The quantities H and  $H_{ex}$  are the applied magnetic field and the exchange field, respectively, where  $H_{ex} = (\nabla . l_{ex}^2(r) \nabla) m(r, t)$ ;  $l_{ex}(r) = \sqrt{\frac{2A(r)}{\mu_0 M_s^2(r)}}$  is the exchange length, and A(r) is the exchange stiffness constant. Under the linear approximation, the component of the magnetization vector  $(M_s(r))$  along the static magnetic field direction (i.e. along z-axis) can be considered to be independent of time, and its magnitude is much larger than that of the perpendicular component m(r, t), so that:

$$M(r, t) = M_s(r) + m(r, t).$$
 (4)

To obtain a solution of the LL equation, the Bloch's theorem with lattice constant a can be used, so that: m  $(r) = \sum_G m_k(G) e^{i(k+G) \cdot r}$ , where  $k = (k_x, k_z)$  is the wavevector in the first Brillouin zone (BZ), and  $G = (G_x, G_z) = \frac{2\pi}{a}(n_x, n_z)$  is the reciprocal lattice vector of the said periodic structure. Next, the Fourier transformations of  $M_s(r)$  and  $l_{ex}^2(r)$  are performed to find the relevant quantities in reciprocal

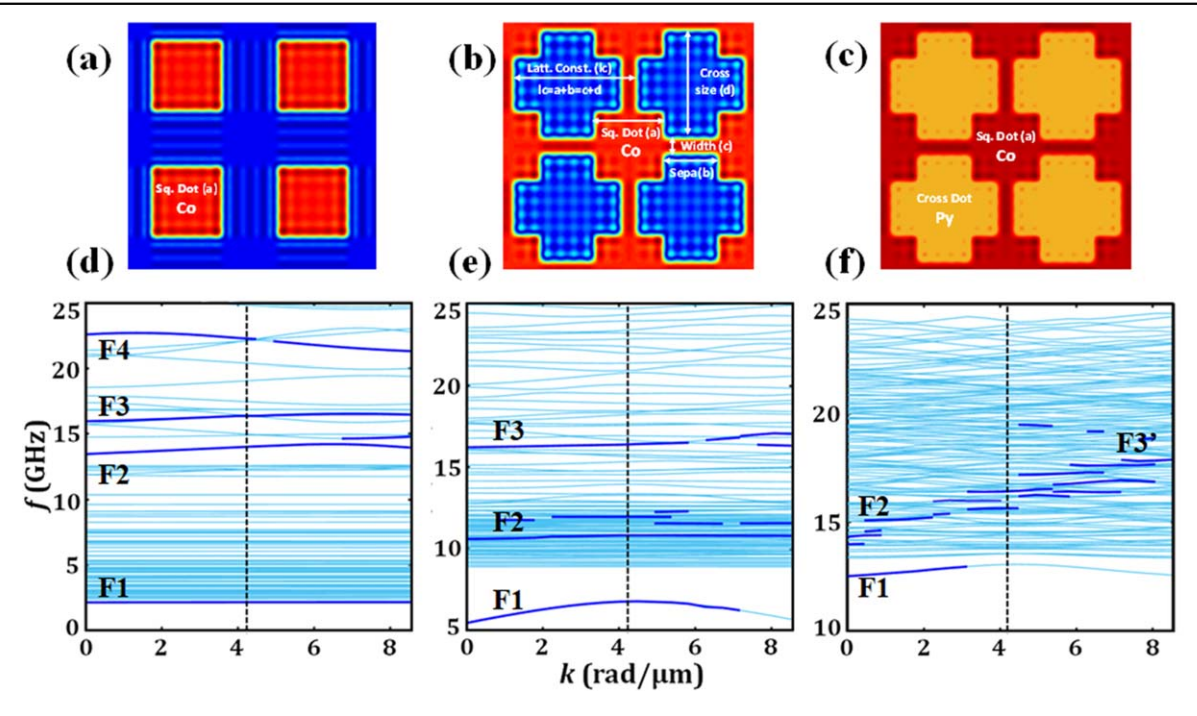


**Figure 6.** (a)–(c) represent the structure of three model 2D MCs, namely, square dot array, connected dot (CD) array and bi-component magnonic crystal (BMC). (d)–(f) Calculated magnonic band structures for the above three different MCs, i.e. square dot array, CD array and BMC, respectively.

space using:

$$M_s(\mathbf{r}) = \sum_G M_s(\mathbf{G}) e^{i\mathbf{G}.\mathbf{r}}$$
 (5)

$$l_{ex}^2(\mathbf{r}) = \sum_{G} l_{ex}^2(\mathbf{G}) e^{i\mathbf{G}.\mathbf{r}}.$$
 (6)

Here

$$M_{s}(G) = \begin{cases} M_{S,A}t + M_{S,B}(1-t) & G = 0\\ (M_{S,A} - M_{S,B})I(G) & G \neq 0 \end{cases}, \tag{7}$$

where, t is the filling fraction of magnetic material in the lattice and  $M_{S,A}$  and  $M_{S,B}$  are saturation magnetization of two magnetic materials A and B, respectively. Finally, I(G) is a function that is specific to the nanodot structure used in this calculation.

3.5.2. Calculation of spin-wave dispersion relation in 2D MCs. In the case of a 1D MC, there is only one symmetry axis with the corresponding lattice symmetry. However, in the cases of a 2D MC and a pseudo-one-dimensional MC, the lattice symmetry can be varied by arranging nanomagnets in different periodic patterns. The 2D MC category can be divided into three sub-categories: (a) physically isolated ferromagnetic dot lattice, (b) antidot lattice and (c) bicomponent MC. There are numerous reports of the study of 2D MC with varying magnetic properties and geometric architectures. Recently, ferromagnetic nano-cross structures have attracted interest owing to some remarkable properties, including magnonic mode softening, mode splitting and strong magnon-magnon coupling induced avoided crossing of SW branches in Ni<sub>80</sub>Fe<sub>20</sub> nano-cross arrays [151]. Hence, we

focus on arrays of nano-cross structures as a case study for the calculation of SW dispersion.

The parameters used in the above calculation are:  $M_{\rm s,Co}=1.15\times10^6\,{\rm A~m^{-1}},\,A_{\rm Co}=28.8~{\rm pJ~m^{-1}},\,M_{\rm s,Py}=0.78\times10^6\,{\rm A~m^{-1}}$  and  $A_{\rm Py}=13.0~{\rm pJ~m^{-1}}$  in the ferromagnetic regions, whereas very small  $M_s$  and A values were assumed for the nonmagnetic regions to avoid nonphysical SW frequencies. We have calculated SW dispersion in DE geometry for (a) square dot array, (b) CD structure, and (c) BMC structure for a fixed lattice constant of 700 nm and square dot width of 400 nm as shown in figures 6(a)–(c). The calculated dispersion of the Co dot array shows four SW modes, of which three modes F2, F3 and F4 are weakly dispersive in nature. To get deeper insight into the nature of these modes, we have calculated the spatial profiles of SW modes at  $k = 1.6 \,\mathrm{rad} \,\mu\mathrm{m}^{-1}$  as shown in figure 7. The nondispersive mode F1 has its power concentrated at the centre of the square dot. The modes F2 and F3, which show weakly positive dispersion, exhibit different spatial characters. The power of mode F2 is primarily concentrated at two horizontal edges of the dots (EM), while the F3 shows standing wave pattern in the DE geometry with quantization number m = 5 as shown in figure 7. The F4 mode is a negatively dispersive mode with standing wave character in the BV geometry with quantization number n = 3. In the CD array, we have considered Co square dots of size  $= 400 \, \text{nm}$ , lattice constant  $= 700 \, \text{nm}$  and connector dimensions (length  $\times$  width) of 300  $\times$  100 nm<sup>2</sup>. In this case, three modes are observed, out of which the mode F1 is weakly dispersive in nature and one band gap is opened at the 1st Brillouin zone (BZ), as shown in figure 6(e). This mode shows DE character with m = 4. The modes F2 and F3 are nondispersive in nature and the power of F2 is concentrated in the horizontal connector channel with m=2. The power in

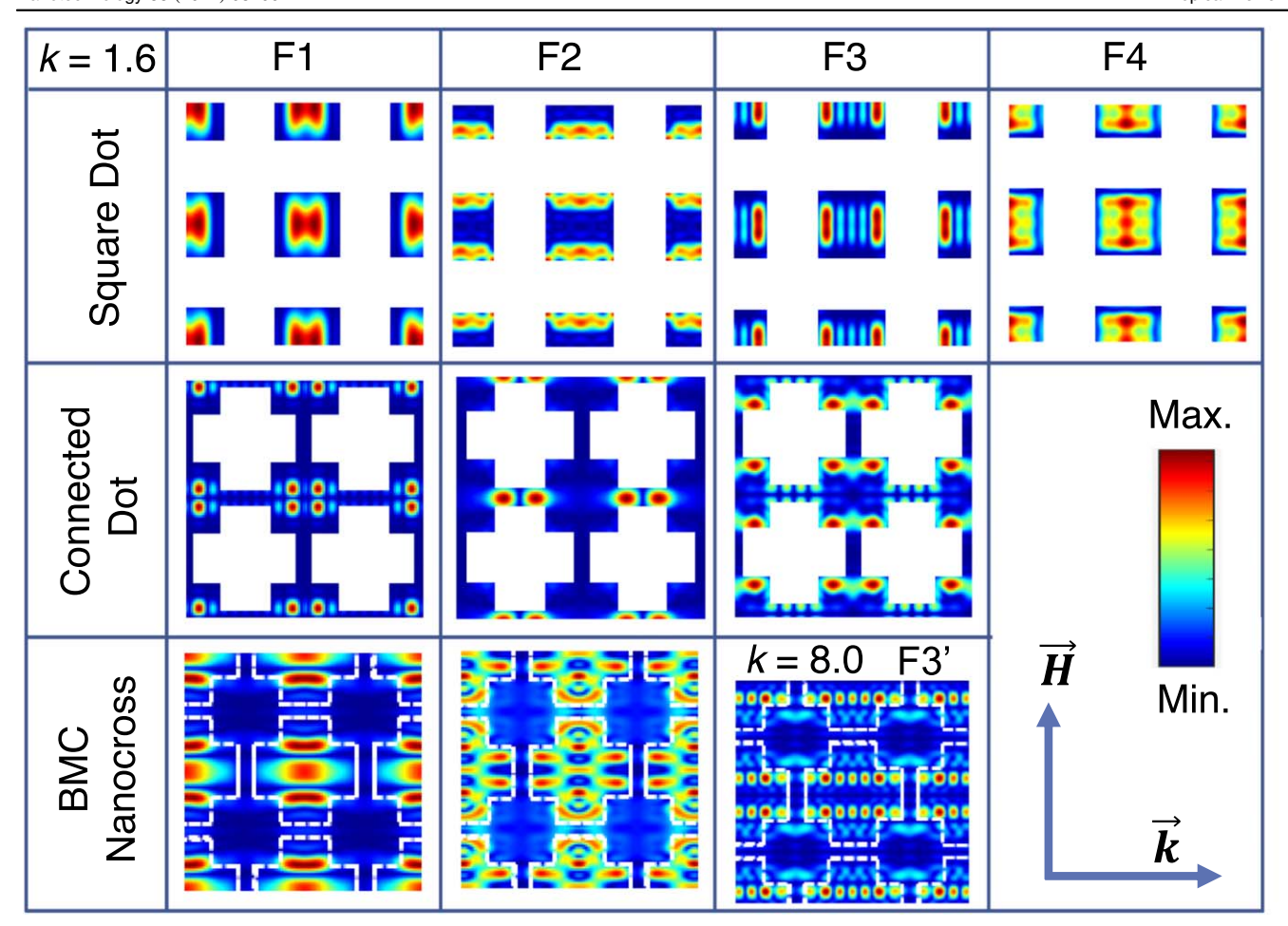


Figure 7. Spatial profiles of selected SW modes at k = 1.6 rad  $\mu m^{-1}$  for three different MCs, namely, square dot array, CD array and BMC.

mode F3 is mainly concentrated at the four corners of the square dot with quantization number (n, m) of (2, 2). The BMC structure is identical to the CD array except for the fact that the blank regions are now filled with Py. In this case, two dispersive modes are observed and an indirect type band gap is present between F1 and F2 modes, as shown in figure 6(f). Figure 7 shows that the two lower frequency dispersive modes F1 and F2 are located inside the Py regions with mode quantization numbers (n, m) being (3, 1) and (7, 3), respectively. A higher frequency dispersive mode F3' also appears with prominent intensity in the 2nd BZ, which again shows power in the Py region with mode quantization number (2, 7).

## 3.6. Effects of geometric parameters on SWs in nanomagnet arrays

Geometric parameters of magnetic dots such as shape, size, aspect ratio (thickness/diameter) and the arrangement of the dots in lattices, have significant impact on the isolated and collective magnetization dynamics of magnetic dots. These geometric parameters basically control the magnetostatic energy inside individual dots and the stray field distribution within the array. Therefore, controlling isolated and collective magnetization dynamics by varying the geometrical parameters have been thoroughly investigated over the last two

decades. Barman et al investigated the magnetization dynamics of isolated magnetic dots with sizes varying from  $5 \,\mu \text{m}$  down to 125 nm as described in section 3.1 [12]. A significant variation of the effective damping with the dot size was also observed [171]. Gubbiotti et al have shown that in 1D periodic arrays of magnetic stripes, the periodic variation of stripe width can be a very useful tool for producing rich magnonic spectra [16]. Later, Tacchi et al also reported that the magnetization ground state in a similar type of stripe array can be either tuned to the ferromagnetic or to the anti-ferromagnetic type of arrangement by judiciously choosing the applied magnetic field. The magnonic spectra can be drastically different in these two cases of magnetic ground states [122]. The precessional dynamics of magnetization in 2D arrays of magnetic dots made of two different dot sizes have also been studied [153, 154]. Effort has been made to prepare 1D nanomagnet array by step modulated thickness either made of a single material [172] or two different materials [128, 173]. In the latter case, the height of the top layer strongly affects the magnonic band structures. Saha et al have shown that the precessional magnetization dynamics in 1D arrays of stripes strongly depends on the width of the stripes as a result of the variation of interdot magnetostatic interactions. In the case of 2D arrays of magnetic dots, the magnetization dynamics become more nonuniform with the

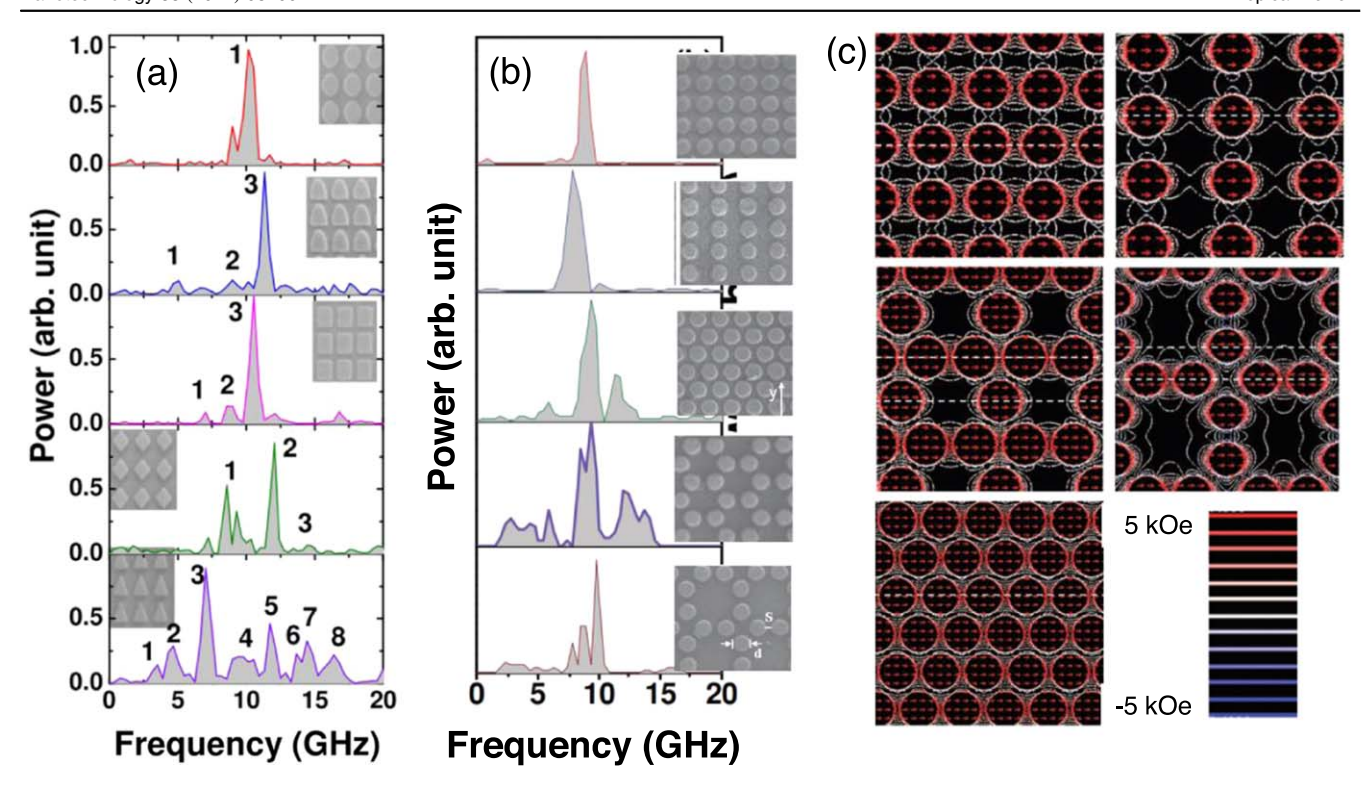


Figure 8. (a) Experimental SW spectra for arrays of  $Ni_{80}Fe_{20}$  (Py) nanodots with varying shapes as shown in the inset. Reprinted from [142], with the permission of AIP Publishing. (b) Experimental SW spectra for circular shaped Py nanodots arranged in varying lattices [139]. (c) Simulated magnetostatic field distributions for arrays of Py nanodots arranged in variable lattices at H = 1.3 kOe. The small arrows inside the dots denote the magnetization distribution within the dots and the colour bar given at the lower right corner of the figure represents the strengths of the stray magnetic fields. [139] John Wiley & Sons. Copyright © 2013 WILEY-VCH Verlag GmbH & Co. KGaA, Weinheim.

reduction of dot diameter [135, 136] and low frequency SW modes, originating from the demagnetized edges of the magnetic dots, become more prominent with the reduction of dot size. Zivieri *et al* [174] and Kostylev *et al* [175] investigated the magnetization dynamics in 1D arrays of rectangular magnonic dots arranged in various ways: such as along long axes, along short axes, in a non-collinear fashion, etc.

Mahato *et al* investigated collective magnetization dynamics of square arrays of magnetic dots made of different shapes [38, 142]. The dot shapes not only affect the dynamics of individual dots, but also significantly modify the collective dynamics of the array (figure 8(a)). The number of resonant modes and the configurational anisotropy strongly depend upon the shape of the dots [38, 142]. Saha *et al* have demonstrated that when circular magnetic dots are arranged in various lattice geometry the collective SW spectra is significantly modified with the variation of lattice arrangement (figure 8(b)) [139, 140]. This is solely due to the distribution of the magnetostatic stray field among the dots, which significantly varies with the lattice arrangement of the dots [139, 140] and also interdot separation [145, 176] (figure 8(c)).

#### 4. External control of nanomagnet dynamics

#### 4.1. Bias magnetic field control

The magnetization dynamics in nanomagnets is mainly decided by the internal magnetization configuration, which can be controlled by the strength and orientation of an external magnetic field. As a result, a bias magnetic field can significantly control the precessional magnetization dynamics of isolated nanomagnets. When the nanomagnets are arranged in a periodic manner, they are coupled via magnetostatic stray field if the interelement distance becomes comparable to the nanomagnet dimension. The magnetostatic coupling can suppress the dynamics of individual nanomagnets leading to the collective dynamics of the array. Therefore, the bias magnetic field strength and orientation can also affect the collective dynamics of the array. A number of reports are found in the literature about biasfield-dependent magnetization dynamics in single magnetic dot, as well as 1D arrays and 2D arrays of magnetic dots. Barman et al demonstrated that the precessional frequency of circular shaped single magnetic dots monotonically increases with increasing bias magnetic field, and the nature of the increment of precessional frequency is different for dots of different size owing to different ground states of magnetization [12]. The effective damping constant, on the other hand, either decreases or remains unchanged as the size of the dots is decreased [171]. Notably, in the case of circular dots, the precessional frequencies may also show an abrupt change due to the change in the magnetization state [112]. In isolated magnetic dots, two types of resonant modes are generally observed—one of which originates from the central part of the dot and other from the oscillation of magnetization taking place at the demagnetized edges perpendicular to the bias magnetic field direction. However, the EM can be suppressed by exciting large amplitude magnetization dynamics

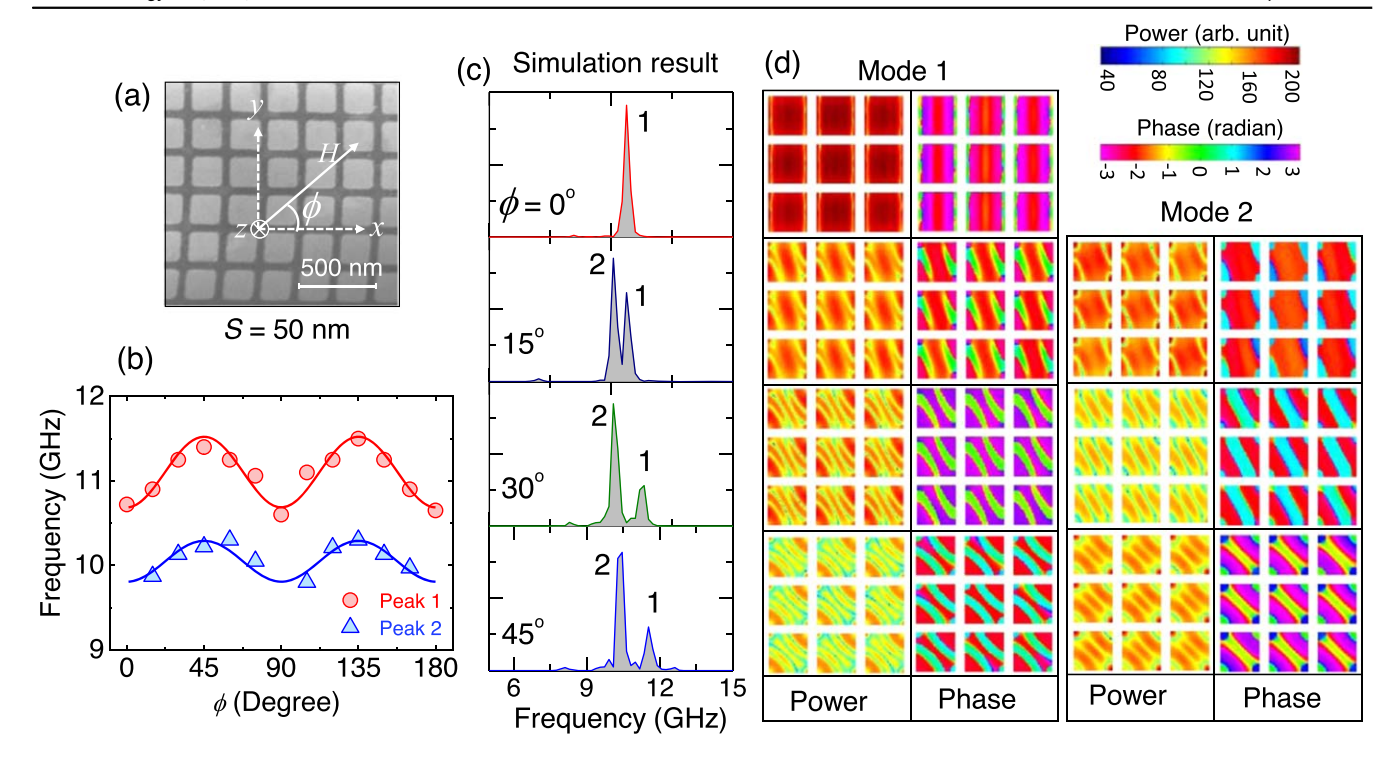


**Figure 9.** (a) Scanning electron micrograph (SEM) of 200 nm wide square permalloy dots with 20 nm thickness and 50 nm interdot separation. (b) Evolution of the collective mode frequencies with the in-plane orientation of the bias magnetic field. (c) Simulation results show the evolution of collective modes with gradually varying azimuthal angle of the bias magnetic field. (d) Simulated spatial profiles of the collective resonant modes. Reprinted from [138], with the permission of AIP Publishing.

[115]. Kostylev et al have shown a systematic variation of the frequencies of the precessional modes in 1D arrays of magnetic stripes with the magnetic field orientation [124]. Similar types of studies were carried out for 1D MCs made of periodic arrays of nanostripes with alternating widths [122], and nanostripes whose dimensions vary from 200 to 50 nm [17]. For 2D arrays of magnetic dots, an anisotropic variation in precessional frequencies was observed where the degree of anisotropy was determined by the lattice symmetry in the magnetic dot array as well as the symmetry in the shape of the individual dots (figures 9(a), (b)) [20, 38, 120, 137-139, 147, 154, 177]. As a general rule, the in-plane magnetic field dependent anisotropy in the resonance frequency is dominated by the dot shape when the dots in the array are well separated, and by the lattice symmetry of the array when the dots are placed sufficiently close to each other to have strong magnetostatic coupling. The magnetic field can not only systematically tune the collective mode frequencies [38, 133, 135, 139, 144, 145, 147–151, 154, 172, 173, 176, 177], but also the magnonic band structures, as well as the band gap widths in 1D [125, 127] and 2D arrays [105, 133] of magnetic dots. Moreover, frequencies of isolated and collective dynamics can change dramatically with the bias magnetic field because of the change in the ground state of magnetization, which can show a transformation from nonuniform state to uniform state with increasing bias magnetic field strength [21, 112, 133, 149]. Rana et al observed that the uniform collective magnetization dynamics in an array of closely shaped square magnetic dot is gradually transformed to the non-collective dynamics when the in-plane bias magnetic field is rotated from 0° to 45° relative to

the symmetry axis of the square lattice (figures 9(c), (d)) [79, 138].

#### 4.2. Electric field based control

In this section, we will mainly confine our discussion to the control of nanomagnet dynamics by VCMA followed by a short description of other electric field-based methods. The mechanisms of VCMA and other electric field-based methods have been discussed earlier in section 8.6 of part I of the topical review. The SW frequency, damping, and band structures in ultrathin ferromagnetic (FM) films strongly depend on the interfacial PMA. Therefore, an electric field applied at FM/oxide interfaces can significantly tune the FMR and SW properties of the FM via VCMA. While studying electric field induced modification of PMA, Nozaki et al [178], Skowroński et al [179] and Kanai et al [180] have experimentally demonstrated a significant modulation of FMR frequency in ultrathin FM films upon the application of an electric field (figure 10(a)). The VCMA induced modulation of SWs was first reported by Nagaoka et al [181]. It was shown that the resonance fields of magnetostatic surface SWs in a 5 nm thick Fe film possessing PMA can be controlled using VCMA. As a thicker FM film was used in this study, the change in the resonance field was smaller, most probably because of weaker PMA. Later on, Rana et al experimentally reported the VCMA induced manipulation of FMR and dipole-exchange SWs frequency in ultrathin CoFeB films with varying thicknesses down to 1.6 nm [8]. A significant modulation in the SW frequency was observed,

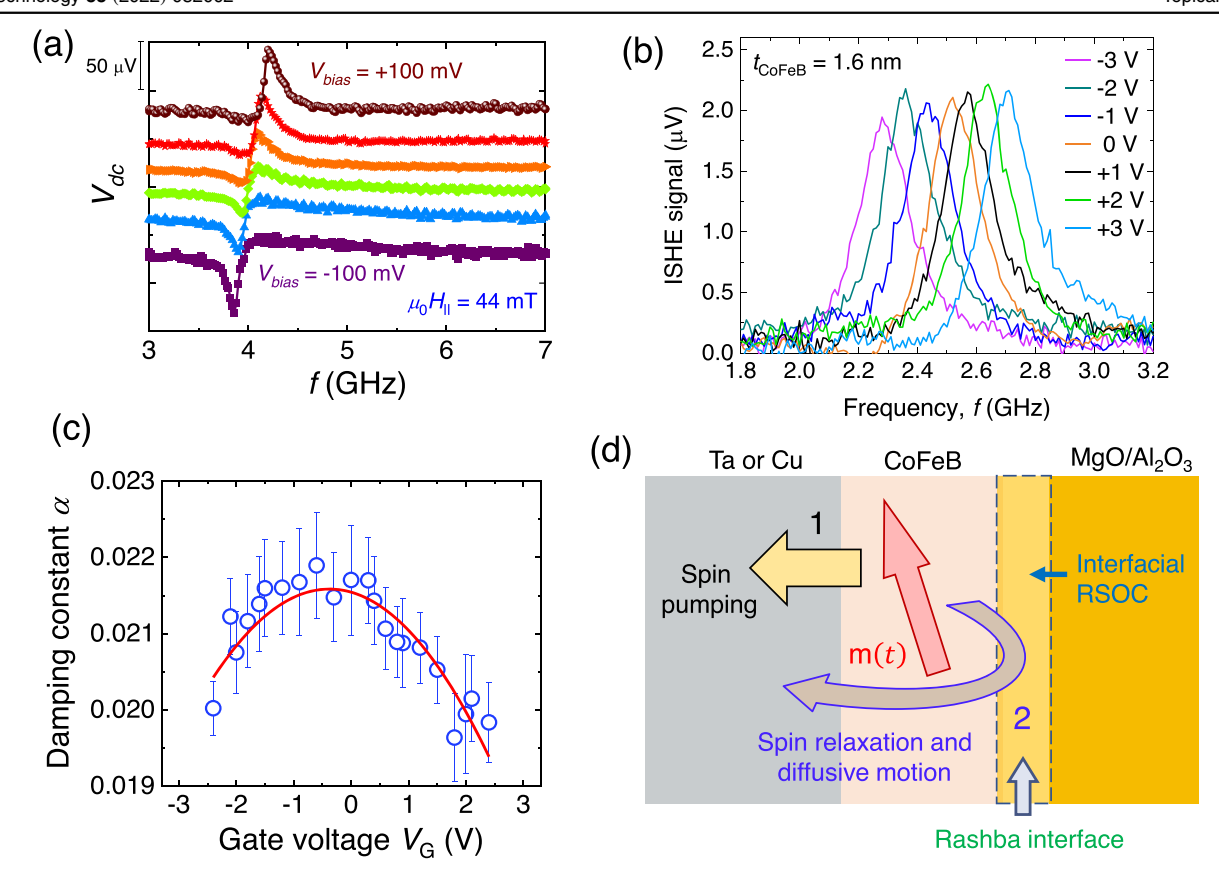


**Figure 10.** (a) Homodyne-detected FMR spectra measured from an ultrathin CoFeB film in presence of an in-plane magnetic field of 44 mT under bias voltage steps of 40 mV. Reprinted from [180], with permission of AIP Publishing. (b) SW signals measured from a 1.6 nm thick CoFeB film with inverse spin Hall effect and spin pumping technique at various values of gate voltage. Reprinted (figure) with permission from [8], Copyright (2019) by the American Physical Society. (c) Dependence of damping constant on gate voltage in a Ta/CoFeB/MgO heterostructure with 1.6 nm CoFeB film thickness. The solid curve represents fitting with a quadratic function. (d) Schematic illustration represents the relaxation mechanism of spin angular momentum in Ta(or, Cu)/CoFeB/MgO/Al<sub>2</sub>O<sub>3</sub> heterostructure through two major processes. Reprinted (figure) with permission from [51], Copyright (2020) by the American Physical Society.

particularly in a 1.6 nm thick CoFeB film, where the interfacial PMA is almost compensated by the demagnetizing field (figure 10(b)). Okada et al demonstrated that an electric field applied at a FM/oxide interface not only modulate the PMAs, but also modulates the damping constant of FMR and the latter modulation is linearly proportional to the applied electric field [182]. Interestingly, a negligible modulation of the damping constant by electric field was observed for CoFeB films thicker than 1.5 nm. However, the reason behind this remains unknown. Later, Rana et al demonstrated nonlinear variation of damping constant with electric field, especially in ultrathin CoFeB films (figure 10(c)) [51]. It was theoretically explained that the nonlinear behavior of damping originates from the electric field dependence of the coefficient of Rashba SOC present at the CoFeB/MgO interface (figure 10(d)), which was confirmed by studying other reference samples. Recently, Fulara et al have demonstrated VCMA induced modulation of effective damping in a spin Hall nano-oscillator. Basically, the mode volume of nano-constriction in the oscillator device and its coupling to propagating SWs are drastically modified by the VCMA induced modulation in the auto-oscillation frequency, resulting in a huge variation (42%) of the effective damping over a moderate range of applied gate voltage [183].

VCMA can also be used to form MCs by periodically modifying the PMA of an ultrathin FM film. Wang et al proposed that reconfigurable MCs can be formed with VCMA by periodically arranging stripe-like gate electrodes on top of an ultrathin FM waveguide [184]. When a dc voltage is applied across gate electrodes and the WG, the PMA of the FM is modulated only underneath the gate electrodes, which then results in the formation of an artificial MC with a lattice constant equal to that of the gate electrodes. These VCMA induced MCs significantly modify frequency versus wavevector band structures of SWs, i.e. magnons, opening a magnonic band gap at the BZ boundary, where the propagation of SWs is prohibited. The width of the band gap and transmission of SWs at BZ boundary in these VCMA induced MCs can be tuned by simply varying the gate voltage magnitude. In a pioneering work, Chaudhury et al experimentally demonstrated the formation of periodic arrays of parallel nanochannels (NCs) by VCMA [185]. These NCs were created by applying dc voltages across the periodically arranged stripe-like gate electrodes delineated on an ultrathin CoFeB film (figure 11(a)). When no gate voltage is applied, a single SW mode with monotonic variation of frequency with the wavevector is observed (figure 11(b)). This SW dispersion looks similar to the SW dispersion of a stand-alone CoFeB

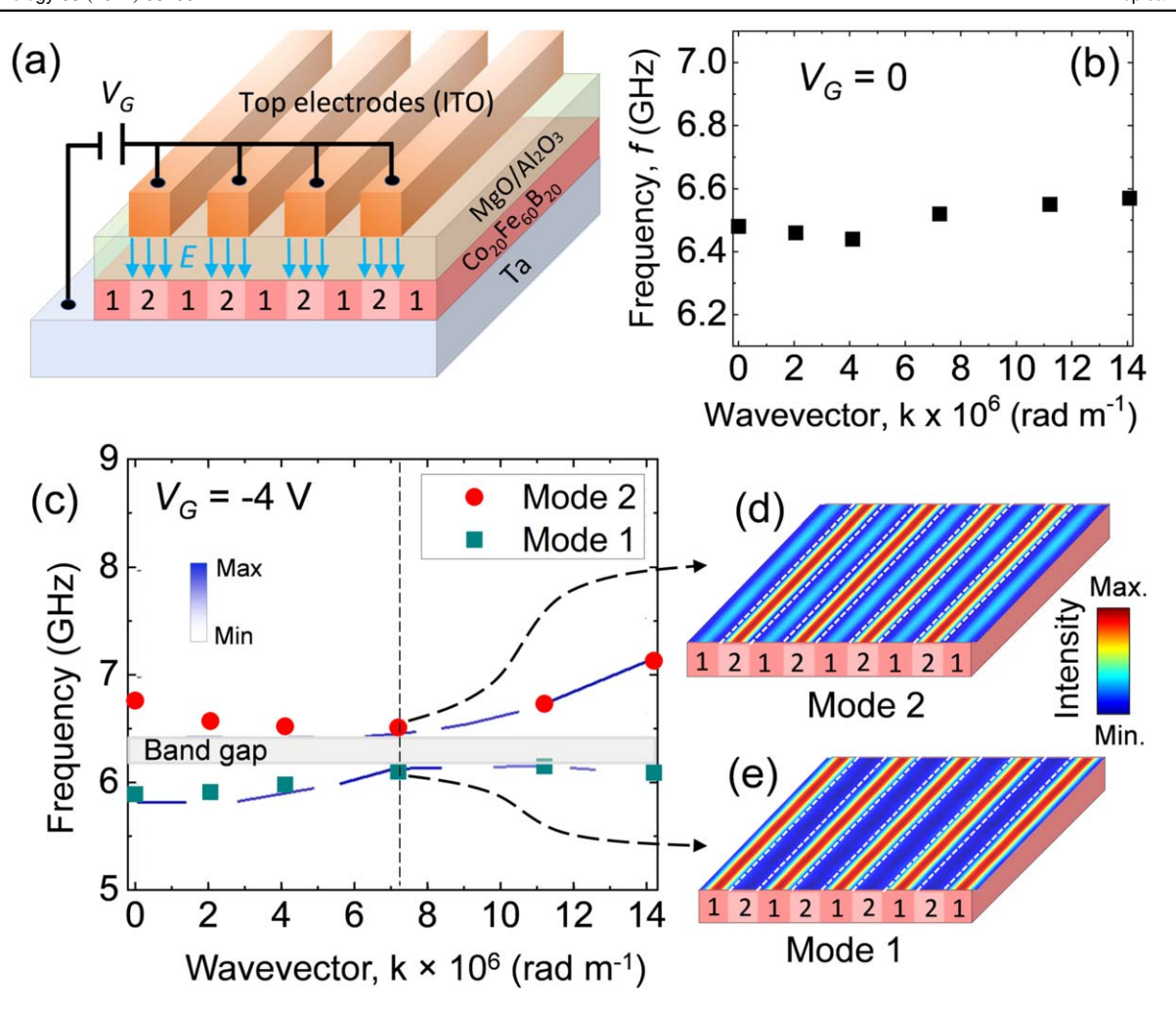


Figure 11. (a) Schematic diagram illustrates the device structure of a VCMA induced NC. A static potential is applied across the periodically arranged gate electrodes and the WG, which gives rise two regions: region outside of top electrodes (i.e. region 1) and region underneath the top electrodes (i.e. region 2). Measured frequency versus wavevector data points at  $V_G = 0 \text{ V}$  (b), and -4 V (c) under the application of 200 mT bias magnetic field [185]. (c) Solid symbols represent measured SW frequencies and the blue curves represent SW intensities calculated by PWM. Inset shows the corresponding colour map. The position of anticrossing is indicated by a vertical dotted line, and the magnonic band gap is shown by the grey region. (d)–(e) Calculated SW mode profiles for wavevector  $k = 7.1 \times 10^6 \text{ rad m}^{-1}$  under the application of  $V_G = -4 \text{ V}$  at  $\mu_0 H = 200 \text{ mT}$  are presented. Mode 1 is confined in region 1 and mode 2 is confined in region 2. From [185]. Reprinted with permission from AAAS.

film without any gate electrodes. When a moderate gate voltage (-4 V) is applied, i.e. when a periodic array of NCs is formed, two SW modes appear with a bandgap (figure 11(c)). Interestingly, the bandgap can be tuned just by changing the gate voltage. After performing a PWM calculation and analysis, it was found that the mode 2, i.e. the higher frequency mode is confined within channel 2 underneath the gate electrodes, while mode 1, i.e. the lower frequency mode is confined within channel 1 interposed between the gate electrodes (figures 11(d), (e)).

#### 5. Spintronic effects in nanomagnets

#### 5.1. Spin current and magnetoresistance

Spintronics utilizes spin current for device operation, i.e. the flow of spin polarized electrons, which requires creation of a nonequilibrium spin population. This can be achieved in many ways. Circularly polarized photons have been used to transfer their angular momenta to electrons and produce a spin-polarized population of electrons in semiconductors [186], but for device applications such as spin transistors, electrical spin injection is preferred. The latter is usually achieved by connecting a ferromagnetic contact to a sample and then injecting electrons from the contact into the sample by connecting a voltage source across the interface between the contact and the sample. A ferromagnet has a spin-split conduction band where the densities of states of electrons at the Fermi level are different for spins parallel and antiparallel to the direction of magnetization. Since the electrons mostly come from around the Fermi level in the contact, the injected current naturally has majority spins and minority spins. The spin injection ratio is defined as  $\eta = \frac{n_{maj} - n_{\min}}{n_{maj} + n_{\min}}$ , where  $n_{maj}$  is the population of majority spins and  $n_{min}$  is the population of minority spins in the injected current. Other methods, which do not require magnets but require such constructs as quantum point contacts, have also been demonstrated for spin injection [187]. In the ferromagnetic contact method, the efficiency of spin injection is increased by interposing a tunnel barrier between the ferromagnet and the non-magnetic sample to overcome the so-called resistivity mismatch problem if the resistivities of the contact and the sample are significantly different [188]. A spin current can also be generated by microwave excitation and by harnessing various spin-orbit effects such as spin pumping, SHE, spin caloric effects (e.g. spin Seebeck and Nernst effect), etc.

Historically, generation of spin polarized current was first demonstrated by Jullieré in 1975 in an experiment involving tunneling of electrons between two ferromagnetic films separated by a spacer layer interposed between them [189]. This trilayer construct is called a 'spin valve' and it led to the concept of tunneling magnetoresistance  $TMR = (R_{AP} - R_P)/R_P =$  $2P_1P_2/(1 - P_1P_2)$ ;  $P_1$  and  $P_2$  being the spin polarizations of the two ferromagnetic layers, while  $R_{AP}$  is the resistance of the spin valve when the polarizations of the two layers are mutually antiparallel and  $R_{\rm P}$  is the resistance when they are parallel. The notion of TMR is a key concept in modern spintronics and is a metric used to gauge the degree of spin selective injection from one layer, and spin-polarized extraction by the other layer, in a spin valve structure. In other words, TMR is a measure of the quality of the 'spin polarizer' layer and the 'spin analyzer' layer. The MTJ is also a spin valve and there, TMR is again a measure of the quality of spin selectivity in the tunneling between the hard and the soft layers.

With the observation of significant room temperature TMR in spin valve structures in 1995 [190, 191], this field has grown substantially leading to the development of magnetoresistive random access memory (MRAM) based on MTJ [192]. Introduction of perfectly ordered (100) oriented MgO tunnel barrier as the spacer layer interposed between CoFeB electrodes as the ferromagnetic layers showed giant TMR value of 220% at room temperature (RT) [193] and even higher value of 604% in  $\text{Co}_{20}\text{Fe}_{60}\text{B}_{20}/\text{MgO}/\text{Co}_{20}\text{Fe}_{60}\text{B}_{20}/\text{Ta}$  at RT demonstrated by Ikeda *et al* [194].

The giant magnetoresistance (GMR) effect was discovered in 1988 by Fert [195] and Grunberg [196] in metallic Fe/Cr multilayers. The effect is manifested as a giant change in the electrical resistance of a device in a magnetic field. The GMR typically occurs due to spin dependent scattering of electrons at the interface, although it can also occur because of other reasons [193]. In analogy with TMR, one defines GMR =  $(R_{AP} - R_P)/R_P$ , where  $R_P$  and  $R_{AP}$  correspond to the resistances of the multilayer structure in parallel and antiparallel magnetization configuration between two FM layers, respectively. GMR is observed both in current-in-plane (CIP) and current-perpendicular-to-plane (CPP) geometries, i.e. when current flows parallel and perpendicular to the heterointerfaces, respectively. Its magnitude depends both on the ferromagnet FM (e.g. Fe) and normal metal NM (e.g. Cr) layer thicknesses as given by the Valet-Fert model [197]. In 1998, IBM introduced a low field GMR sensor which is a key component for data reading in magnetic hard disk drives today.

In early 1993, a pioneering work on lateral spin valve was reported [198], which spurred intense interest in early 2000 when Jedema et al demonstrated diffusive spin-injection in a nonlocal geometry from a Py nanowire electrode followed by spin accumulation in a Cu nanowire and subsequent spin detection by another Py nanoelectrode [199]. An estimated spin diffusion length in Cu of 350 nm at room temperature was obtained. Later they demonstrated electrical spin injection and detection in diffusive metallic conductor from metallic FM electrodes through Al-O tunnel barrier and studied controlled spin precession of the injected electrons [200]. An increasing spin signal due to ballistic spin injection was reported. Efforts on increasing spin injection efficiency continued and an efficiency up to 27% was reported using halfmetallic Co<sub>2</sub>FeSi FM electrode [201] (figure 12), and a temperature independent 70% spin injection efficiency in a CoFe/MgO/GaAs device [202] were reported.

#### 5.2. Spin transfer torque (STT)

The STT effect, mentioned earlier in this review, requires spin polarized injection of current into or extraction of current from the soft layer of an MTJ to reverse its magnetization. Here, the MTJ's hard layer acts as the spin polarizer. STT was demonstrated first in a point contact [203] and subsequently in CPP-GMR [204] and TMR nanopillars. There is a critical current density in STT below which magnetic reversal does not take place in the soft layer. Jiang et al found a way to reduce the critical current density in a CPP pseudo-spin-valve nanopillar. They showed that the critical current density for STT can be reduced by an order of magnitude through the insertion of a spin-scattering ultrathin Ru layer and an additional FM layer [205, 206]. More recently, Vautrin et al reported the angular and thickness dependence of the magnetocurrent of hot electrons in a magnetic tunnel transistor (MTT) with crossed magnetic anisotropies. They showed an increase in magnetocurrent up to 85% with the variation of FM layer thickness, which is very close to the theoretical maximum value of 100% for MTTs [207]. Spin-polarized current driven magnetic switching in nanoscale MTJ with Al-O barrier showed TMR up to 30% at current densities less than  $10^7 \,\mathrm{A \, cm^{-2}}$  [208]. Introduction of a MgO barrier and post-processing annealing in low-resistance  $Co_{40}Fe_{40}B_{20}/MgO/Co_{40}Fe_{40}B_{20}$  MTJs showed reduction of critical current density  $J_{\rm C}$  to as low as  $7.8 \times 10^5 \,\mathrm{A\,cm^{-2}}$  (TMR = 49%) and increase of TMR ratio to as high as 160% ( $J_C = 2.5 \times 10^6 \,\mathrm{A \, cm}^{-2}$ ) [209]. The improved scalability of ultrasmall out-of-plane magnetized MTJs for STT-MRAM cells has been made possible by using magnetic shape anisotropy in combination with interface anisotropy [44]. Recently, insertion of a double tunneling barrier in a double MTJ has led to the formation of a resonant tunnelling junction, which showed TMR oscillation up to 12 nm thick FM layer [210]. More recently, quantum resonant tunneling has been observed in a double MTJ incorporating a double quantum well [211]. In recent years spintronics has branched off into new areas by merging with various ancillary

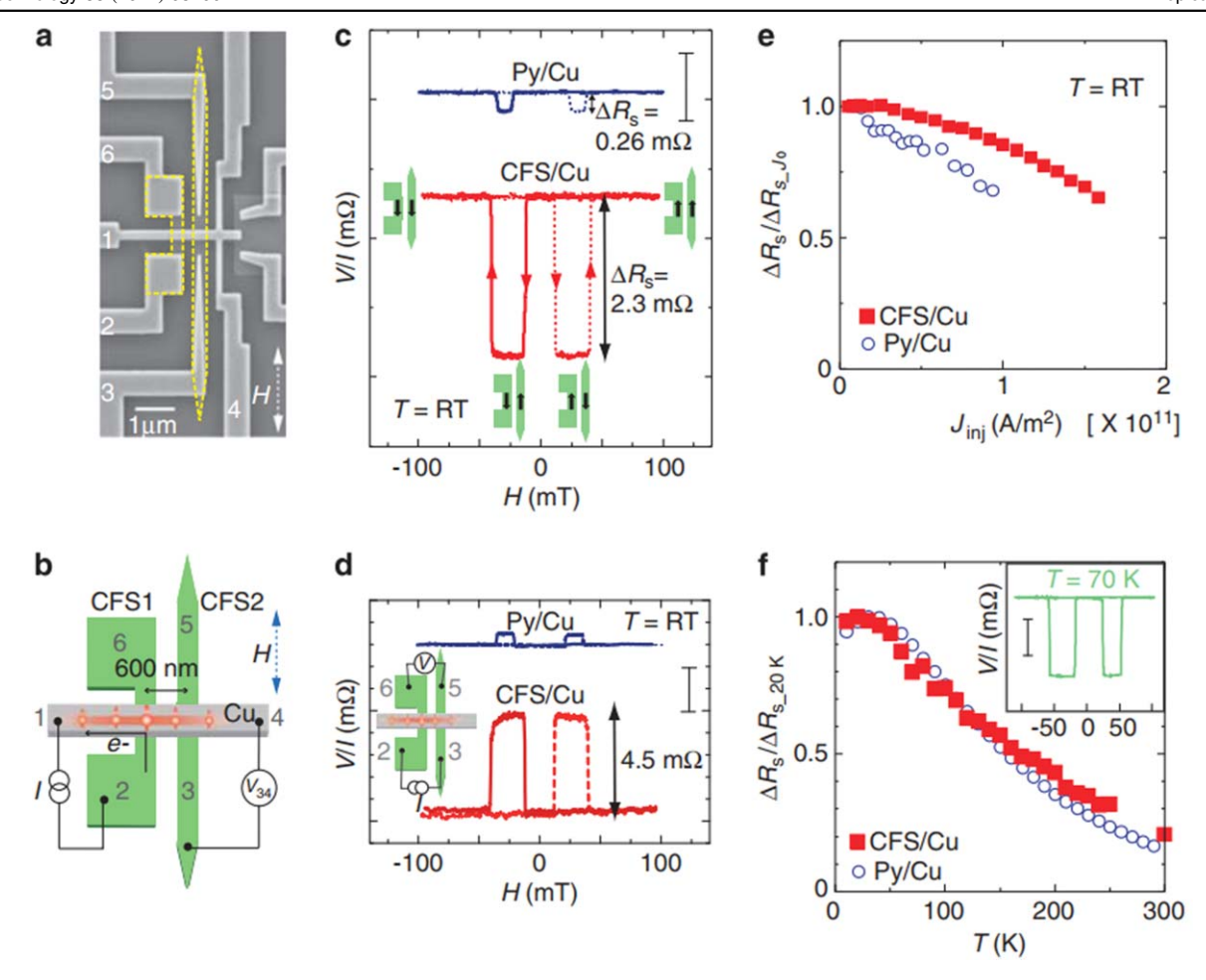


Figure 12. Enhanced nonlocal spin valve effect. (a) SEM image of the fabricated Co<sub>2</sub>FeSi(CFS)/Cu lateral spin valve (LSV). (b) Schematic diagram of a nonlocal spin valve measurement is presented where spin polarized electron is injected into Cu through contact 2, and a nonlocal voltage between contact 3 and contact 4 is measured. (c) A measured nonlocal spin-valve signal at room temperature for the CFS/Cu LSV, together with that for the Py/Cu LSV is shown. As illustrated in the inset, the spin-valve signal varies according to the relative orientation of magnetization in two wire-shaped CFS electrodes. (d) Local spin-valve signals measured from the Py/Cu and CFS/Cu LSVs at room temperature. The inset shows the current (*I*)–voltage (*V*) probe configuration. The low and high resistance states are associated with the parallel and anti-parallel magnetization alignments, which agree well with those observed in the nonlocal spin valve signal. (e) Injected current density dependent nonlocal spin signal  $\Delta R_{\rm S}$ , normalized by  $\Delta R_{\rm S}$  at a small bias current density of  $J_0 \sim 10^9$  A m<sup>-2</sup>, are plotted for the CFS/Cu LSV (red solid squares) and the Py/Cu LSV (blue open circles). (f) Evolution of  $\Delta R_{\rm S}$  with the measurement temperature, normalized by  $\Delta R_{\rm S}$  measured at 20 K, for the CFS/Cu LSV (red solid squares) and the Py/Cu LSV (blue open circles). The inset shows a nonlocal spin-valve effect of the CFS/Cu LSV at T = 70 K. The scale bars in (c), (d), and the inset of (f) are 1, 2 and 5 mΩ, respectively. Reprinted by permission from Springer Nature Customer Service Centre GmbH: Springer Nature, NPG Asia Materials, [201], Copyright © 2012, The Author(s).

fields, namely magnon spintronics [5], spin–orbitronics [212], antiferromagnetic spintronics [213], topological spintronics [214], flexible spintronics [215], organic spintronics [216], spin-based quantum [217, 218], neuromorphic [219] and probabilistic computing [220], and so on. The overriding goals are: further miniaturization, faster operation, greater functionality, energy efficiency, integration on flexible substrate etc.

#### 5.3. Spin orbitronics

In STT, the exchange interaction between injected electron spins and resident spins in magnetic materials mediates transfer of spin angular momenta from the injected spins to the resident spins. Spin-orbitronics is a new avenue of spintronics, which relies upon the SOC in nonmagnetic materials instead of the exchange interaction in magnetic materials for the generation, detection and use of pure spin currents. This opens the pathway to building magnetic materials less spin-based devices which can be operated without magnetic fields. A number of effects originating from SOC are important in the fields of nanomagnetism and spintronics. These range from the fundamental magnetic anisotropy energy, namely magnetocrystalline anisotropy to more advanced topics such as anisotropic magnetoresistance, SHE, Rashba effect, Edelstein effect, SOT, spin pumping effect, DMI, spin caloric effects etc. Two of the most important aspects arising from the above effects are the generation of pure spin current, i.e. the so-called spin-charge interconversion and appearance of chiral spin textures.

The intrinsic SOC is a fundamental interaction occurring between an electron's spin and its orbital motion around the nucleus. Hence it is sometimes called  $\mathbf{L} \cdot \mathbf{S}$  coupling. An electron moving around a nucleus experiences an electric field due to the positively charged nucleus and this electric field Lorentz transforms into a magnetic field in the rest frame of the electron. The interaction of this magnetic field with the spin angular momentum of the electron gives rise to SOC. The SOC increases as  $Z^4$  (Z is the atomic number) in hydrogen-like atom [64]. The general derivation of SOC starting from the Dirac equation for an electron of charge -e and mass m under an external electrical field  $E(r) = -\nabla \phi(r)$  yields:

$$H_{SO} = \frac{e\hbar}{4m^2c^2}\hat{\sigma} \cdot [\vec{E}(r) \times \vec{P}], \tag{8}$$

where  $\vec{P}$  and  $\hat{\sigma}$  are the momentum operator and the Pauli spin matrix, respectively. In addition to the intrinsic SOC or  $\mathbf{L} \cdot \mathbf{S}$ coupling, there may be other types of SOC. Two major contributions to such SOC in the conduction band of semiconductor crystals with direct band gap are: (a) the Dresselhaus contribution occurring in crystals with bulk inversion asymmetry, leading to a net electric field along specific crystal directions [221] and (b) the Rashba SOC occurring in systems with net electric field due to structural inversion asymmetry [222]. The intrinsic SOC is usually absent in the conduction band of direct gap semiconductors since the electron orbitals are S-type (L = 0) but it can be present in the conduction band of indirect gap semiconductors like Ge where the electron orbitals are not S-type. The Rashba and Dresselhaus SOC can produce momentum-dependent splitting of spin bands in bulk material and low-dimensional condensed phase systems such as surface and interface states. The splitting occurs due to the SOC and asymmetry of the crystal potential, perpendicular to the 2D plane. It can also give rise to the spinmomentum locking. The spin-momentum locking in 2D geometries can influence the interplay between the charge and spin transport. The Edelstein effect is an intrinsic charge to spin conversion mechanism. When a charge current flows through the spin-polarized surface states, a spin accumulation occurs [223]. In the case of a 2D Rashba electron gas, where this spin-dependent band splitting occurs [224], this effect is known as Rashba-Edelstein effect.

Topological insulators (TI) exhibit a spin-split linear dispersion character on their surfaces, while showing a band gap in the bulk. This spin-split surface states occur due to the presence of surface topology, irrespective of the Rashba effect. Besides, they also exhibit spin-momentum locking [225]. When a charge current flows through the spin-polarized surface states of a TI, a spin accumulation is generated and the effect is called the Edelstein effect [223].

The SHE acts as the leading mechanism for the conversion of charge to transverse spin current inside a nonmagnetic metallic system with large spin-charge conversion ratio (spin Hall angle or SHA). Dyakonov and Perel first proposed this phenomenon in 1971 [226] which was later expounded by Hirsch [227]. Subsequently, optical and electrical measurement techniques were used to study SHE and inverse SHE in different non-magnetic systems [228–230]. Its origin lies in the intrinsic effect, namely Berry curvature effect associated

with the spin dependent band structure of the crystalline material and extrinsic mechanisms associated with the asymmetric scattering of conduction electrons from impurity potential, namely skew scattering and side-jump mechanism. There is also an *intrinsic* universal SHE that is due to spin-orbit interaction in a 2D system which yields a universal spin Hall coefficient of  $q/8\pi$  (q= electron charge) [231]. Among nonmagnetic metals, heavy metals like Pt, Ta, Ir, Hf, W show large SHA, with W and its oxides exhibiting the highest value of  $\sim$ 0.5 for the SHA [232]. On the other hand, TIs show giant SHA with spin Hall angles well above unity associated with the topological surface state and unique valley degree of freedom [233].

Spin pumping is another efficient method for generating pure spin current. It is a non-local effect, which refers to the flow of pure spin current generated by the precession of magnetization, from a ferromagnet (FM) into a normal metal (NM). The magnetization precession results in spin accumulation at the interface of NM/FM heterostructure. The accumulated spins then enter into adjacent NM layer through diffusive motion. The NM layer plays the role of a spin sink to absorb the spin current through spin-flip scattering. This leads to an increase of the Gilbert damping coefficient of the FM layer. Tserkovnyak, Brataas and Bauer theoretically formulated the spin pumping led increase in damping in NM/ FM heterostructures in 2002, using time-dependent adiabatic scattering theory [234]. There, time dependent magnetization in the presence of spin pumping can be expressed by a modified LLG equation as [235, 236]:

$$\frac{d\mathbf{m}}{dt} = -\gamma(\mathbf{m} \times \mathbf{H}_{\text{eff}}) + \alpha_0 \left(\mathbf{m} \times \frac{d\mathbf{m}}{dt}\right) + \frac{\gamma}{V M_s} \mathbf{I}_s, \quad (9)$$

where  $I_s$  is the total spin current,  $\gamma$  is the gyromagnetic ratio,  $H_{eff}$  is the effective magnetic field,  $\alpha_0$  is the intrinsic Gilbert damping parameter, V is the volume of the FM and  $M_s$  is the saturation magnetization of the FM. The spin current  $I_s$  generally consists of three terms: a direct current contribution  $(I_s^0)$ , spin current  $(I_s^{pump})$  pumped from the FM to NM, and spin current backflow  $(I_s^{back})$  into the FM due to reflection from the NM/substrate interface assuming it as a perfect reflector. This can be written as:

$$I_s = I_s^0 + I_s^{\text{pump}} + I_s^{\text{back}}.$$
 (10)

The contribution  $I_s^{back}$  is determined by the spin diffusion length of the NM layer. The spin transport through NM/FM interface is determined by the spin-mixing conductance, which is nothing but the conductance properties of the spin channels at the NM/FM interface. The spin mixing conductance can be of two types: (a) the intrinsic spin-mixing conductance ( $G_{f,l}$ ), where the contribution of spin angular momentum backflow is ignored, and (b) the effective spin-mixing conductance ( $G_{eff}$ ), where the backflow contribution is included [237]. The interfacial spin transparency (T) takes into account various effects leading to the reflection of electrons from the interface instead of transmission during transport [238]. Moreover, T also depends upon intrinsic and extrinsic interfacial factors, for instance, Fermi velocity, band-structure mismatch, interface imperfections, structural

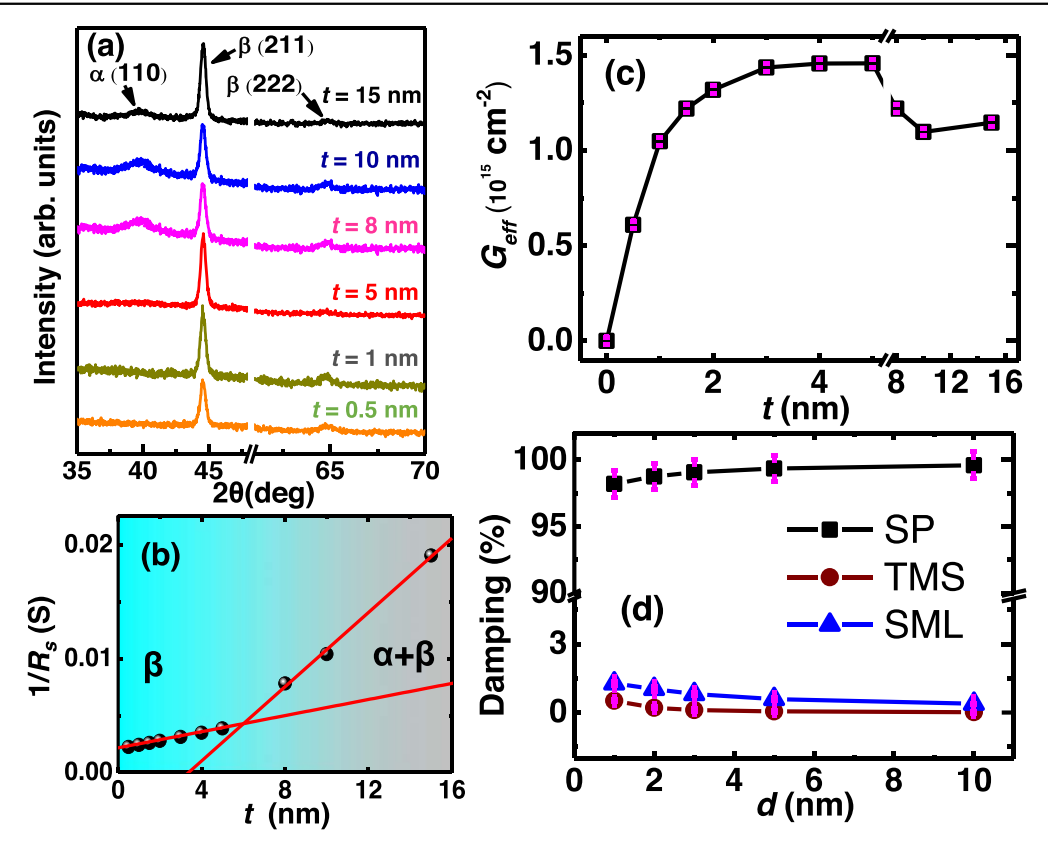


Figure 13. (a) X-ray diffraction (XRD) data measured at  $2^{\circ}$  grazing incidence angle for varying thicknesses of W are plotted. (b) Variation of the inverse of sheet resistance with W thickness. (c) Variation of effective spin-mixing conductance ( $G_{eff}$ ) with the thickness t of W layer (symbol). The solid line represents a guide to the eye. (b) Contributions of spin pumping (SP), two magnon scattering (TMS) and spin memory loss (SML) to the modulation of damping for different  $Co_{20}Fe_{60}B_{20}$  layer thicknesses d (symbol). The solid lines represent a guide to the eye. Adapted from [240] with permission from the American Chemical Society.

phase etc [239, 240]. Panda *et al* showed a giant value of T exceeding 80% in a W(t)/CoFeB(d) heterostructures, which strongly depends on the structural phase of W. A subtle variation of W thickness across 5 nm exhibited a sudden change of structural phase from  $\beta$ -W ( $t \le 5$  nm) to mixed  $\alpha + \beta - W$  (t > 5 nm) and an ensuing decrease in  $G_{eff}$  (figure 13) and T value from  $0.81 \pm 0.03$  to  $0.60 \pm 0.02$  [240]. Analyses showed that the contribution of spin pumping (SP) is heavily dominant over other possible contributions like two-magnon scattering (TMS) and spin memory loss (SML) to damping.

Another important effect arising from SOC is the DMI. This has its root in the seminal work in 1958, when the phenomenological theory of antisymmetric exchange coupling between spins to explain the phenomenon of weak ferromagnetism in antiferromagnetic compounds [241] was developed. In 1960 Moriya derived this interaction as a SOC between electrons within the framework of super-exchange theory [242, 243]. This anisotropic exchange interaction, i.e. DMI arises in the materials that lack inversion symmetry in the presence of strong SOC. This spans over non-centrosymmetric bulk ferromagnets, multiferroics, perovskites and cuprates. Interfacial DMI, which is observed in FM thin film heterostructures, helps to stabilize various chiral spin textures, for example, skyrmions, skyrmion lattices, magnetic helices and chiral domain walls. Early theoretical effort

considered the RKKY interaction, i.e. spin-orbit scattering of the conduction electron gas from the heavy metal impurities to explain DMI [244]. Later, proximity induced magnetic moment in heavy metal was claimed to be responsible for DMI [245], which was immediately contradicted and was found to have no role to play in Co/Pt [246]. The sign and magnitude of DMI depends upon the degree of 3d-5d orbital hybridization around the Fermi level [247]. It depends on filling of 5d orbitals (electronegativity) in heavymetals (HMs) [248]. DMI is driven by spin-flip transitions between 3d states (in the FM) involving intermediate states (from the adjacent layer) with strong SOC strength [249] and is correlated with spin-mixing conductance. BLS has emerged as one of the most popular and reliable techniques to investigate interfacial DMI in various HM (or other NM)/FM heterostructures from the asymmetric spin-wave dispersion (figure 14) in the DE geometry [21, 250, 251].

The SOC related effects are generally studied in HM systems but other candidates like TI and 2D materials are gradually making inroads. For example, the SOC magnitude for the sp2 bonded structure of pristine graphene is quite small (about 10  $\mu$ eV) [252]. However, SOC can be significantly enhanced by some techniques, for instance, by proximity effect and hybridization with adjacent materials. The SOC can also be enhanced by introducing in-plane and out-of-plane deformations that mix the sp2 and sp3 orbitals in

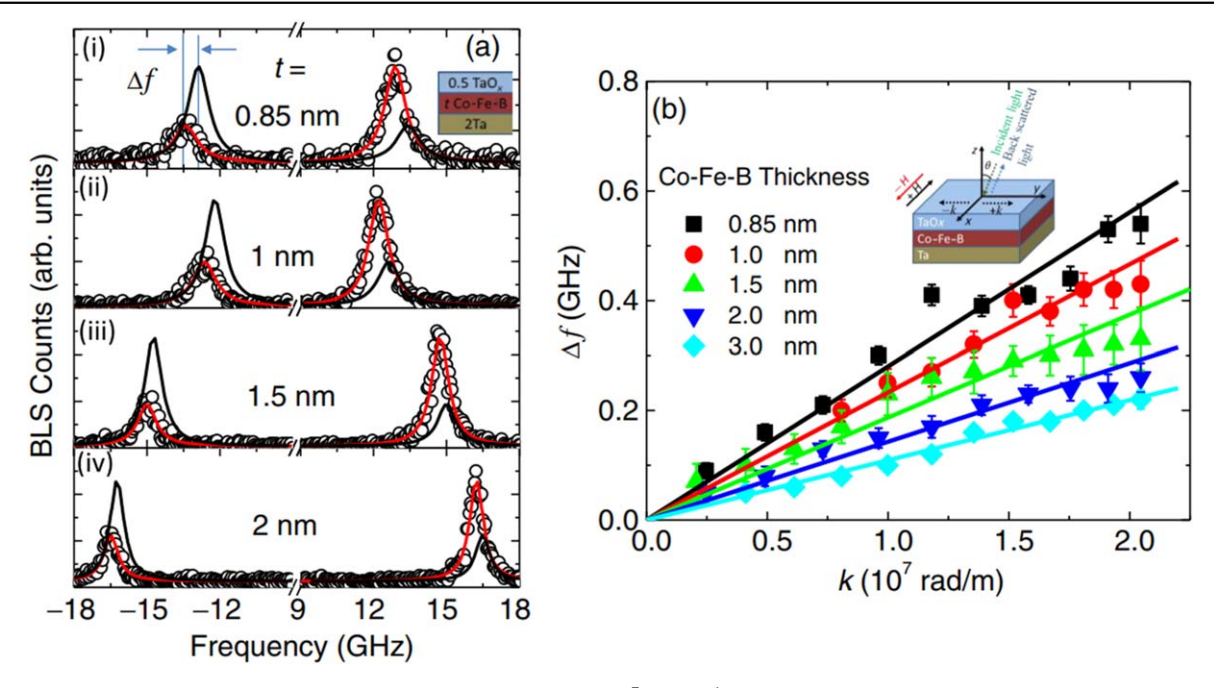


Figure 14. (a) BLS spectra measured at SW wave vector  $k = 2.04 \times 10^7$  rad m<sup>-1</sup> from a Ta(2 nm)/CoFeB(t)/TaO<sub>x</sub>(0.5 nm) sample for two counterpropagating directions. The corresponding CoFeB thicknesses are indicated in each panel. The solid curves represent the fit with the Lorentzian function. (b) Plot of frequency difference ( $\Delta f$ ) between two counterpropagating SWs as a function of k for Ta(2 nm)/CoFeB(t)/TaO<sub>x</sub>(0.5 nm) samples with various values of t. Solid symbols represent the experimentally obtained values and solid lines are the theoretical fits. Inset: Schematic of the film stack and measurement geometry of BLS. Adapted from [251] with permission from the American Physical Society.

strained or buckled graphene and also by employing interactions with adatoms and electric fields. SOC-induced splitting of graphene bands further leads to the spin-momentum locking and chiral spin orientations; for example, the large SOC splitting ( $\sim 100 \text{ meV}$ ) in graphene on Au originates from the strong hybridization between the Dirac-cone states and the d states of Au [253].

#### 5.4. Spin mechatronics

Spin mechatronics utilizes mechanical motion of nanomagnets for generation and control of spin currents. The angular momentum conservation between mechanical motion and spins triggers the spin current generation by mechanical motion [254]. To understand this phenomenon, a spinning top driven by external torque can be considered. When mechanical rotation is applied to this system, the rotation axis of a spinning top aligns with the axis of external torque due to the Coriolis force given by:  $H_{Cor} = -\mathbf{L} \cdot \mathbf{\Omega}$ , where  $\mathbf{L}$  represents the mechanical angular momentum of the spinning top and  $\Omega$ represents the angular velocity of the applied rotation field. Analogously, classical Coriolis force can be replaced by quantum mechanical spin-rotation coupling (SRC), i.e. coupling between spin angular momentum S and mechanical rotation given by:  $H_{SRC} = -\mathbf{S} \cdot \mathbf{\Omega}$ . In 1915, Barnett discovered a gyromagnetic effect known as Barnett effect, which stipulates that when a magnetic element is rotated, the spins inside the element are aligned along the rotation axis, i.e. the element is magnetized (figure 15(a)) [255]. This is caused by the Zeeman coupling of S with the emergent magnetic field  $B_{\Omega} = \Omega/\gamma$  created by the rotation of the element, where  $\gamma$  is the gyromagnetic ratio.

The converse phenomenon of the Barnett effect is known as Einstein-de Haas effect. Einstein and de Haas experimentally demonstrated that a freely suspended FM starts to rotate under the application of an external magnetic field (figure 15(b)) [260]. Basically, the magnetic moment in the FM is changed once the magnetic field is switched on. This triggers a mechanical angular momentum to compensate the modulation of the spin angular momentum of the FM because of angular momentum conservation principle. In the Barnett effect, the mechanical rotation not only couples to the electronic spin system, but also couples with the nuclear spin system. Chudo et al measured the Barnett field in non-ferromagnetic system by observing the shift of the nuclear magnetic resonance (NMR) frequency due to the SRC between nuclear spin and mechanical rotation [261]. By measuring the induced magnetic moment in a polycrystalline Gd (paramagnetic) sample, Ono et al also estimated the Barnett field [262]. Interestingly, SRC not only modulates spin angular momentum, but also can generate spin current by two routes: first, mechanically induced SOC due to the rigid motion, and second, coupling of spin with vorticity due to the local rotational motion of elastic or fluid materials. In the first case, SHEs can be induced by rigid [263] and vibrational [264] mechanical motion even in the absence of conventional SOC, which enables spin current generation. As an example, if a Pt film vibrates at 10 GHz frequency with an amplitude of 0.1 nm, then the amplitude of the generated ac spin current can be estimated as  $10^5$  A m<sup>-2</sup> [264]. In the second case, the

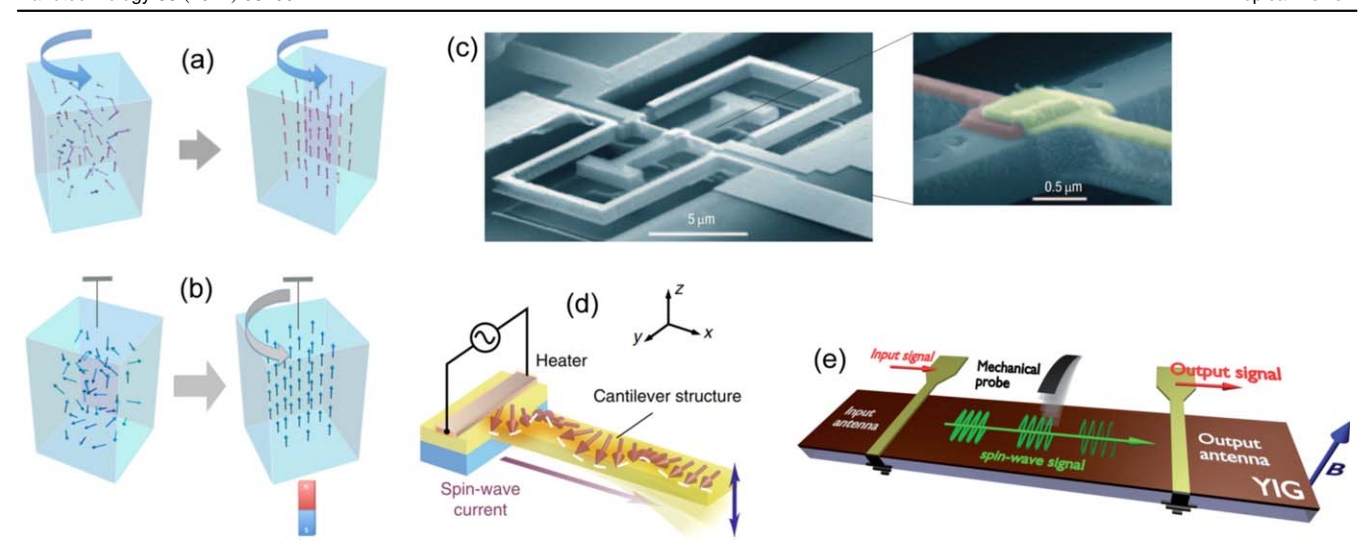


**Figure 15.** (a) Schematic illustration of the Barnett effect. The magnetic moments in a FM material are aligned along the rotation axis of the external mechanical rotation due to spin-rotation coupling [254, 256]. (b) Einstein—de Haas effect, the converse of the Barnett effect, which causes mechanical rotation owing to magnetization, is illustrated. When a suspended magnetic material is magnetized, the spins are aligned along the direction of the external magnetic field, leading to the induction of mechanical angular momentum to compensate the modulation of spin angular momentum. Reproduced from [256] with permission of Frontiers Media. (c) SEM image of a nanomechanical device along with the enlarged image showing the FM/NM interface (cobalt and gold are represented by red and yellow colors, respectively). The structure is fully suspended and rigidly clamped at the large support pads. Reproduced from [257] with permission of Springer Nature. (d) The schematic illustration of a YIG cantilever connected to one edge of a YIG film. A heater is placed on top of the YIG film. When electric current is applied to the heater, heat current is generated, which creates SW (i.e. magnon) accumulation at the top and bottom surfaces of the YIG film. The accumulated magnons then inject spin current into the YIG cantilever. Reproduced from [258] with permission of Springer Nature. (e) The schematic diagram of the experimental setup that demonstrated the feasibility of utilizing mechanical coupling to propagate magnetostatic SWs through a YIG waveguide. The amplitude modulated SWs, excited by a microstrip antenna, are used to generate out-of-plane oscillations of a magnetic micro-mechanical probe (nickel, diameter 10 μm) suspended above the surface of YIG film. A laser interferometric vibrometer is used to measure the displacements of the probe. Reproduced from [259] with permission of the authors.

vorticity gradient gives rise to a spin-dependent force given by  $F_S = \mathbf{S} \cdot \nabla \omega$ , where  $\nabla \omega$  is the gradient of vorticity. This shows that spin current can be generated along the vorticity gradient. When SAWs propagate through a nonmagnetic film, the atoms attached to the lattice points oscillate around their equilibrium position and a gradient of vorticity is established across the thickness of the film. This generates a spin current across the thickness [265–267]. Interestingly, this mechanism allows one to utilize materials with relatively small SOC (e.g. Cu, Al and even carbon nanotubes) to generate spin current with reasonable density. Takahashi *et al* demonstrated that the spin-vorticity coupling caused by the gradient of vorticity field in a liquid metal flow, such as flow of GaInSn or Hg in a fine quartz pipe, can also generate spin current [268].

In spintronics, the spin current, i.e. flow of spin angular momentum is utilized for transmission and processing of information. Either the translational motion of conduction electrons or the SWs can be used to carry spin angular momentum. A spin-flip or spin-transfer process always involves a change in the angular momentum, which can induce a mechanical torque and hence mechanical oscillation to the nanoelement attached to the system. Based on this principle, Mohanty *et al* proposed a spin-mechanical device for the manipulation and detection of spin currents by mechanical torque [269], which was experimentally demonstrated later [257]. It was demonstrated that when a spin-polarized current flows through a metallic nanowire, half of which is made of FM and other half is made of nonmagnetic

material, the spins of the conduction electrons are 'flipped' at the interface between the two materials, which then produces a nanomechanical torque (figure 15(c)). The spin torque was determined from a measurement of the magnetic field dependence of the magnetomotive voltage. That enables nanomechanical detection of spin flip phenomenon. This idea was later extended for nanomechanical detection of the spin Hall coefficient. Recently, Harii et al have experimentally demonstrated transmission of mechanical angular momentum and force generation due to SWs injected into a yttrium iron garnet (YIG) film by the spin-Seebeck effect [258]. The SW current, transmitted through a YIG microcantilever, was observed to create a mechanical force on the cantilever as a nonlocal reaction to the spin-Seebeck effect (figure 15(d)). Karenowska et al proposed a hybrid spin mechatronic structure in which information encoded in the phases and amplitudes of propagating SWs are written and read by resonant magno-mechanical elements [259]. The principle of operation is very similar to MRFM, where short wavelength, highly spatially localized standing SWs are detected by a cantilever tipped with a ferromagnetic particle. They have proposed to use a YIG waveguide for SW transmission and a magnetic cantilever suspended above the film as a micromechanical probe (figure 15(e)). The probe is movable in the x-, y-, and zdirections. An optical vibrometer having resolution of 0.1 nm is used to detect the displacements of the cantilever due to the stray field generated by propagating SWs. This magnetic

cantilever movement can even perturb the SW amplitude and phase at sub-millimeter approach distances.

#### 6. Future perspectives and challenges

The field of magnonics offers the tantalizing possibility of replacing traditional charge-based logic, communication and information processing approaches with an alternate paradigm that may eclipse the traditional paradigm in many aspects [270]. As magnonics is a young and rapidly evolving research field, it naturally faces many challenges. Successful application of nanomagnets in future magnonic devices has to contend with many obstacles, and strategies for overcoming them can be broadly classified into three major tasks as discussed below.

#### 6.1. Searching for new nanomagnets

Nanomagnets are proven to be the backbone of magnonics. Various types of nanomagnets have been tested as dynamical systems. The SW properties and various operations of magnonic devices have already been demonstrated in those nanomagnets as discussed in this topical review. However, the quest for new types of nanomagnets with emerging properties and new functionalities is still ongoing [271–274]. The recently discovered 2D materials with spontaneous magnetization below and above room temperature have ushered in a renaissance in this field. A huge variety of 2D materials such as metals, semimetals, TIs, semiconductors and insulators have been discovered so far. The breakthrough occurred in 2017 when ferromagnetism in atomically thin CrI<sub>3</sub> [275] and Cr<sub>2</sub>Ge<sub>2</sub>Te<sub>6</sub> [276] layer were experimentally demonstrated. This was quickly followed by the discovery of magnetism in Fe<sub>3</sub>GeTe<sub>2</sub> [277, 278] and FePS<sub>3</sub> [279]. However, the Curie temperature for all of them is well below room temperature. Very recently, magnetism has also been discovered in 2D layers of MnSe<sub>2</sub> [280], VSe<sub>2</sub> [281] and Fe<sub>5</sub>GeTe<sub>2</sub> [282] at room temperature. Due to very weak van der Waals (vdW) interaction, the single layers of 2D materials are easily cleavable from bulk materials and the absence of any dangling bond allows one to stack 2D materials in any sequence with almost perfect interfaces. This creates vast opportunities to study various fascinating phenomena originating at the interfaces, such as PMA [283], Rashba SOC [284] and DMI [285–289]. Being low dimensional systems, the magnetic 2D materials have always become a popular platform to study various quantum aspects of magnons. Also, topological magnonics is another vibrant research field drawing more attention over the past few years [290–292]. All these reports prove that the new materials can show some intriguing properties of magnons and also demonstrate a potential for application in future magnonic devices. However, as of this writing, investigation and control of the SW properties in magnetic 2D materials, especially, in the form of nanostructured arrays, has not been done.

Three-dimensional (3D) nanomagnetism [293] has the potential to revolutionize ultrahigh density data storage

devices, neuromorphic computing, and 2.5D spintronic devices. However, the major challenges in this field are the difficult fabrication and characterization techniques. A combination of various 3D patterning techniques including two-photon lithography, focused electron beam-ion deposition with other physical and electrochemical deposition techniques are being used to grow different kinds of 3D nanomagnets [294, 295]. Investigation of high frequency spin-wave dynamics is another major challenge in these systems and recently TR-MOKE [296] and BLS [297] techniques have been successfully used to investigate the confined and extended SWs in different kinds of 3D magnetic nanostructures. The field is still wide open with huge opportunities both from fundamental and application perspectives and will be a subject of intense interest in the coming years.

Apart from the conventional materials, efforts have also been made to explore new type of materials such as complex organic molecules. They have already been tested for the generation of spin current [298], spin-charge interconversion [299] and for controlling localized spin [300]. In this regard, single molecule magnets have been very popular owing to various potential applications in spintronics [300]. Chiral molecules are promising as another potential candidate for spintronics and possibly for magnonics applications as well. It has been demonstrated that chiral molecules can transport spin current with chosen spin polarization depending upon the handedness of the molecule [301]. This phenomenon, popularly known as chiral-induced spin selectivity (CISS), originates from the centripetal force experienced by the spins of electrons moving through the curvature of the potential energy associated with the chiral molecule. The CISS effect can be used to create magnetic material free magnetic memory [302] and an efficient source of spin current [303]. When chiral molecules are deposited on top of magnetic materials, they can switch the magnetization without the requirement of charge current and magnetic field [304]. The spin current generated by the CISS effect can also be utilized to effectively amplify SWs and to implement STNOs.

Antiferromagnets are also drawing attention because of their huge potential in ultrahigh-frequency spintronics. Although antiferromagnetic materials and their properties drew attention a few decades ago, they were initially thought to be useless due to zero net magnetic moment which makes them invisible to common magnetic probes. However, this common perception has recently been changed after discovering its several advantages over ferromagnetic materials related to spintronics, especially in magnonics [213]. Antiferromagnetic thin films have been tested as efficient spin current generator [305]. Coherent propagating SWs with very short wavelength and very high frequency up to THz can be excited in antiferromagnetic materials [306, 307], which offers the development of ultrafast miniaturized magnonic devices. Moreover, magnon transport up to several micrometers has also been reported in van der Waals antiferromagnets [308]. One interesting advantage of antiferromagnets over ferromagnets is that they can accommodate SWs with both right and left circular polarization. Hence an antiferromagnetic domain wall can be used as the polarizer and

retarder of SWs [309]. Despite all these promises, the study of SWs in aniferromagnetic nanostructures like single and periodic arrays of dots, stripes, wires, antidots have not been done as of this writing. Moreover, suitable methods for controlling, detecting SW and demonstration of SW logic operations in antiferromagnetic materials are still lacking and will be the subject of intense interest in the coming years.

#### 6.2. Hybrid magnonics

The quest for ever increasing functionality of magnonics demands the hybridization of magnons with other entities such as phonons (i.e. lattice vibration in solid), skyrmions, superconducting qubits, fluxons and magnons themselves [310]. The interaction of magnons with phonons, i.e. MPC can give rise to novel device functionalities such as nonreciprocal transport, efficient excitation of magnons, manipulation and amplification of magnons, spin current generation due to lattice vibration and magneto-elastic antennas. The current challenge is to enhance the coupling efficiency between magnons and phonons such that the information can be exchanged back and forth without losing information [311]. The phonons can propagate over much longer distances than magnons and hence can act as pilot waves to steer magnons. Thus MPC can significantly increase the magnon propagation distance or magnon lifetime. Being topologically protected objects, skyrmions can store data with a very high density, carry information and serve even as microwave oscillators. Moreover, periodic arrays of skyrmions can serve as refractor or MCs where the propagation direction and the propagation properties of magnons can be reconfigured. Therefore, presence of skyrmions in a lattice form can significantly influence the magnon properties. Moreover, the study of magnon interaction with other magnetic structures such as magnetic domain walls, magnetic vortices, etc are equally important. Magnon-magnon coupling is another form of hybrid magnonic phenomena having potential in quantum information processing where quantum states can be coherently transferred from one medium to another. Despite the initial progress in magnon-magnon coupling in ferromagnetic heterostructures [312], little has been done to study this phenomenon in arrays of ferromagnetic nanostructures. This is more challenging since the coupling strength varies as the square root of the number of spins in the system, which falls off drastically in nanoscale systems. However, the recent demonstrations of dipolar-coupling mediated moderate to strong magnon-magnon coupling in ferromagnetic nanostructures raise hope in this field [151, 313].

Spin polarized current and pure spin currents have traditionally been used for the amplification of SWs, where the spin polarized current is generated by sending a charge current through ferromagnetic materials and a pure spin current is generated by utilizing the SHE. The orbital angular momentum of electrons has always been neglected. However, the recently discovered orbital Hall effect which represents the generation of a transverse flow of orbital angular momentum by a longitudinally applied electric field can add some new insights in this direction [314, 315]. The orbital torques may be utilized for amplifying SWs and can have great importance for developing novel spin-orbitronic devices.

#### 6.3. Emergent properties and new functionalities of magnons

Another new direction of research in this area is to explore emergent properties of magnons in nanomagnets and demonstration of new functionalities of magnons. The Bose–Einstein condensation of magnons [316, 317], excitation of nuclear SWs, excitation of ultrashort wavelength SW, application of SWs in neuromorphic computing, i.e. the human brain inspired alternative computing architectures, etc are some of those classic examples. Nuclear SWs are a new type of SWs excited in anisotropic antiferromagnet using nuclear magnetic resonance by utilizing the Suhl–Nakamura interaction mechanism [318]. This nuclear SWs can even generate pure spin current into an adjacent metallic layer. It is expected that more studies in this direction will be performed in the near future to show the potential of these nuclear SWs.

Excitation and detection of SWs with shorter wavelength, especially, with the sub-100 nm wavelength and study of their properties are of great importance owing to possible technological applications in faster and miniaturized magnonic devices. However, excitation and detection of exchange dominated shorter SWs has always been very challenging. Several approaches, such as ferromagnetic antennas [319], magnonic nanogratings [320, 321], spin textures [322], parametric pumping [323] etc have been adopted to excite SWs with wavelength below 100 nm. The recent report on the excitation and directional emission of short wavelength exchange SWs by magnetic nanostructures such as skyrmions has fueled interest in this direction [324]. It is anticipated that magnetic nanostructures such as arrays of magnetic dots, antidots, wires and topological spin structures such as skyrmions, domain walls, vortices, etc can be used for the excitation and directional propagation of SWs.

Recently, it has been proposed that SWs can be used in neuromorphic computing by utilizing oscillator, interference and propagation properties [325–327] although actual implementation has remained elusive. Additionally, the study of the quantum properties of SWs in superconductor/ferromagnet hybrid structures [328, 329] and exploring topological magnons [290, 292, 330] are also very interesting new directions of magnonic research. In summary, magnonic devices based on magnetic nanomaterials is a very promising and active research field bristling with the possibility that it may eventually surpass the performance of modern CMOS based electronic devices in some respects. Although many challenges remain, the excitement that permeates this field is likely to propel and take this field to new heights.

#### **Acknowledgments**

The work of BR described in this article was partially supported by RIKEN Incentive Research Project Grant No. FY2019. The work of SB in this field has been supported over the last decade by the US National Science Foundation under

grants ECCS-1124714, CCF-1216614, CMMI-301013, ECCS-1609303, CCF-1815033, CCF-2001255 and CCF-2006843, the Semiconductor Research Corporation under task 2203.001, the State of Virginia CRCF Fund and the Virginia Commonwealth University Commercialization Fund. AB and SB acknowledge travel support from the Indo-US Science and Technology Fund Center Grant titled 'Center for Nanomagnetics for Energy-Efficient Computing, Communications and Data Storage' (IUSSTF/JC-030/2018). AKM thanks the S N Bose National Centre for Basic Sciences for a senior research fellowship.

#### Data availability statement

All data that support the findings of this study are included within the article (and any supplementary files).

#### **ORCID iDs**

Bivas Rana https://orcid.org/0000-0002-1076-4165 Amrit Kumar Mondal https://orcid.org/0000-0003-3038-7253

Supriyo Bandyopadhyay https://orcid.org/0000-0001-6074-1212

Anjan Barman https://orcid.org/0000-0002-4106-5658

#### References

- [1] Mahmoud A, Ciubotaru F, Vanderveken F, Chumak A V, Hamdioui S, Adelmann C and Cotofana S 2020 Introduction to spin wave computing *J. Appl. Phys.* 128 161101
- [2] Neusser S and Grundler D 2009 Magnonics: spin waves on the nanoscale Adv. Mater. 21 2927
- [3] Kruglyak V V, Demokritov S O and Grundler D 2010 Magnonics J. Phys. D: Appl. Phys. 43 260301
- [4] Krawczyk M and Grundler D 2014 Review and prospects of magnonic crystals and devices with reprogrammable band structure J. Phys. Condens. Matter 26 123202
- [5] Chumak A V, Vasyuchka V I, Serga A A and Hillebrands B 2015 Magnon spintronics *Nat. Phys.* 11 453–61
- [6] Bailleul M, Olligs D and Fermon C 2003 Propagating spin wave spectroscopy in a permalloy film: a quantitative analysis Appl. Phys. Lett. 83 972–4
- [7] Rousseau O, Rana B, Anami R, Yamada M, Miura K, Ogawa S and Otani Y 2015 Realization of a micrometrescale spin-wave interferometer *Sci. Rep.* 5 9873
- [8] Rana B, Choudhury S, Miura K, Takahashi H, Barman A and Otani Y 2019 Electric field control of spin waves in ultrathin CoFeB films *Phys. Rev.* B 100 224412
- [9] Baumgaertl K, Gräfe J, Che P, Mucchietto A, Förster J, Träger N, Bechtel M, Weigand M, Schütz G and Grundler D 2020 Nanoimaging of ultrashort magnon emission by ferromagnetic grating couplers at GHz frequencies *Nano Lett.* 20 7281–6
- [10] Dieterle G et al 2019 Coherent excitation of heterosymmetric spin waves with ultrashort wavelengths Phys. Rev. Lett. 122 117202
- [11] Hiebert W, Stankiewicz A and Freeman M 1997 Direct observation of magnetic relaxation in a small permalloy disk

- by time-resolved scanning Kerr microscopy *Phys. Rev. Lett.* **79** 1134–7
- [12] Barman A, Wang S, Maas J D, Hawkins A R, Kwon S, Liddle A, Bokor J and Schmidt H 2006 Magneto-optical observation of picosecond dynamics of single nanomagnets *Nano Lett.* 6 2939–44
- [13] Laraoui A, Vénuat J, Halté V, Albrecht M, Beaurepaire E and Bigot J-Y 2007 Study of individual ferromagnetic disks with femtosecond optical pulses J. Appl. Phys. 101 09C105
- [14] Rana B, Kumar D, Barman S, Pal S, Fukuma Y, Otani Y and Barman A 2011 Detection of picosecond magnetization dynamics of 50 nm magnetic dots down to the single dot regime ACS Nano 5 9559–65
- [15] Gubbiotti G, Tacchi S, Carlotti G, Vavassori P, Singh N, Goolaup S, Adeyeye A O, Stashkevich A and Kostylev M 2005 Magnetostatic interaction in arrays of nanometric permalloy wires: a magneto-optic Kerr effect and a Brillouin light scattering study *Phys. Rev.* B 72 224413
- [16] Gubbiotti G, Tacchi S, Carlotti G, Singh N, Goolaup S, Adeyeye A O and Kostylev M 2007 Collective spin modes in monodimensional magnonic crystals consisting of dipolarly coupled nanowires Appl. Phys. Lett. 90 092503
- [17] Saha S, Barman S, Otani Y and Barman A 2015 All-optical investigation of tunable picosecond magnetization dynamics in ferromagnetic nanostripes with a width down to 50 nm *Nanoscale* 7 18312–9
- [18] Banerjee C, Choudhury S, Sinha J and Barman A 2017 Pseudo-one-dimensional magnonic crystals for highfrequency nanoscale devices *Phys. Rev. Appl.* 8 014036
- [19] Shaw J M, Silva T J, Schneider M L and McMichael R D 2009 Spin dynamics and mode structure in nanomagnet arrays: effects of size and thickness on linewidth and damping *Phys. Rev.* B 79 184404
- [20] Mahato B K, Rana B, Mandal R, Kumar D, Barman S, Fukuma Y, Otani Y and Barman A 2013 Configurational anisotropic spin waves in cross-shaped Ni80Fe20 nanoelements Appl. Phys. Lett. 102 192402
- [21] Mondal A K, Banerjee C, Adhikari A, Chaurasiya A K, Choudhury S, Sinha J, Barman S and Barman A 2020 Spintexture driven reconfigurable magnonics in chains of connected Ni80Fe20 submicron dots *Phys. Rev.* B 101 224426
- [22] Buchanan K S, Zhu X, Meldrum A and Freeman M R 2005 Ultrafast dynamics of a ferromagnetic nanocomposite *Nano Lett.* 5 383–7
- [23] Rana B and Barman A 2015 Ultrafast magnetization dynamics of chemically synthesized Ni nanoparticles J. Phys. Chem. C 119 17444–9
- [24] Martyanov O N, Yudanov V F, Lee R N, Nepijko S A, Elmers H J, Hertel R, Schneider C M and Schönhense G 2007 Ferromagnetic resonance study of thin film antidot arrays: experiment and micromagnetic simulations *Phys. Rev.* B 75 174429
- [25] Mandal R, Saha S, Kumar D, Barman S, Pal S, Das K, Raychaudhuri A K, Fukuma Y, Otani Y and Barman A 2012 Optically induced tunable magnetization dynamics in nanoscale Co antidot lattices ACS Nano 6 3397–403
- [26] Pal S, Saha S, Kamalakar M V and Barman A 2016 Field-dependent spin waves in high-aspect-ratio single-crystal ferromagnetic nanowires *Nano Res.* 9 1426–33
- [27] Haldar A, Kumar D and Adeyeye A O 2016 A reconfigurable waveguide for energy-efficient transmission and local manipulation of information in a nanomagnetic device *Nat. Nanotechnol.* 11 437–43
- [28] Chumak A V, Serga A A and Hillebrands B 2017 Magnonic crystals for data processing J. Phys. D: Appl. Phys. 50 244001

- [29] Rana B and Otani Y 2018 Voltage-controlled reconfigurable spin-wave nanochannels and logic devices *Phys. Rev. Appl.* 9 014033
- [30] Wang Q, Pirro P, Verba R, Slavin A, Hillebrands B and Chumak A V 2018 Reconfigurable nanoscale spin-wave directional coupler Sci. Adv. 4 e1701517
- [31] Szulc K, Graczyk P, Mruczkiewicz M, Gubbiotti G and Krawczyk M 2020 Spin-wave diode and circulator based on unidirectional coupling *Phys. Rev. Appl.* 14 034063
- [32] Xing X, Zhou Y and Braun H B 2020 Magnetic skyrmion tubes as nonplanar magnonic waveguides *Phys. Rev. Appl.* 13 034051
- [33] Rana B and Otani Y 2019 Towards magnonic devices based on voltage-controlled magnetic anisotropy *Commun. Phys.* 2 90
- [34] Covington M, Crawford T M and Parker G J 2002 Timeresolved measurement of propagating spin waves in ferromagnetic thin films *Phys. Rev. Lett.* 89 237202
- [35] Demidov V E, Demokritov S O, Hillebrands B, Laufenberg M and Freitas P P 2004 Radiation of spin waves by a single micrometer-sized magnetic element *Appl. Phys.* Lett. 85 2866–8
- [36] Yu H, Huber R, Schwarze T, Brandl F, Rapp T, Berberich P, Duerr G and Grundler D 2012 High propagating velocity of spin waves and temperature dependent damping in a CoFeB thin film Appl. Phys. Lett. 100 262412
- [37] Demidov V E, Demokritov S O, Birt D, O'Gorman B, Tsoi M and Li X 2009 Radiation of spin waves from the open end of a microscopic magnetic-film waveguide *Phys. Rev.* B 80 014429
- [38] Mahato B K, Choudhury S, Mandal R, Barman S, Otani Y and Barman A 2015 Tunable configurational anisotropy in collective magnetization dynamics of Ni80Fe20 nanodot arrays with varying dot shapes *J. Appl. Phys.* 117 213909
- [39] Khasanvis S, Li M, Rahman M, Biswas A K, Salehi-Fashami M, Atulasimha J, Bandyopadhyay S and Moritz C A 2015 Architecting for causal intelligence at nanoscale *Computer* 48 54–64
- [40] Deac A M, Fukushima A, Kubota H, Maehara H, Suzuki Y, Yuasa S, Nagamine Y, Tsunekawa K, Djayaprawira D D and Watanabe N 2008 Bias-driven high-power microwave emission from MgO-based tunnel magnetoresistance devices *Nat. Phys.* 4 803–9
- [41] Chen T, Dumas R K, Eklund A, Muduli P K, Houshang A, Awad A A, Dürrenfeld P, Malm B G, Rusu A and Åkerman J 2016 Spin-torque and spin-Hall nano-oscillators Proc. IEEE 104 1919–45
- [42] Dutta S, Chang S-C, Kani N, Nikonov D E, Manipatruni S, Young I A and Naeemi A 2015 Non-volatile clocked spin wave interconnect for beyond-CMOS nanomagnet pipelines Sci. Rep. 5 9861
- [43] Hellman F et al 2017 Interface-induced phenomena in magnetism Rev. Mod. Phys. 89 025006
- [44] Ikeda S, Miura K, Yamamoto H, Mizunuma K, Gan H D, Endo M, Kanai S, Hayakawa J, Matsukura F and Ohno H 2010 A perpendicular-anisotropy CoFeB–MgO magnetic tunnel junction *Nat. Mater.* 9 721–4
- [45] Maruyama T et al 2009 Large voltage-induced magnetic anisotropy change in a few atomic layers of iron Nat. Nanotechnol. 4 158–61
- [46] Belmeguenai M, Adam J-P, Roussigné Y, Eimer S, Devolder T, Kim J-V, Cherif S M, Stashkevich A and Thiaville A 2015 Interfacial Dzyaloshinskii-Moriya interaction in perpendicularly magnetized Pt/Co/AlOx ultrathin films measured by Brillouin light spectroscopy *Phys. Rev.* B 91 180405

- [47] Cho J et al 2015 Thickness dependence of the interfacial Dzyaloshinskii–Moriya interaction in inversion symmetry broken systems Nat. Commun. 6 7635
- [48] Chaurasiya A K, Banerjee C, Pan S, Sahoo S, Choudhury S, Sinha J and Barman A 2016 Direct observation of interfacial Dzyaloshinskii-Moriya interaction from asymmetric spinwave propagation in W/CoFeB/SiO2 heterostructures down to sub-nanometer CoFeB thickness Sci. Rep. 6 32592
- [49] Puebla J, Auvray F, Xu M, Rana B, Albouy A, Tsai H, Kondou K, Tatara G and Otani Y 2017 Direct optical observation of spin accumulation at nonmagnetic metal/ oxide interface Appl. Phys. Lett. 111 092402
- [50] Lesne E et al 2016 Highly efficient and tunable spin-to-charge conversion through Rashba coupling at oxide interfaces Nat. Mater. 15 1261
- [51] Rana B, Akosa C A, Miura K, Takahashi H, Tatara G and Otani Y 2020 Nonlinear control of damping constant by electric field in ultrathin ferromagnetic films *Phys. Rev. Appl.* 14 014037
- [52] Cowburn R P, Koltsov D K, Adeyeye A O, Welland M E and Tricker D M 1999 Single-domain circular nanomagnets Phys. Rev. Lett. 83 1042–5
- [53] Wu Y, Wang Y, Qin X, Rong X and Du J 2019 A programmable two-qubit solid-state quantum processor under ambient conditions npj Quantum Inf. 5 9
- [54] Xu C, Feng J, Prokhorenko S, Nahas Y, Xiang H and Bellaiche L 2020 Topological spin texture in Janus monolayers of the chromium trihalides Cr(I, X)3 Phys. Rev. B 101 060404
- [55] Bandyopadhyay S and Cahay M 2009 Electron spin for classical information processing: a brief survey of spinbased logic devices, gates and circuits *Nanotechnology* 20 412001
- [56] Khitun A, Bao M and Wang K L 2010 Magnonic logic circuits J. Phys. D: Appl. Phys. 43 264005
- [57] Datta S and Das B 1990 Electronic analog of the electro-optic modulator Appl. Phys. Lett. 56 665–7
- [58] Bandyopadhyay S and Cahay M 2004 Alternate spintronic analog of the electro-optic modulator Appl. Phys. Lett. 85 1814–6
- [59] Ralph D C 2011 The electromotive force of MnAs nanoparticles *Nature* 474 E6–6
- [60] Ganichev S D 2008 Spin-galvanic effect and spin orientation by current in non-magnetic semiconductors *J. Mod. Phys.* B 22 1–26
- [61] Salahuddin S and Datta S 2006 Electrical detection of spin excitations *Phys. Rev.* B 73 081301
- [62] Md Iftekhar H, Bandyopadhyay S, Atulasimha J and Bandyopadhyay S 2015 Modulating spin relaxation in nanowires with infrared light at room temperature *Nanotechnology* 26 281001
- [63] Hirohata A and Takanashi K 2014 Future perspectives for spintronic devices J. Phys. D: Appl. Phys. 47 193001
- [64] Bandyopadhyay S and Cahay M 2015 Introduction to Spintronics 2nd edn (Boca Raton, FL: CRC Press)
- [65] Barman A and Sinha J 2018 Spin Dynamics and Damping in Ferromagnetic Thin Films and Nanostructures (Cham, Switzerland: Springer) (https://doi.org/10.1007/978-3-319-66296-1)
- [66] Yu H, d' Allivy Kelly O, Cros V, Bernard R, Bortolotti P, Anane A, Brandl F, Heimbach F and Grundler D 2016 Approaching soft x-ray wavelengths in nanomagnet-based microwave technology Nat. Commun. 7 11255
- [67] Demidov V E, Demokritov S O, Rott K, Krzysteczko P and Reiss G 2008 Mode interference and periodic self-focusing of spin waves in permalloy microstripes *Phys. Rev.* B 77 064406

- [68] Barman A, Kimura T, Otani Y, Fukuma Y, Akahane K and Meguro S 2008 Benchtop time-resolved magneto-optical Kerr magnetometer Rev. Sci. Instrum. 79 123905
- [69] Kalarickal S S, Krivosik P, Wu M, Patton C E, Schneider M L, Kabos P, Silva T J and Nibarger J P 2006 Ferromagnetic resonance linewidth in metallic thin films: comparison of measurement methods J. Appl. Phys. 99 093909
- [70] Patton C E 1968 Linewidth and relaxation processes for the main resonance in the spin-wave spectra of Ni–Fe alloy films J. Appl. Phys. 39 3060–8
- [71] Madami M, Bonetti S, Consolo G, Tacchi S, Carlotti G, Gubbiotti G, Mancoff F B, Yar M A and Akerman J 2011 Direct observation of a propagating spin wave induced by spin-transfer torque *Nat. Nanotechnol.* 6 635–8
- [72] Demidov V E, Urazhdin S, Liu R, Divinskiy B, Telegin A and Demokritov S O 2016 Excitation of coherent propagating spin waves by pure spin currents *Nat. Commun.* 7 10446
- [73] Savochkin I V et al 2017 Generation of spin waves by a train of fs-laser pulses: a novel approach for tuning magnon wavelength Sci. Rep. 7 5668
- [74] Rana B, Fukuma Y, Miura K, Takahashi H and Otani Y 2017 Excitation of coherent propagating spin waves in ultrathin CoFeB film by voltage-controlled magnetic anisotropy Appl. Phys. Lett. 111 052404
- [75] Kos A B, Silva T J and Kabos P 2002 Pulsed inductive microwave magnetometer Rev. Sci. Instrum. 73 3563–9
- [76] Au Y, Ahmad E, Dmytriiev O, Dvornik M, Davison T and Kruglyak V V 2012 Resonant microwave-to-spin-wave transducer Appl. Phys. Lett. 100 182404
- [77] Poimanov V D, Kuchko A N and Kruglyak V V 2018 Magnetic interfaces as sources of coherent spin waves *Phys. Rev.* B 98 104418
- [78] Divinskiy B, Demidov V E, Urazhdin S, Freeman R, Rinkevich A B and Demokritov S O 2018 Excitation and amplification of spin waves by spin–orbit torque *Adv. Mater.* 30 1802837
- [79] Rana B and Barman A 2013 Magneto-optical measurements of collective spin dynamics of two-dimensional arrays of ferromagnetic nanoelements SPIN 03 1330001
- [80] Ando Y, Lee Y M, Aoki T, Miyazaki T, Schultheiß H and Hillebrands B 2007 Thermally excited spin wave modes in synthetic antiferromagnetic stripes J. Magn. Magn. Mater. 310 1949–51
- [81] Nozaki T et al 2012 Electric-field-induced ferromagnetic resonance excitation in an ultrathin ferromagnetic metal layer Nat. Phys. 8 491–6
- [82] Zhu J *et al* 2012 Voltage-induced ferromagnetic resonance in magnetic tunnel junctions *Phys. Rev. Lett.* **108** 197203
- [83] Khitun A and Wang K L 2011 Non-volatile magnonic logic circuits engineering J. Appl. Phys. 110 034306
- [84] Zografos O, Raghavan P, Sherazi Y, Vaysset A, Ciubatoru F, Sorée B, Lauwereins R, Radu I and Thean A 2015 Area and routing efficiency of SWD circuits compared to advanced CMOS (1-3 June 2015 pp 1-4
- [85] Demidov V E, Urazhdin S and Demokritov S O 2010 Direct observation and mapping of spin waves emitted by spintorque nano-oscillators *Nat. Mater.* 9 984–8
- [86] Chang L-J et al 2020 Spin wave injection and propagation in a magnetic nanochannel from a vortex core Nano Lett. 20 3140-6
- [87] Vlaminck V and Bailleul M 2010 Spin-wave transduction at the submicrometer scale: experiment and modeling *Phys. Rev.* B 81 014425
- [88] Shukla A S, Chouhan A, Pandey R, Raghupathi M, Yamamoto T, Kubota H, Fukushima A, Yuasa S, Nozaki T and Tulapurkar A A 2020 Generation of charge current from magnetization oscillation via the inverse of

- voltage-controlled magnetic anisotropy effect Sci. Adv. 6 eabc2618
- [89] Demokritov S O, Hillebrands B and Slavin A N 2001 Brillouin light scattering studies of confined spin waves: linear and nonlinear confinement *Phys. Rep.* 348 441–89
- [90] van der Sar T, Casola F, Walsworth R and Yacoby A 2015 Nanometre-scale probing of spin waves using single electron spins Nat. Commun. 6 7886
- [91] Klein O, de Loubens G, Naletov V V, Boust F, Guillet T, Hurdequint H, Leksikov A, Slavin A N, Tiberkevich V S and Vukadinovic N 2008 Ferromagnetic resonance force spectroscopy of individual submicron-size samples *Phys. Rev.* B 78 144410
- [92] An T et al 2013 Unidirectional spin-wave heat conveyer Nat. Mater. 12 549–53
- [93] Bocklage L, Swoboda C, Schlage K, Wille H-C, Dzemiantsova L, Bajt S, Meier G and Röhlsberger R 2015 Spin precession mapping at ferromagnetic resonance via nuclear resonant scattering of synchrotron radiation *Phys. Rev. Lett.* 114 147601
- [94] Martin T, Woltersdorf G, Stamm C, Dürr H A, Mattheis R, Back C H and Bayreuther G 2008 Layer resolved magnetization dynamics in interlayer exchange coupled Ni81Fe19/Ru/Co90Fe10 by time resolved x-ray magnetic circular dichroism J. Appl. Phys. 103 07B112
- [95] Jorzick J, Demokritov S O, Hillebrands B, Bailleul M, Fermon C, Guslienko K Y, Slavin A N, Berkov D V and Gorn N L 2002 Spin wave wells in nonellipsoidal micrometer size magnetic elements *Phys. Rev. Lett.* 88 047204
- [96] Barman A, Kruglyak V V, Hicken R J, Kundrotaite A and Rahman M 2003 Anisotropy, damping, and coherence of magnetization dynamics in a 10 μm square Ni81Fe19 element *Appl. Phys. Lett.* 82 3065–7
- [97] Barman A, Kruglyak V V, Hicken R J, Kundrotaite A and Rahman M 2003 Observation of incoherent picosecond magnetisation dynamics in micron sized Ni81Fe19 elements by time resolved scanning Kerr effect microscopy *IIEE Proc.-Sci. Meas. Technol.* 150 260–3
- [98] Barman A, Kruglyak V V, Hicken R J, Rowe J M, Kundrotaite A, Scott J and Rahman M 2004 Imaging the dephasing of spin wave modes in a square thin film magnetic element *Phys. Rev.* B 69 174426
- [99] Barman A, Kruglyak V V, Hicken R J, Kundrotaite A and Rahman M 2004 Shape-dependent anisotropy and damping of picosecond magnetisation dynamics in a micron sized Ni81Fe19 element J. Magn. Magn. Mater. 272–276 2121–2
- [100] Barman A, Kruglyak V V, Hicken R J, Scott J, Kundrotaite A and Rahman M 2004 Dependence of anisotropy and damping on shape and aspect ratio in micron sized Ni81Fe19 elements J. Appl. Phys. 95 6998–7000
- sized Ni81Fe19 elements *J. Appl. Phys.* **95** 6998–7000 [101] Barman A and Sharma R C 2007 Micromagnetic study of picosecond dephasing of spin waves in a square magnetic element *J. Appl. Phys.* **102** 053912
- [102] Belov M, Liu Z, Sydora R D and Freeman M R 2004 Modal oscillation control in internally patterned Ni80Fe20 thin film microstructures *Phys. Rev.* B 69 094414
- [103] Barman A, Kruglyak V V, Hicken R J, Scott J and Rahman M 2005 Dependence of spatial coherence of coherent suppression of magnetization precession upon aspect ratio in Ni81Fe19 microdots J. Appl. Phys. 97 10A710
- [104] Jung S, Watkins B, DeLong L, Ketterson J B and Chandrasekhar V 2002 Ferromagnetic resonance in periodic particle arrays *Phys. Rev.* B 66 132401
- [105] Gubbiotti G, Carlotti G, Okuno T, Shinjo T, Nizzoli F and Zivieri R 2003 Brillouin light scattering investigation of dynamic spin modes confined in cylindrical Permalloy dots *Phys. Rev.* B 68 184409

- [106] Ney A, Pampuch C, Koch R and Ploog K H 2003 Programmable computing with a single magnetoresistive element *Nature* 425 485–7
- [107] Koch R H, Katine J A and Sun J Z 2004 Time-resolved reversal of spin-transfer switching in a nanomagnet *Phys. Rev. Lett.* 92 088302
- [108] Krivorotov I N, Emley N C, Sankey J C, Kiselev S I, Ralph D C and Buhrman R A 2005 Time-domain measurements of nanomagnet dynamics driven by spintransfer torques *Science* 307 228
- [109] Slonczewski J C 1996 Current-driven excitation of magnetic multilayers J. Magn. Magn. Mater. 159 L1-7
- [110] Acremann Y, Strachan J P, Chembrolu V, Andrews S D, Tyliszczak T, Katine J A, Carey M J, Clemens B M, Siegmann H C and Stöhr J 2006 Time-resolved imaging of spin transfer switching: Beyond the macrospin concept Phys. Rev. Lett. 96 217202
- [111] Laraoui A, Halté V, Vomir M, Vénuat J, Albrecht M, Beaurepaire E and Bigot J-Y 2007 Ultrafast spin dynamics of an individual CoPt3 ferromagnetic dot Eur. Phys. J. D 43 251–3
- [112] Liu Z, Sydora R D and Freeman M R 2008 Shape effects on magnetization state transitions in individual 160-nm diameter Permalloy disks *Phys. Rev.* B 77 174410
- [113] Gao D, Yang G, Zhang J, Zhu Z, Si M and Xue D 2011 d0 ferromagnetism in undoped sphalerite ZnS nanoparticles Appl. Phys. Lett. 99 052502
- [114] Naletov V V et al 2011 Identification and selection rules of the spin-wave eigenmodes in a normally magnetized nanopillar Phys. Rev. B 84 224423
- [115] Keatley P S, Gangmei P, Dvornik M, Hicken R J, Childress J R and Katine J A 2011 Large amplitude magnetization dynamics and the suppression of edge modes in a single nanomagnet Appl. Phys. Lett. 98 082506
- [116] Demidov V E, Urazhdin S, Ulrichs H, Tiberkevich V, Slavin A, Baither D, Schmitz G and Demokritov S O 2012 Magnetic nano-oscillator driven by pure spin current *Nat. Mater.* 11 1028
- [117] Berk C, Jaris M, Yang W, Dhuey S, Cabrini S and Schmidt H 2019 Strongly coupled magnon–phonon dynamics in a single nanomagnet *Nat. Commun.* 10 2652
- [118] Sampath V, D'Souza N, Atkinson G. M., Bandyopadhyay S and Atulasimha J 2016 Experimental demonstration of acoustic wave induced magnetization switching in dipole coupled magnetostrictive nanomagnets for ultralow power computing Appl. Phys. Lett. 109 102403
- [119] Mondal S, Abeed M A, Dutta K, De A, Sahoo S, Barman A and Bandyopadhyay S 2018 Hybrid magnetodynamical modes in a single magnetostrictive nanomagnet on a piezoelectric substrate arising from magnetoelastic modulation of precessional dynamics ACS Appl. Mater. Interfaces 10 43970–7
- [120] Barman A, Mondal S, Sahoo S and De A 2020 Magnetization dynamics of nanoscale magnetic materials: a perspective J. Appl. Phys. 128 170901
- [121] Goolaup S, Adeyeye A O, Singh N and Gubbiotti G 2007 Magnetization switching in alternating width nanowire arrays *Phys. Rev.* B 75 144430
- [122] Tacchi S, Madami M, Gubbiotti G, Carlotti G, Goolaup S, Adeyeye A O, Singh N and Kostylev M P 2010 Analysis of collective spin-wave modes at different points within the hysteresis loop of a one-dimensional magnonic crystal comprising alternative-width nanostripes *Phys. Rev.* B 82 184408
- [123] Topp J, Heitmann D, Kostylev M P and Grundler D 2010 Making a reconfigurable artificial crystal by ordering bistable magnetic nanowires *Phys. Rev. Lett.* 104 207205
- [124] Kostylev M, Schrader P, Stamps R L, Gubbiotti G, Carlotti G, Adeyeye A O, Goolaup S and Singh N 2008 Partial

- frequency band gap in one-dimensional magnonic crystals *Appl. Phys. Lett.* **92** 132504
- [125] Wang Z K, Zhang V L, Lim H S, Ng S C, Kuok M H, Jain S and Adeyeye A O 2009 Observation of frequency band gaps in a one-dimensional nanostructured magnonic crystal Appl. Phys. Lett. 94 083112
- [126] Wang Z K, Zhang V L, Lim H S, Ng S C, Kuok M H, Jain S and Adeyeye A O 2010 Nanostructured magnonic crystals with size-tunable bandgaps ACS Nano 4 643–8
- [127] Gubbiotti G, Tacchi S, Madami M, Carlotti G, Yang Z, Ding J, Adeyeye A O and Kostylev M 2016 Collective spin excitations in bicomponent magnonic crystals consisting of bilayer permalloy/Fe nanowires *Phys. Rev.* B 93 184411
- [128] Gubbiotti G, Silvani R, Tacchi S, Madami M, Carlotti G, Yang Z, Adeyeye A O and Kostylev M 2017 Tailoring the spin waves band structure of 1D magnonic crystals consisting of L-shaped iron/permalloy nanowires J. Phys. D: Appl. Phys. 50 105002
- [129] Gubbiotti G, Zhou X, Adeyeye A O, Varvaro G and Kostylev M 2020 Effect of exchange and dipolar interlayer interactions on the magnonic band structure of dense Fe/ Cu/Py nanowires with symmetric and asymmetric layer widths *Phys. Rev.* B 101 224431
- [130] Stamps R L and Camley R E 1998 Frustration and finite size effects of magnetic dot arrays J. Magn. Magn. Mater. 177–181 813–4
- [131] Stamps R L and Camley R E 1999 High-frequency response and reversal dynamics of two-dimensional magnetic dot arrays *Phys. Rev.* B 60 12264–9
- [132] Gubbiotti G, Albini L, Carlotti G, Crescenzi M D, Fabrizio E D, Gerardino A, Donzelli O, Nizzoli F, Koo H and Gomez R D 2000 Finite size effects in patterned magnetic permalloy films J. Appl. Phys. 87 5633–5
- [133] Giovannini L, Montoncello F, Nizzoli F, Gubbiotti G, Carlotti G, Okuno T, Shinjo T and Grimsditch M 2004 Spin excitations of nanometric cylindrical dots in vortex and saturated magnetic states *Phys. Rev.* B 70 172404
- [134] Kakazei G N, Wigen P E, Guslienko K Y, Novosad V, Slavin A N, Golub V O, Lesnik N A and Otani Y 2004 Spinwave spectra of perpendicularly magnetized circular submicron dot arrays Appl. Phys. Lett. 85 443–5
- [135] Kruglyak V V, Barman A, Hicken R J, Childress J R and Katine J A 2005 Precessional dynamics in microarrays of nanomagnets J. Appl. Phys. 97 10A706
- [136] Kruglyak V V, Barman A, Hicken R J, Childress J R and Katine J A 2005 Picosecond magnetization dynamics in nanomagnets: crossover to nonuniform precession *Phys. Rev.* B 71 220409
- [137] Kruglyak V V, Keatley P S, Hicken R J, Childress J R and Katine J A 2007 Dynamic configurational anisotropy in nanomagnets *Phys. Rev.* B 75 024407
- [138] Rana B, Kumar D, Barman S, Pal S, Mandal R, Fukuma Y, Otani Y, Sugimoto S and Barman A 2012 Anisotropy in collective precessional dynamics in arrays of Ni80Fe20 nanoelements J. Appl. Phys. 111 07D503
- [139] Saha S, Mandal R, Barman S, Kumar D, Rana B, Fukuma Y, Sugimoto S, Otani Y and Barman A 2013 Tunable magnonic spectra in two-dimensional magnonic crystals with variable lattice symmetry Adv. Funct. Mater. 23 2378–86
- [140] Saha S, Barman S, Sugimoto S, Otani Y and Barman A 2015 Tunable picosecond spin dynamics in two dimensional ferromagnetic nanodot arrays with varying lattice symmetry RSC Adv. 5 34027–31
- [141] Choudhury S, Barman S, Otani Y and Barman A 2017 Efficient modulation of spin waves in two-dimensional octagonal magnonic crystal ACS Nano 11 8814–21
- [142] Mahato B K, Rana B, Kumar D, Barman S, Sugimoto S, Otani Y and Barman A 2014 Tunable spin wave dynamics

- in two-dimensional Ni80Fe20 nanodot lattices by varying dot shape *Appl. Phys. Lett.* **105** 012406
- [143] Choudhury S, Saha S, Mandal R, Barman S, Otani Y and Barman A 2016 Shape- and interface-induced control of spin dynamics of two-dimensional bicomponent magnonic crystals ACS Appl. Mater. Interfaces 8 18339–46
- [144] Rana B, Pal S, Barman S, Fukuma Y, Otani Y and Barman A 2011 All-optical excitation and detection of picosecond dynamics of ordered arrays of nanomagnets with varying areal density Appl. Phys. Express 4 113003
- [145] Mondal S, Choudhury S, Barman S, Otani Y and Barman A 2016 Transition from strongly collective to completely isolated ultrafast magnetization dynamics in twodimensional hexagonal arrays of nanodots with varying inter-dot separation RSC Adv. 6 110393–9
- [146] Ciuciulkaite A, Östman E, Brucas R, Kumar A, Verschuuren M A, Svedlindh P, Hjörvarsson B and Kapaklis V 2019 Collective magnetization dynamics in nanoarrays of thin FePd disks *Phys. Rev.* B 99 184415
- [147] Choudhury S, Pan S, Barman S, Otani Y and Barman A 2019 Anisotropic spin waves in two-dimensional triangular shaped bi-component magnonic crystal J. Magn. Magn. Mater. 490 165484
- [148] Kruglyak V V, Keatley P S, Neudert A, Hicken R J, Childress J R and Katine J A 2010 Imaging collective magnonic modes in 2D arrays of magnetic nanoelements *Phys. Rev. Lett.* 104 027201
- [149] Adhikari K, Choudhury S, Mandal R, Barman S, Otani Y and Barman A 2017 Bias field tunable magnetic configuration and magnetization dynamics in Ni80Fe20 nano-cross structures with varying arm length *J. Appl. Phys.* 121 043909
- [150] Adhikari K, Barman S, Mandal R, Otani Y and Barman A 2018 Tunable angle-dependent magnetization dynamics in Ni80Fe20 nanocross structures of varying size *Phys. Rev.* Appl. 10 044010
- [151] Adhikari K, Sahoo S, Mondal A K, Otani Y and Barman A 2020 Large nonlinear ferromagnetic resonance shift and strong magnon-magnon coupling in Ni80Fe20 nanocross array Phys. Rev. B 101 054406
- [152] De A, Mondal S, Banerjee C, Chaurasiya A K, Mandal R, Otani Y, Mitra R K and Barman A 2017 Investigation of magnetization dynamics in 2D Ni80Fe20 diatomic nanodot arrays J. Phys. D: Appl. Phys. 50 385002
- [153] De A, Banerjee C, Kumar Chaurasiya A, Mandal R, Otani Y, Kumar Mitra R and Barman A 2019 Anisotropic spin-wave dispersion in two-dimensional Ni80Fe20 diatomic nanodot array J. Magn. Magn. Mater. 491 165557
- [154] Porwal N, Dutta K, Mondal S, Choudhury S, Sinha J, Barman A and Datta P K 2020 Observation of spectral narrowing and mode conversion in two-dimensional binary magnonic crystal J. Magn. Magn. Mater. 501 166378
- [155] Abeed M A, Sahoo S, Winters D, Barman A and Bandyopadhyay S 2019 The effect of material defects on resonant spin wave modes in a nanomagnet *Sci. Rep.* 9
- [156] Bhat V S, Heimbach F, Stasinopoulos I and Grundler D 2016 Magnetization dynamics of topological defects and the spin solid in a kagome artificial spin ice *Phys. Rev.* B 93 140401
- [157] Sokolovskyy M L and Krawczyk M 2011 The magnetostatic modes in planar one-dimensional magnonic crystals with nanoscale sizes J. Nanopart. Res. 13 6085–91
- [158] Lisiecki F et al 2019 Reprogrammability and scalability of magnonic Fibonacci quasicrystals Phys. Rev. Appl. 11 054003
- [159] Mieszczak S, Busel O, Gruszecki P, Kuchko A N, Kłos J W and Krawczyk M 2020 Anomalous refraction of spin waves as a way to guide signals in curved magnonic multimode waveguides *Phys. Rev. Appl.* 13 054038

- [160] Adhikari A, Banerjee C, Mondal A K, Chaurasiya A K, Choudhury S, Sinha J, Barman S and Barman A 2021 Anisotropic spin-wave propagation in asymmetric width modulated Ni80Fe20 nanostripes *Mater. Sci. Eng.* B 272 115385
- [161] Sahoo S, Panda S N, Barman S, Otani Y and Barman A 2021 Nanochannels for spin-wave manipulation in Ni80Fe20 nanodot arrays J. Magn. Magn. Mater. 522 167550
- [162] Mouadili A, Boudouti E H E, Akjouj A, Al-Wahsh H, Djafari-Rouhani B and Dobrzynski L 2019 Y-shaped magnonic demultiplexer using induced transparency resonances AIP Adv. 9 035011
- [163] Gartside J C, Arroo D M, Burn D M, Bemmer V L, Moskalenko A, Cohen L F and Branford W R 2018 Realization of ground state in artificial kagome spin ice via topological defect-driven magnetic writing *Nat*. *Nanotechnol.* 13 53–8
- [164] Kumar D, Dmytriiev O, Ponraj S and Barman A 2011 Numerical calculation of spin wave dispersions in magnetic nanostructures J. Phys. D: Appl. Phys. 45 015001
- [165] Hillebrands B, Mathieu C, Bauer M, Demokritov S O, Bartenlian B, Chappert C, Decanini D, Rousseaux F and Carcenac F 1997 Brillouin light scattering investigations of structured permalloy films J. Appl. Phys. 81 4993–5
- [166] Krawczyk M and Puszkarski H 2008 Plane-wave theory of three-dimensional magnonic crystals *Phys. Rev.* B 77 054437
- [167] Grimsditch M, Giovannini L, Montoncello F, Nizzoli F, Leaf G K and Kaper H G 2004 Magnetic normal modes in ferromagnetic nanoparticles: a dynamical matrix approach *Phys. Rev.* B 70 054409
- [168] Donahue M J and Porter D G 1999 OOMMF User's Guide, Version 1.0, Interagency Report NISTIR 6376 (Gaithersburg, MD: National Institute of Standards and Technology)
- [169] Vansteenkiste A, Leliaert J, Dvornik M, Helsen M, Garcia-Sanchez F and Waeyenberge B V 2014 The design and verification of MuMax3 AIP Adv. 4 107133
- [170] Vasseur J O, Dobrzynski L, Djafari-Rouhani B and Puszkarski H 1996 Magnon band structure of periodic composites *Phys. Rev.* B 54 1043–9
- [171] Barman A, Wang S, Maas J, Hawkins A R, Kwon S, Bokor J, Liddle A and Schmidt H 2007 Size dependent damping in picosecond dynamics of single nanomagnets *Appl. Phys.* Lett. 90 202504
- [172] Gubbiotti G et al 2014 Collective spin waves on a nanowire array with step-modulated thickness J. Phys. D: Appl. Phys. 47 105003
- [173] Gubbiotti G, Zhou X, Haghshenasfard Z, Cottam M G, Adeyeye A O and Kostylev M 2019 Interplay between intraand inter-nanowires dynamic dipolar interactions in the spin wave band structure of Py/Cu/Py nanowires Sci. Rep. 9 4617
- [174] Zivieri R, Montoncello F, Giovannini L, Nizzoli F, Tacchi S, Madami M, Gubbiotti G, Carlotti G and Adeyeye A O 2011 Collective spin modes in chains of dipolarly interacting rectangular magnetic dots *Phys. Rev.* B 83 054431
- [175] Kostylev M, Zhong S, Ding J and Adeyeye A O 2013 Resonance properties of bi-component arrays of magnetic dots magnetized perpendicular to their planes *J. Appl. Phys.* 114 113910
- [176] Mondal S, Barman S, Choudhury S, Otani Y and Barman A 2018 Influence of anisotropic dipolar interaction on the spin dynamics of Ni80Fe20 nanodot arrays arranged in honeycomb and octagonal lattices J. Magn. Magn. Mater. 458 95–104
- [177] De A, Mondal S, Choudhury S, Sahoo S, Majumder S, Barman S, Otani Y and Barman A 2019 Shape dependent high frequency spin-wave dynamics in nanoscale magnonic crystals J. Magn. Magn. Mater. 487 165263

- [178] Nozaki T, Shiota Y, Shiraishi M, Shinjo T and Suzuki Y 2010 Voltage-induced perpendicular magnetic anisotropy change in magnetic tunnel junctions Appl. Phys. Lett. 96 022506
- [179] Witold S, Takayuki N, Yoichi S, Shingo T, Kay Y, Hitoshi K, Akio F, Shinji Y and Yoshishige S 2015 Perpendicular magnetic anisotropy of Ir/CoFeB/MgO trilayer system tuned by electric fields Appl. Phys. Express 8 053003
- [180] Kanai S, Gajek M, Worledge D C, Matsukura F and Ohno H 2014 Electric field-induced ferromagnetic resonance in a CoFeB/MgO magnetic tunnel junction under dc bias voltages Appl. Phys. Lett. 105 242409
- [181] Nawaoka K, Shiota Y, Miwa S, Tomita H, Tamura E, Mizuochi N, Shinjo T and Suzuki Y 2015 Voltage modulation of propagating spin waves in Fe J. Appl. Phys. 117 17A905
- [182] Okada A, Kanai S, Yamanouchi M, Ikeda S, Matsukura F and Ohno H 2014 Electric-field effects on magnetic anisotropy and damping constant in Ta/CoFeB/MgO investigated by ferromagnetic resonance Appl. Phys. Lett. 105 052415
- [183] Fulara H, Zahedinejad M, Khymyn R, Dvornik M, Fukami S, Kanai S, Ohno H and Åkerman J 2020 Giant voltagecontrolled modulation of spin Hall nano-oscillator damping *Nat. Commun.* 11 4006
- [184] Wang Q, Chumak A V, Jin L, Zhang H, Hillebrands B and Zhong Z 2017 Voltage-controlled nanoscale reconfigurable magnonic crystal *Phys. Rev.* B 95 134433
- [185] Choudhury S, Chaurasiya A K, Mondal A K, Rana B, Miura K, Takahashi H, Otani Y and Barman A 2020 Voltage controlled on-demand magnonic nanochannels Sci. Adv. 6 eaba5457
- [186] Žutić I, Fabian J and Das Sarma S 2004 Spintronics: fundamentals and applications Rev. Mod. Phys. 76 323–410
- [187] Debray P, Rahman S M S, Wan J, Newrock R S, Cahay M, Ngo A T, Ulloa S E, Herbert S T, Muhammad M and Johnson M 2009 All-electric quantum point contact spinpolarizer *Nat. Nanotechnol.* 4 759–64
- [188] Rashba E I 2000 Theory of electrical spin injection: tunnel contacts as a solution of the conductivity mismatch problem *Phys. Rev.* B 62 R16267–70
- [189] Julliere M 1975 Tunneling between ferromagnetic films *Phys. Lett.* A 54 225–6
- [190] Miyazaki T and Tezuka N 1995 Giant magnetic tunneling effect in Fe/Al<sub>2</sub>O<sub>3</sub>/Fe junction J. Magn. Magn. Mater. 139 L231-4
- [191] Moodera J S, Kinder L R, Wong T M and Meservey R 1995 Large magnetoresistance at room temperature in ferromagnetic thin film tunnel junctions *Phys. Rev. Lett.* 74 3273
- [192] Parkin S S P et al 1999 Exchange-biased magnetic tunnel junctions and application to nonvolatile magnetic random access memory (invited) J. Appl. Phys. 85 5828–33
- [193] Parkin S S P, Kaiser C, Panchula A, Rice P M, Hughes B, Samant M and Yang S-H 2004 Giant tunnelling magnetoresistance at room temperature with MgO (100) tunnel barriers *Nat. Mater.* 3 862–7
- [194] Ikeda S, Hayakawa J, Ashizawa Y, Lee Y M, Miura K, Hasegawa H, Tsunoda M, Matsukura F and Ohno H 2008 Tunnel magnetoresistance of 604% at 300K by suppression of Ta diffusion in CoFeB/MgO/CoFeB pseudo-spinvalves annealed at high temperature Appl. Phys. Lett. 93 082508
- [195] Baibich M N, Broto J M, Fert A, Van Dau F N, Petroff F, Etienne P, Creuzet G, Friederich A and Chazelas J 1988 Giant magnetoresistance of (001) Fe/(001) Cr magnetic superlattices *Phys. Rev. Lett.* 61 2472
- [196] Binasch G, Grünberg P, Saurenbach F and Zinn W 1989 Enhanced magnetoresistance in layered magnetic structures with antiferromagnetic interlayer exchange *Phys. Rev.* B 39 4828–30 (R)

- [197] Valet T and Fert A 1993 Theory of the perpendicular magnetoresistance in magnetic multilayers *Phys. Rev.* B 48 7099–113
- [198] Johnson M 1991 Analysis of anomalous multilayer magnetoresistance within the thermomagnetoelectric system *Phys. Rev. Lett.* 67 3594
- [199] Jedema F J, Filip A T and Van Wees B J 2001 Electrical spin injection and accumulation at room temperature in an allmetal mesoscopic spin valve *Nature* 410 345–8
- [200] Jedema F J, Heersche H B, Filip A T, Baselmans J J A and Van Wees B J 2002 Electrical detection of spin precession in a metallic mesoscopic spin valve *Nature* 416 713–6
- [201] Kimura T, Hashimoto N, Yamada S, Miyao M and Hamaya K 2012 Room-temperature generation of giant pure spin currents using epitaxial Co2FeSi spin injectors NPG Asia Mater. 4 e9–9
- [202] Salis G, Wang R, Jiang X, Shelby R M, Parkin S S P, Bank S R and Harris J S 2005 Temperature independence of the spin-injection efficiency of a MgO-based tunnel spin injector Appl. Phys. Lett. 87 262503
- [203] Albert F J, Katine J A, Buhrman R A and Ralph D C 2000 Spin-polarized current switching of a Co thin film nanomagnet Appl. Phys. Lett. 77 3809–11
- [204] Bass J 2016 CPP magnetoresistance of magnetic multilayers: a critical review J. Magn. Magn. Mater. 408 244–320
- [205] Jiang Y, Abe S, Ochiai T, Nozaki T, Hirohata A, Tezuka N and Inomata K 2004 Effective reduction of critical current for current-induced magnetization switching by a Ru layer insertion in an exchange-biased spin valve *Phys. Rev.* Lett. 92 167204
- [206] Jiang Y, Nozaki T, Abe S, Ochiai T, Hirohata A, Tezuka N and Inomata K 2004 Substantial reduction of critical current for magnetization switching in an exchangebiased spin valve *Nat. Mater.* 3 361-4
- [207] Vautrin C, Lacour D, Sala G, Lu Y, Montaigne F and Hehn M 2017 Thickness and angular dependence of the magnetocurrent of hot electrons in a magnetic tunnel transistor with crossed anisotropies *Phys. Rev.* B 96 174426
- [208] Fuchs G, Emley N, Krivorotov I, Braganca P, Ryan E, Kiselev S, Sankey J, Ralph D, Buhrman R and Katine J 2004 Spin-transfer effects in nanoscale magnetic tunnel junctions Appl. Phys. Lett. 85 1205–7
- [209] Hayakawa J, Ikeda S, Lee Y M, Sasaki R, Meguro T, Matsukura F, Takahashi H and Ohno H 2005 Current-driven magnetization switching in CoFeB/MgO/CoFeB magnetic tunnel junctions *Japan. J. Appl. Phys.* 44 L1267
- [210] Tao B, Yang H, Zuo Y, Devaux X, Lengaigne G, Hehn M, Lacour D, Andrieu S, Chshiev M and Hauet T 2015 Longrange phase coherence in double-barrier magnetic tunnel junctions with a large thick metallic quantum well *Phys. Rev. Lett.* 115 157204
- [211] Tao B, Wan C, Tang P, Feng J, Wei H, Wang X, Andrieu S P, Yang H, Chshiev M and Devaux X 2019 Coherent resonant tunneling through double metallic quantum well states *Nano Lett.* 19 3019–26
- [212] Soumyanarayanan A, Reyren N, Fert A and Panagopoulos C 2016 Emergent phenomena induced by spin-orbit coupling at surfaces and interfaces *Nature* 539 509-17
- [213] Jungwirth T, Marti X, Wadley P and Wunderlich J 2016 Antiferromagnetic spintronics Nat. Nanotechnol. 11 231
- [214] Wang K, Che X, Wu H and Shao Q 2019 Topological Spintronics and Majorana Fermions (Proc. SPIE 10982, Micro- and Nanotechnology Sensors, Systems, and Applications XI 1098206) (https://doi.org/10.1117/ 12.2520183)
- [215] Bedoya-Pinto A, Donolato M, Gobbi M, Hueso L E and Vavassori P 2014 Flexible spintronic devices on Kapton Appl. Phys. Lett. 104 062412

- [216] Vardeny E Z V 2017 Organic Spintronics (Boca Raton, FL: CRC Press)
- [217] Bandyopadhyay S 1997 Switching in a reversible spin logic gate Superlattices Microstruct. 22 411–6
- [218] Loss D and DiVincenzo D P 1998 Quantum computation with quantum dots *Phys. Rev.* A 57 120–6
- [219] See, example f, Grollier J, Querlioz D, Camsari K Y, Everschor-Sitte K, Fukami S and Stiles M D 2020 Neuromorphic spintronics *Nat. Electron.* 3 360–70
- [220] Camsari K Y, Sutton B M and Datta S 2019 p-bits for probabilistic spin logic Appl. Phys. Rev. 6 011305
- [221] Dresselhaus G 1955 Spin–orbit coupling effects in Zinc blende structures *Phys. Rev.* **100** 580–6
- [222] Rashba E I 1960 Properties of semiconductors with an extremum loop: cyclotron and combinational resonance in a magnetic field perpendicular to the plane of the loop Sov. Phys. Solid State 2 1224–38
- [223] Bottegoni F, Zucchetti C, Isella G, Bollani M, Finazzi M and Ciccacci F 2020 Spin-charge interconversion in heterostructures based on group-IV semiconductors *Riv*. *Nuovo Cim.* 43 45–96
- [224] Schliemann J and Loss D 2003 Anisotropic transport in a two-dimensional electron gas in the presence of spin-orbit coupling *Phys. Rev.* B 68 165311
- [225] Moore J E 2010 The birth of topological insulators *Nature* **464** 194–8
- [226] Dyakonov M and Perel V I 1971 Possibility of orienting electron spins with current Sov. Phys. JETP 33 657–60
- [227] Hirsch J E 1999 Spin Hall effect Phys. Rev. Lett. 83 1834-7
- [228] Valenzuela S O and Tinkham M 2006 Direct electronic measurement of the spin Hall effect *Nature* 442 176–9
- [229] Kato Y K, Myers R C, Gossard A C and Awschalom D D 2004 Observation of the spin Hall effect in semiconductors Science 306 1910
- [230] Saitoh E, Ueda M, Miyajima H and Tatara G 2006 Conversion of spin current into charge current at room temperature: inverse spin-Hall effect Appl. Phys. Lett. 88 182509
- [231] Sinova J, Culcer D, Niu Q, Sinitsyn N A, Jungwirth T and MacDonald A H 2004 universal intrinsic spin Hall effect *Phys. Rev. Lett.* 92 126603
- [232] Demasius K-U, Phung T, Zhang W, Hughes B P, Yang S-H, Kellock A, Han W, Pushp A and Parkin S S P 2016 Enhanced spin-orbit torques by oxygen incorporation in tungsten films *Nat. Commun.* 7 10644
- [233] Khang N H D, Ueda Y and Hai P N 2018 A conductive topological insulator with large spin Hall effect for ultralow power spin-orbit torque switching *Nat. Mater.* 17 808–13
- [234] Tserkovnyak Y, Brataas A and Bauer G E W 2002 Enhanced Gilbert damping in thin ferromagnetic films *Phys. Rev. Lett.* 88 117601
- [235] Tserkovnyak Y, Brataas A, Bauer G E W and Halperin B I 2005 Nonlocal magnetization dynamics in ferromagnetic heterostructures Rev. Mod. Phys. 77 1375–421
- [236] Tserkovnyak Y, Brataas A and Bauer G E W 2002 Spin pumping and magnetization dynamics in metallic multilayers *Phys. Rev.* B 66 224403
- [237] Shaw J M, Nembach H T and Silva T J 2012 Determination of spin pumping as a source of linewidth in sputtered Co90Fe10/Pd multilayers by use of broadband ferromagnetic resonance spectroscopy *Phys. Rev.* B 85 054412
- [238] Zhang W, Han W, Jiang X, Yang S-H and Parkin S S P 2015 Role of transparency of platinum–ferromagnet interfaces in determining the intrinsic magnitude of the spin Hall effect Nat. Phys. 11 496–502
- [239] Panda S N, Mondal S, Sinha J, Choudhury S and Barman A 2019 All-optical detection of interfacial spin transparency

- from spin pumping in  $\beta$ -Ta/CoFeB thin films *Sci. Adv.* **5** eaav7200
- [240] Panda S N, Majumder S, Bhattacharyya A, Dutta S, Choudhury S and Barman A 2021 Structural phasedependent giant interfacial spin transparency in W/CoFeB thin-film heterostructures ACS Appl. Mater. Interfaces 13 20875–84
- [241] Dzyaloshinsky I 1958 A thermodynamic theory of 'weak' ferromagnetism of antiferromagnetics J. Phys. Chem. Solids 4 241–55
- [242] Moriya T 1960 New mechanism of anisotropic superexchange interaction *Phys. Rev. Lett.* 4 228–30
- [243] Moriya T 1960 Anisotropic superexchange interaction and weak ferromagnetism *Phys. Rev.* **120** 91–8
- [244] Fert A and Levy P M 1980 Role of anisotropic exchange interactions in determining the properties of spin-glasses Phys. Rev. Lett. 44 1538–41
- [245] Ryu K-S, Yang S-H, Thomas L and Parkin S S P 2014 Chiral spin torque arising from proximity-induced magnetization *Nat. Commun.* 5 3910
- [246] Yang H, Thiaville A, Rohart S, Fert A and Chshiev M 2015 Anatomy of Dzyaloshinskii-Moriya interaction at Co/Pt interfaces *Phys. Rev. Lett.* 115 267210
- [247] Belabbes A, Bihlmayer G, Bechstedt F, Blügel S and Manchon A 2016 Hund's rule-driven Dzyaloshinskii-Moriya interaction at 3d-5d interfaces *Phys. Rev. Lett.* 117 247202
- [248] Torrejon J, Kim J, Sinha J, Mitani S, Hayashi M, Yamanouchi M and Ohno H 2014 Interface control of the magnetic chirality in CoFeB/MgO heterostructures with heavy-metal underlayers *Nat. Commun.* 5 4655
- [249] Ma X, Yu G, Razavi S A, Chang L, Deng L, Chu Z, He C, Wang K L and Li X 2018 Correlation between the Dzyaloshinskii-Moriya interaction and spin-mixing conductance at an antiferromagnet/ferromagnet interface *Phys. Rev.* B 98 104428
- [250] Nembach H T, Shaw J M, Weiler M, Jué E and Silva T J 2015 Linear relation between Heisenberg exchange and interfacial Dzyaloshinskii–Moriya interaction in metal films *Nat. Phys.* 11 825–9
- [251] Chaurasiya A K, Choudhury S, Sinha J and Barman A 2018
  Dependence of interfacial Dzyaloshinskii-Moriya interaction
  on layer thicknesses in Ta/Co-Fe-B/TaOx heterostructures
  from Brillouin light scattering *Phys. Rev. Appl.* 9
- [252] Castro Neto A H, Guinea F, Peres NMR, Novoselov K S and Geim A K 2009 The electronic properties of graphene Rev. Mod. Phys. 81 109–62
- [253] Marchenko D, Varykhalov A, Scholz M R, Bihlmayer G, Rashba E I, Rybkin A, Shikin A M and Rader O 2012 Giant Rashba splitting in graphene due to hybridization with gold Nat. Commun. 3 1232
- [254] Matsuo M, Saitoh E and Maekawa S 2016 Spin-mechatronics J. Phys. Soc. Japan 86 011011
- [255] Barnett S J 1915 Magnetization by rotation *Phys. Rev.* 6 239–70
- [256] Matsuo M, Ieda J and Maekawa S 2015 Mechanical generation of spin current Front. Phys. 3 54
- [257] Zolfagharkhani G, Gaidarzhy A, Degiovanni P, Kettemann S, Fulde P and Mohanty P 2008 Nanomechanical detection of itinerant electron spin flip *Nat. Nanotechnol.* 3 720–3
- [258] Harii K, Seo Y-J, Tsutsumi Y, Chudo H, Oyanagi K, Matsuo M, Shiomi Y, Ono T, Maekawa S and Saitoh E 2019 Spin Seebeck mechanical force *Nat. Commun.* 10 2616
- [259] Karenowska A D, Gregg J F, Chumak A V, Serga A A and Hillebrands B 2011 Spin information transfer and transport in hybrid spinmechatronic structures J. Phys. Conf. Ser. 303 012018

- [260] Einstein A, de Haas W J 1915 Experimenteller Nachweis der Ampereschen Molekularströme Verh. Dtsch. Phys. Ges. 17 152–70
- [261] Chudo H, Ono M, Harii K, Matsuo M, Ieda J I, Haruki R, Okayasu S, Maekawa S, Yasuoka H and Saitoh E 2014 Observation of Barnett fields in solids by nuclear magnetic resonance Appl. Phys. Express 7 063004
- [262] Ono M, Chudo H, Harii K, Okayasu S, Matsuo M, Ieda J I, Takahashi R, Maekawa S and Saitoh E 2015 Barnett effect in paramagnetic states *Phys. Rev.* B 92 174424
- [263] Matsuo M, Ieda J i, Saitoh E and Maekawa S 2011 Effects of mechanical rotation on spin currents *Phys. Rev. Lett.* 106 076601
- [264] Matsuo M, Ieda J i, Saitoh E and Maekawa S 2011 Spindependent inertial force and spin current in accelerating systems *Phys. Rev.* B 84 104410
- [265] Matsuo M, Ieda J I, Harii K, Saitoh E and Maekawa S 2013 Mechanical generation of spin current by spin-rotation coupling *Phys. Rev.* B 87 180402
- [266] Ieda J I, Matsuo M and Maekawa S 2014 Theory of mechanical spin current generation via spin–rotation coupling Solid State Commun. 198 52–6
- [267] Kobayashi D, Yoshikawa T, Matsuo M, Iguchi R, Maekawa S, Saitoh E and Nozaki Y 2017 Spin current generation using a surface acoustic wave generated via spinrotation coupling *Phys. Rev. Lett.* 119 077202
- [268] Takahashi R, Matsuo M, Ono M, Harii K, Chudo H, Okayasu S, Ieda J, Takahashi S, Maekawa S and Saitoh E 2016 Spin hydrodynamic generation *Nat. Phys.* 12 52–6
- [269] Mohanty P, Zolfagharkhani G, Kettemann S and Fulde P 2004 Spin-mechanical device for detection and control of spin current by nanomechanical torque *Phys. Rev.* B 70 195301
- [270] Barman A et al 2021 The 2021 magnonics roadmap J. Phys. Condens.: Matter 33 413001
- [271] Pan S, Mondal S, Zelent M, Szwierz R, Pal S, Hellwig O, Krawczyk M and Barman A 2020 Edge localization of spin waves in antidot multilayers with perpendicular magnetic anisotropy *Phys. Rev.* B 101 014403
- [272] De A, Drobitch J L, Majumder S, Barman S, Bandyopadhyay S and Barman A 2021 Resonant amplification of intrinsic magnon modes and generation of new extrinsic modes in a two-dimensional array of interacting multiferroic nanomagnets by surface acoustic waves *Nanoscale* 13 10016–23
- [273] De A, Dutta K, Mondal S, Barman S, Otani Y and Barman A 2021 Magnonic crystals with complex geometry *Phys. Rev.* B 103 064402
- [274] Chaurasiya A K, Mondal A K, Gartside J C, Stenning K D, Vanstone A, Barman S, Branford W R and Barman A 2021 Comparison of spin-wave modes in connected and disconnected artificial spin ice nanostructures using brillouin light scattering spectroscopy ACS Nano 15 11734–42
- [275] Huang B et al 2017 Layer-dependent ferromagnetism in a van der Waals crystal down to the monolayer limit Nature 546 270
- [276] Gong C *et al* 2017 Discovery of intrinsic ferromagnetism in two-dimensional van der Waals crystals *Nature* **546** 265
- [277] Deng Y *et al* 2018 Gate-tunable room-temperature ferromagnetism in two-dimensional Fe<sub>3</sub>GeTe<sub>2</sub> *Nature* **563** 94–9
- [278] Fei Z et al 2018 Two-dimensional itinerant ferromagnetism in atomically thin Fe<sub>3</sub>GeTe<sub>2</sub> Nat. Mater. 17 778–82
- [279] Lee J-U, Lee S, Ryoo J H, Kang S, Kim T Y, Kim P, Park C-H, Park J-G and Cheong H 2016 Ising-type magnetic ordering in atomically thin FePS<sub>3</sub> Nano Lett. 16 7433–8
- [280] O'Hara D J et al 2018 Room temperature intrinsic ferromagnetism in epitaxial manganese selenide films in the monolayer limit Nano Lett. 18 3125–31

- [281] Bonilla M, Kolekar S, Ma Y, Diaz H C, Kalappattil V, Das R, Eggers T, Gutierrez H R, Phan M-H and Batzill M 2018 Strong room-temperature ferromagnetism in VSe<sub>2</sub> monolayers on van der Waals substrates *Nat. Nanotechnol.* 13 289–93
- [282] May A F, Ovchinnikov D, Zheng Q, Hermann R, Calder S, Huang B, Fei Z, Liu Y, Xu X and McGuire M A 2019 Ferromagnetism near room temperature in the cleavable van der Waals crystal Fe<sub>5</sub>GeTe<sub>2</sub> ACS Nano 13 4436–42
- [283] Zhang W et al 2019 Ferromagnet/two-dimensional semiconducting transition-metal dichalcogenide interface with perpendicular magnetic anisotropy ACS Nano 13 2253–61
- [284] Shao Q, Yu G, Lan Y-W, Shi Y, Li M-Y, Zheng C, Zhu X, Li L-J, Amiri P K and Wang K L 2016 Strong Rashba-Edelstein effect-induced spin-orbit torques in monolayer transition metal dichalcogenide/ferromagnet bilayers *Nano Lett.* 16 7514-20
- [285] Yang H et al 2018 Significant Dzyaloshinskii–Moriya interaction at graphene–ferromagnet interfaces due to the Rashba effect Nat. Mater. 17 605–9
- [286] Chaurasiya A K, Kumar A, Gupta R, Chaudhary S, Muduli P K and Barman A 2019 Direct observation of unusual interfacial Dzyaloshinskii-Moriya interaction in graphene/NiFe/Ta heterostructures *Phys. Rev.* B 99 035402
- [287] Ajejas F et al 2018 Unraveling Dzyaloshinskii–Moriya interaction and chiral nature of graphene/cobalt interface Nano Lett. 18 5364–72
- [288] Wu Y et al 2020 Néel-type skyrmion in WTe<sub>2</sub>/Fe<sub>3</sub>GeTe<sub>2</sub> van der Waals heterostructure Nat. Commun. 11 3860
- [289] Kumar A et al 2020 Direct measurement of interfacial Dzyaloshinskii–Moriya interaction at the MoS<sub>2</sub>/Ni80Fe20 interface Appl. Phys. Lett. 116 232405
- [290] Yao W, Li C, Wang L, Xue S, Dan Y, Iida K, Kamazawa K, Li K, Fang C and Li Y 2018 Topological spin excitations in a three-dimensional antiferromagnet *Nat. Phys.* 14 1011–5
- [291] Bao S et al 2018 Discovery of coexisting Dirac and triply degenerate magnons in a three-dimensional antiferromagnet Nat. Commun. 9 2591
- [292] Chen L, Chung J-H, Gao B, Chen T, Stone M B, Kolesnikov A I, Huang Q and Dai P 2018 Topological spin excitations in honeycomb ferromagnet CrI3 *Phys. Rev.* X 8 041028
- [293] Fernández-Pacheco A, Streubel R, Fruchart O, Hertel R, Fischer P and Cowburn R P 2017 Three-dimensional nanomagnetism Nat. Commun. 8 15756
- [294] Sanz-Hernández D, Hamans R F, Liao J-W, Welbourne A, Lavrijsen R and Fernández-Pacheco A 2017 Fabrication, detection, and operation of a three-dimensional nanomagnetic conduit ACS Nano 11 11066–73
- [295] Williams G et al 2018 Two-photon lithography for 3D magnetic nanostructure fabrication Nano Res. 11 845–54
- [296] Sahoo S, Mondal S, Williams G, May A, Ladak S and Barman A 2018 Ultrafast magnetization dynamics in a nanoscale three-dimensional cobalt tetrapod structure *Nanoscale* 10 9981–6
- [297] Sahoo S, May A, van Den Berg A, Mondal A K, Ladak S and Barman A 2021 Observation of coherent spin waves in a three-dimensional artificial spin ice structure *Nano Lett.* 21 4629–35
- [298] Dediu V A, Hueso L E, Bergenti I and Taliani C 2009 Spin routes in organic semiconductors Nat. Mater. 8 707–16
- [299] Nakayama H, Yamamoto T, An H, Tsuda K, Einaga Y and Ando K 2018 Molecular engineering of Rashba spin-charge converter Sci. Adv. 4 eaar3899
- [300] Bogani L and Wernsdorfer W 2008 Molecular spintronics using single-molecule magnets Nat. Mater. 7 179–86
- [301] Naaman R, Paltiel Y and Waldeck D H 2019 Chiral molecules and the electron spin Nat. Rev. Chem. 3 250–60

- [302] Dor O B, Yochelis S, Mathew S P, Naaman R and Paltiel Y 2013 A chiral-based magnetic memory device without a permanent magnet *Nat. Commun.* 4 2256
- [303] Al-Bustami H, Koplovitz G, Primc D, Yochelis S, Capua E, Porath D, Naaman R and Paltiel Y 2018 Single nanoparticle magnetic spin memristor *Small* 14 1801249
- [304] Ben Dor O et al 2017 Magnetization switching in ferromagnets by adsorbed chiral molecules without current or external magnetic field Nat. Commun. 8 14567
- [305] Naka M, Hayami S, Kusunose H, Yanagi Y, Motome Y and Seo H 2019 Spin current generation in organic antiferromagnets *Nat. Commun.* 10 4305
- [306] Hortensius J R, Afanasiev D, Matthiesen M, Leenders R, Citro R, Kimel A V, Mikhaylovskiy R V, Ivanov B A and Caviglia A D 2021 Coherent spin-wave transport in an antiferromagnet *Nat. Phys.* 17 1001–6
- [307] Li J *et al* 2020 Spin current from sub-terahertz-generated antiferromagnetic magnons *Nature* **578** 70–4
- [308] Xing W, Qiu L, Wang X, Yao Y, Ma Y, Cai R, Jia S, Xie X C and Han W 2019 Magnon transport in quasi-twodimensional van der Waals antiferromagnets *Phys. Rev.* X 9 011026
- [309] Lan J, Yu W and Xiao J 2017 Antiferromagnetic domain wall as spin wave polarizer and retarder *Nat. Commun.* 8 178
- [310] Li Y, Zhang W, Tyberkevych V, Kwok W-K, Hoffmann A and Novosad V 2020 Hybrid magnonics: physics, circuits and applications for coherent information processing J. Appl. Phys. 128 130902
- [311] Hwang Y, Puebla J, Xu M, Lagarrigue A, Kondou K and Otani Y 2020 Enhancement of acoustic spin pumping by acoustic distributed Bragg reflector cavity *Appl. Phys. Lett.* 116 252404
- [312] Klingler S et al 2018 Spin-torque excitation of perpendicular standing spin waves in coupled YIG/Co heterostructures Phys. Rev. Lett. 120 127201
- [313] Adhikari K, Choudhury S, Barman S, Otani Y and Barman A 2021 Observation of magnon–magnon coupling with high cooperativity in Ni80Fe20 cross-shaped nanoring array *Nanotechnology* 32 395706
- [314] Go D, Jo D, Kim C and Lee H-W 2018 Intrinsic spin and orbital Hall effects from orbital texture *Phys. Rev. Lett.* 121
- [315] Kim J, Go D, Tsai H, Jo D, Kondou K, Lee H-W and Otani Y 2021 Nontrivial torque generation by orbital angular momentum injection in ferromagnetic-metal/Cu/Al<sub>2</sub>O<sub>3</sub> trilayers *Phys. Rev.* B 103 L020407
- [316] Demokritov S O, Demidov V E, Dzyapko O, Melkov G A, Serga A A, Hillebrands B and Slavin A N 2006 Bose–Einstein

- condensation of quasi-equilibrium magnons at room temperature under pumping *Nature* **443** 430–3
- [317] Bozhko D A, Serga A A, Clausen P, Vasyuchka V I, Heussner F, Melkov G A, Pomyalov A, L'vov V S and Hillebrands B 2016 Supercurrent in a room-temperature Bose–Einstein magnon condensate *Nat. Phys.* 12 1057–62
- [318] Shiomi Y, Lustikova J, Watanabe S, Hirobe D, Takahashi S and Saitoh E 2019 Spin pumping from nuclear spin waves *Nat. Phys.* 15 22–6
- [319] Che P, Baumgaertl K, Kúkol'ová A, Dubs C and Grundler D 2020 Efficient wavelength conversion of exchange magnons below 100 nm by magnetic coplanar waveguides *Nat. Commun.* 11 1445
- [320] Yu H, Duerr G, Huber R, Bahr M, Schwarze T, Brandl F and Grundler D 2013 Omnidirectional spin-wave nanograting coupler *Nat. Commun.* 4 2702
- [321] Liu C et al 2018 Long-distance propagation of shortwavelength spin waves Nat. Commun. 9 738
- [322] Sluka V *et al* 2019 Emission and propagation of 1D and 2D spin waves with nanoscale wavelengths in anisotropic spin textures *Nat. Nanotechnol.* **14** 328–33
- [323] Sandweg C W, Kajiwara Y, Chumak A V, Serga A A, Vasyuchka V I, Jungfleisch M B, Saitoh E and Hillebrands B 2011 Spin pumping by parametrically excited exchange magnons *Phys. Rev. Lett.* 106 216601
- [324] Chen J, Hu J and Yu H 2021 Chiral emission of exchange spin waves by magnetic skyrmions *ACS Nano* **15** 4372–9
- [325] Torrejon J *et al* 2017 Neuromorphic computing with nanoscale spintronic oscillators *Nature* **547** 428–31
- [326] Zeng L, Zhang D, Zhang Y, Gong F, Gao T, Tu S, Yu H and Zhao W 2016 Spin Wave Based Synapse and Neuron for Ultra Low Power Neuromorphic Computation System (22–25 May 2016) pp 918–21
- [327] Papp A, Porod W and Csaba G 2020 Nanoscale neural network using non-linear spin-wave interference arXiv:2012.04594
- [328] Jeon K-R et al 2019 Effect of Meissner screening and trapped magnetic flux on magnetization dynamics in thick Nb/ Ni80Fe20/Nb trilayers Phys. Rev. Appl. 11 014061
- [329] Golovchanskiy I A, Abramov N N, Stolyarov V S, Bolginov V V, Ryazanov V V, Golubov A A and Ustinov A V 2018 Ferromagnet/superconductor hybridization for magnonic applications Adv. Funct. Mater. 28 1802375
- [330] Emil Viñas Boström M, Claassen J W, McIver G, Jotzu A, Rubio and Sentef M A 2020 Light-induced topological magnons in two-dimensional van der Waals magnets SciPost Phys. 9 061